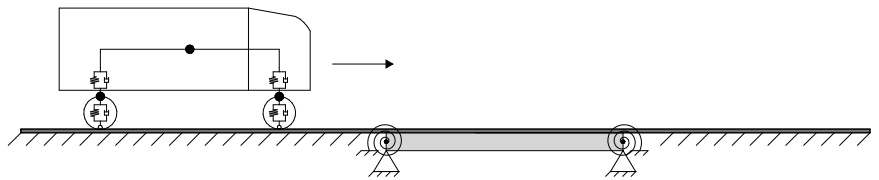




LUND
UNIVERSITY



REFINED MODEL FOR CALCULATING THE DYNAMIC AMPLIFICATION FACTOR FOR ROAD BRIDGES

JENS BERGENUDD

Structural
Mechanics

Master's Dissertation

DEPARTMENT OF CONSTRUCTION SCIENCES
DIVISION OF STRUCTURAL MECHANICS

ISRN LUTVDG/TVSM--20/5248--SE (1-144) | ISSN 0281-6679

MASTER'S DISSERTATION

REFINED MODEL FOR CALCULATING THE DYNAMIC AMPLIFICATION FACTOR FOR ROAD BRIDGES

JENS BERGENUDD

Supervisor: Professor **KENT PERSSON**, Division of Structural Mechanics, LTH.
Assistant Supervisor: **CHRISTOFFER SVEDHOLM**, PhD, ELU Konsult AB.
Examiner: Professor **PER-ERIK AUSTRELL**, Division of Structural Mechanics, LTH.

Copyright © 2020 Division of Structural Mechanics,
Faculty of Engineering LTH, Lund University, Sweden.

Printed by V-husets tryckeri LTH, Lund, Sweden, July 2020 (*PI*).

For information, address:
Division of Structural Mechanics,
Faculty of Engineering LTH, Lund University, Box 118, SE-221 00 Lund, Sweden.
Homepage: www.byggmek.lth.se

Abstract

The objective of the thesis is to simulate and evaluate vehicle-bridge interaction (VBI) due to road surface irregularities and soil-structure interaction (SSI) with different vehicle models and suspension properties. Parameter studies will be carried out for integral and slab bridges. The aim is to compare the results with the current formula for the dynamic amplification factor (DAF) according to Trafikverket (2019b) and provide appropriate recommendations. The difference between two suspension types, i.e. air and leaf suspension, will be evaluated as well. Suggestions of measures taken for platoons if they prove to be a problem concerning resonance in bridges will also be presented. The aim is also to evaluate the influence of SSI and other parameters that affect the DAF.

A toolbox in MATLAB that solves the VBI has been verified and used. The vehicles are modeled as mass-spring-damper systems moving across the bridge. The two subsystems, i.e. bridge and vehicle, are coupled using the contact forces and displacements. The coupled equations are solved with the finite element method (FEM) and the time-varying dynamic response is solved with the Newmark- β integration scheme. Road surface irregularities are generated using Power Spectral Density (PSD) functions according to ISO-8608.

Vehicle properties are taken from previous studies for both air and leaf suspension. Bridge properties are retrieved from constructional drawings from ELU Konsult and damping according to SS-EN 1991-2. Soil properties are gathered from previous studies and a simplified soil model is used. Information of traffic composition and flow rate is gathered from weigh-in-motion (WIM) measurements of Swedish bridges. Traffic is simulated using statistical assumptions from previous studies. Information of distances between trucks in a platoon is gathered from the results of different European projects.

The results from the parameter studies shows that the DAF exceeds the Swedish norm for both single and multiple truck events. The main factor to

the exceeding is coincidental frequencies, i.e. when the eigenfrequencies of the vehicles coincide with the bridge's fundamental frequency, f_1 . An example of a refined model of the DAF based on bridge f_1 is therefore presented, which also includes the speed limit of the bridge. It is shown that heavier vehicles provides a lower DAF compared to lighter vehicles. Air suspension is also shown to give a lower response than leaf suspension when the lowest vehicle modes (suspension modes) are close to the bridge's f_1 . When the bridge f_1 exceed the highest vehicle modes the response is similar for the two suspension types.

Platoons are shown to induce resonance which is largest for the slab bridges due to their larger mass and lack of rotational stiffness at the boundaries compared to the integral bridges. Having random distances between vehicles as a safety measure is therefore recommended. SSI provides an amplified response for the VBI and it is shown that the response is attenuated with increasing stiffness and damping on the soil.

Keywords — Dynamics, Dynamic amplification factor, Dynamic impact factor, Platooning, Soil-structure interaction, Vehicle-bridge interaction.

Sammanfattning

Målet med examensarbetet är att simulera och utvärdera fordon-bro interaktion med avseende på ojämnheter i vägbana och jord-bro interaktion med olika fordonsmodeller och egenskaper på fjädringen. Parameterstudier kommer genomföras för plattram- och plattbroar. Syftet är att jämföra resultatet med den dynamiska förstöringsfaktorn enligt Trafikverket (2019b) och att föreslå lämpliga rekommendationer. Skillnaden mellan två typer av fjädring, dvs. luft- och bladfjädring, kommer också att utvärderas. Förslag på åtgärder för framtida lastbilskonvojer om de ger problem med resonans hos broar kommer också att utföras. Syftet är också att utvärdera påverkan från jord-bro interaktion och andra parametrar som påverkar förstöringsfaktorn.

En toolbox i MATLAB som löser fordon-bro interaktion har verifierats och använts. Fordonen är modellerade som massa-fjäder-dämpare system som rör sig över bron. De två delsystemen, dvs. bro och fordon, är kopplade genom att använda kontaktkrafter och förskjutningar. De kopplade ekvationerna löses med finita elementmetoden (FEM) och den tidsvarierande responsen löses med Newmark- β metoden. Ojämnheter i vägbana är genererade med Power Spectral Density funktioner (PSD) enligt ISO-8608.

Egenskaper för fordonen är hämtade från tidigare studier för både luft- och bladfjädring. Egenskaper för broarna är tagna från konstruktionsritningar från ELU Konsult och dämpning enligt SS-EN 1991-2. Jordegenskaper är hämtade från tidigare studier och en förenklad jordmodell används. Information om sammansättning av trafik och flöde är hämtat från weigh-in motion (WIM) mätningar på svenska broar. Trafiken är simulerad genom att använda statistiska antaganden från tidigare studier. Information om avstånd mellan lastbilar i en konvoj är hämtat från olika Europeiska projekt.

Resultaten från parameterstudierna visar att förstöringsfaktorn överstiger den svenska normen för både enskilda och multipla lastbilspassager. Den huvudsakliga faktorn för överstigandet är sammafällande frekvenser, dvs. när egenfrekvenserna för fordonen sammanfaller med bronns fundamentala

frekvens, f_1 . Ett exempel på en förfinad modell av förstoringfaktorn som baseras på bronns f_1 presenteras därmed, vilken dessutom inkluderar bronns hastighetsgräns. Det visas att tyngre fordon ger en mindre förstoringfaktor jämfört med lättare fordon. Det visas också att luftfjädring ger en lägre respons än bladfjädring när de lägsta fordonsmoderna (fjädringsmoder) är nära bronns f_1 . När bronns f_1 är större än de högsta fordonsmoderna är responsen likvärdig för de två fjädringstyperna.

Det visas att konvojer inducerar resonans vilket är störst för plattbroarna till följd av broarnas större massa och avsaknad av rotationstyvhet vid upplagen jämfört med plattrambroarna. Att använda slumpmässiga avstånd mellan fordonen som en säkerhetsåtgärd är därför rekommenderat. Jord-bro interaktion ger en förstärkt respons för fordon-bro interaktionen och det visas att responsen minskar med ökad styvhet och dämpning på jorden.

Nyckelord — Dynamik, Dynamisk förstoringfaktor, Dynamiskt tillskott, Lastbilskonvojer, Jord-bro interaktion, Fordon-bro interaktion.

Acknowledgements

This thesis has been written at the Division of Structural Mechanics at the Faculty of Engineering, Lund University, in cooperation with ELU Konsult during the spring of 2020. I would like to thank ELU Konsult for their suggestion of the thesis and for letting me see a bit of the work that they do at their office. I want to give a special thanks to my supervisor at ELU, Christoffer Svedholm, who provided great insights and ideas to the project and my supervisor at LTH Kent Persson. Thanks also to Daniel Cantero at NTNU for letting me use the MATLAB toolbox he has developed that solves the VBI. I also want to thank my family who always offer their support and help. A big thanks to all my teachers and classmates who have provided great insights and help throughout the years.

June 2020

Lund, Sweden

Jens Bergenudd

Contents

1	Introduction	1
1.1	Background	1
1.2	Aim and objectives	2
1.3	Method	2
1.4	Limitations	3
I	Literature study	5
2	Dynamics	7
2.1	Equation of motion	7
2.2	Eigenfrequencies	7
2.3	Modal truncation	8
2.4	Forced harmonic vibration	9
2.5	Damping	10
2.6	Newmark- β	11
2.7	Bernoulli dynamic beam	12
3	Dynamic amplification factor	15
3.1	DAF in national codes	16
3.1.1	Trafikverket	16
3.1.2	Eurocode	18
3.1.3	AASHTO	19
3.1.4	British standard	19
3.1.5	New Zealand	19
3.1.6	Summary	20
4	Vehicle-bridge interaction	23
4.1	Solving VBI	23
4.1.1	Load models	23
4.1.2	Coupled equations	24

4.1.3	Uncoupled equations	27
4.2	Road	28
4.2.1	Road irregularities	29
4.2.2	Swedish road network	30
4.2.3	Road modeling	31
4.3	Bridge	32
4.3.1	Eigenfrequencies	32
4.3.2	Resonance	34
4.3.3	Cancellation	34
4.4	Vehicles	34
4.4.1	Vehicle dynamics	34
4.4.2	Suspension	36
4.4.3	Vehicle models	37
4.4.4	Vehicle properties	40
4.4.5	Truck 2: Eigenmodes	42
4.5	Frequency and mass	45
4.6	Vehicle events	46
4.7	Suspension	46
5	Soil-structure interaction	49
5.1	Dynamic stiffness	49
5.2	Standard lumped parameter model	52
6	Traffic	55
6.1	Platooning	55
6.1.1	Vehicle distance	56
6.2	Traffic	57
6.2.1	WIM measurements	57
6.2.2	Headway	57
II	Results	59
7	Verification of VBI	61
7.1	Toolbox in MATLAB	61
8	Modelling aspects	63
8.1	Finite element modelling	63
8.2	Maximum DAF	63
8.3	Static systems	64
8.3.1	Slab bridge	64
8.3.2	Integral bridge	65

8.4	Bridge properties	66
8.4.1	Material weight	66
8.4.2	Integral bridge	67
8.4.3	Slab bridge	73
8.4.4	Damping	74
8.5	Soil properties	74
8.6	Vehicle properties	77
8.7	Vehicle velocity	77
8.8	Convergence	79
8.8.1	Mesh	79
8.8.2	Vehicle events	80
8.8.3	Frequency	82
8.9	Platooning	84
8.9.1	Resonance distance	84
8.9.2	Number of vehicles	85
8.10	Multiple truck event	87
8.11	Road irregularities	88
8.11.1	Simulated distance	89
9	Parameter study	91
9.1	Vehicle and bridge frequencies	91
9.2	Single truck event	92
9.2.1	Slab bridges	93
9.2.2	Integral bridges	96
9.2.3	Summary	100
9.3	Multiple truck event	102
9.3.1	Slab bridges	102
9.3.2	Integral bridges	104
9.3.3	Summary	106
9.4	Platooning	107
9.4.1	Slab bridges	108
9.4.2	Integral bridges	110
9.4.3	Summary	112
9.5	Soil-structure interaction	113
9.5.1	Integral bridges	114
III	Review	123
10	Discussion	125
10.1	Bridges	125

10.2	Convergence	125
10.3	Trafikverket	126
10.4	Platooning	126
10.5	Soil	127
11	Conclusions	129
12	Further work	133
12.1	Bridges	133
12.2	Vehicles	133
12.3	Speed limit	134
12.4	Platooning	134
12.5	Soil	134
	References	135

List of abbreviations

AASHTO	American Association of State Highway and Transportation Officials
BM	Bending moment
BS	British standard
CI	Confidence interval
DAF	Dynamic amplification factor
DOF	Degree of freedom
EC	Eurocode
EOM	Equation of motion
FEM	Finite element method
FFT	Fast Fourier transform
IM	Dynamic impact factor
IRI	International roughness index
MDOF	Multi degree of freedom
Mn	Moraine
MTE	Multiple truck event
NZ	New Zealand
PDF	Probability density function
PSD	Power spectral density
SDOF	Single degree of freedom
SSI	Soil-structure interaction

STE	Single truck event
TRVR	Trafikverket
VBI	Vehicle-bridge interaction
WIM	Weigh-in-motion

Chapter 1

Introduction

1.1 Background

When classifying bridges in Sweden, a bearing capacity calculation shall be carried out according to Trafikverket (2019b). 14 different types of vehicle scenarios with axle loads A and B shall be used in the calculation and the values of these axle loads shall be determined in order to classify the bridge. A vehicle moving on a bridge provides a dynamic load in addition to the static load. This is due to irregularities in the roadway, curvature of the bridge and the dynamic response of both the bridge and vehicle. The calculation according to Trafikverket (2019b) therefore includes a dynamic amplification factor (DAF) which depends on the length of the bridge and the vehicle velocity, which is set to a constant value of 80 km/h.

In a proposal for a pilot study by Plos and Svedholm (2019), it is considered possible to develop a refined model of the DAF. The present formulation of the DAF in the Swedish norm is assumed to be inaccurate since there are many parameters that are not taken into account, such as suspension type, soil-structure interaction (SSI) etc. The proposal mentions that the increased use of air suspension in vehicles introduced to the market provides a reduced DAF. This was demonstrated in a study by Raid Karoumi and Andersson (2006) where the use of air suspension provided a smaller DAF compared to the traditional leaf suspension. This was also shown by Ludescher and Brühwiler (2009) and Cantero, Gonzalez, and Eugene OBrien (2011) and mentioned by McLean et al. (1998), Deng et al. (2014) and Gonzalez (2010).

A smaller value on the DAF can subsequently give existing bridges a higher classification which means that measurements, such as reinforcing or replac-

ing the bridge, to allow for heavier vehicles to pass might not be needed. This in turn provides economical and environmental benefits. Heavier trucks also emits more fuel per truck than lighter trucks, but less fuel per tonnes, which is environmentally beneficial (Lumsden 2004).

Previous studies such as Jung, G. Kim, and Park (2013) have also shown that a DAF based on bridge span is insufficient. The study shows that basing it on fundamental frequency instead might be a more appropriate approach.

A new concept that might exist on European roads in a near future is platoons of trucks. The concept is to have a leading vehicle where other vehicles can connect to this vehicle. The following vehicles uses sensors in order to follow the leading vehicle and match its speed and movement. The vehicles uses the same distance between each other which might induce the phenomena of resonance in bridges. This might need consideration when developing the platooning system in order to not damage existing bridges and to not increase the value on the DAF in the national code.

1.2 Aim and objectives

The objective of the thesis is to simulate and evaluate vehicle-bridge interaction (VBI) due to road surface irregularities and SSI with different vehicle models and suspension properties. Parameter studies will be carried out for integral and slab bridges.

The aim is to compare the results with the current formula for the DAF according to Trafikverket (2019b) and provide appropriate recommendations. The difference between two suspension types, i.e. air and leaf suspension, will be evaluated as well. Suggestions of measures taken for platoons if they prove to be a problem concerning resonance in bridges will also be presented. The aim is also to evaluate the influence of SSI and other parameters that affect the DAF. Suggestions of further work will also be mentioned.

1.3 Method

A toolbox in MATLAB developed by Daniel Cantero at NTNU that solves the VBI will be verified and used. The vehicles are modeled as mass-spring-damper systems moving across the bridge. The two subsystems, i.e. bridge and vehicle, are coupled using the contact forces and displacements. The coupled equations are solved with the finite element method (FEM) and the time-varying dynamic response is solved with the Newmark- β integra-

tion scheme. Road surface irregularities are generated using Power Spectral Density (PSD) functions according to ISO-8608.

Vehicle properties are taken from previous studies for both air and leaf suspension. Bridge properties are retrieved from constructional drawings from ELU Konsult and damping according to SS-EN 1991-2. Soil properties are gathered from previous studies and a simplified soil model will be used. Information of traffic composition and flow rate is gathered from weigh-in-motion (WIM) measurements of Swedish bridges. Traffic is simulated using statistical assumptions from previous studies. Information of distances between trucks in a platoon is gathered from the results of different European projects.

Four different studies will be performed:

1. Single truck event (STE).
2. Multiple truck event (MTE).
3. Platooning.
4. Soil-structure interaction (SSI).

The results from the 1st and 2nd study will be compared with the DAF according to Trafikverket (2019b). They will also be the basis of evaluating the difference between air and leaf suspension. The 3rd study will evaluate resonance in bridges due to platooning. The 4th study will evaluate the effect of SSI with a simple soil model which consists of vertical stiffness and damping.

1.4 Limitations

Only vertical vehicle and bridge dynamics is considered, i.e. no horizontal translations are considered. Four different vehicle models are used which are some of the most common vehicles on European roads. The vehicle properties are set to constant values for each vehicle model. The bridge lengths are limited to 5-40 m and only slab and integral bridges are evaluated. Simplifications in order to transform integral to slab properties are made. The soil model is limited to moraine which is the most common soil in Sweden.

Part I

Literature study

Chapter 2

Dynamics

2.1 Equation of motion

A dynamic system can contain springs with stiffness k_i , dampers with viscous damping c_i and masses with mass m_i . The equation of motion for the system is derived by using Newton's 2nd law. By setting up a force equivalence and noting that the forces in the springs and dampers should equal the inertial effects of the masses and the external forces $p_i(t)$, the equation of motion (EOM) for a multi degree of freedom (MDOF) system becomes (Chopra 2013):

$$\mathbf{M}\ddot{\mathbf{u}} + \mathbf{C}\dot{\mathbf{u}} + \mathbf{K}\mathbf{u} = \mathbf{P}(t) \quad (2.1)$$

2.2 Eigenfrequencies

A dynamic system contains eigenfrequencies where resonance occur if an excitation coincides with these frequencies. The eigenfrequencies are solved by performing an eigenvalue analysis of the dynamic system:

$$(\mathbf{K} - \omega^2\mathbf{M})\Phi = 0 \quad (2.2)$$

By solving the determinant of a MDOF system the angular frequencies $\omega_1, \omega_2, \dots, \omega_n$ can be determined, where n is the amount of degrees of freedom:

$$\det(\mathbf{K} - \omega^2\mathbf{M}) = 0 \quad (2.3)$$

The angular frequencies can thereafter be substituted into equation 2.2 and the eigenvectors Φ_i can be solved for. The eigenvectors are the mode shapes of the eigenfrequencies. For a single degree of freedom (SDOF) system the eigenfrequency is simply determined as:

$$\omega_n = \sqrt{\frac{k}{m}} \quad (2.4)$$

The eigenfrequency also depends on the damping ratio, ζ , and the natural frequency of damped vibration is determined as (Chopra 2013):

$$\omega_D = \omega_n \sqrt{1 - \zeta^2} \quad (2.5)$$

2.3 Modal truncation

When the modes of a dynamic system have been determined the displacements can be expressed as a superposition of all N modes with the modal coordinate $q_i(t)$:

$$\mathbf{u}(t) = \sum_{i=1}^N q_i(t) \Phi_i = \Phi \mathbf{q} \quad (2.6)$$

The velocity and acceleration can be derived from this expression by differentiation. By inserting equation 2.6 into the equation of motion, see equation 2.1, and multiplying with Φ^T , a new system of equations can be established:

$$\Phi^T \mathbf{M} \Phi \ddot{\mathbf{q}} + \Phi^T \mathbf{C} \Phi \dot{\mathbf{q}} + \Phi^T \mathbf{K} \Phi \mathbf{q} = \Phi^T \mathbf{P}(t) \quad (2.7)$$

In order to make computations more efficient, a modal truncation can be performed where not all modes of a system are used. The amount of modes used should ensure that the smallest error possible is achieved. The lowest modes are the most important since higher modes give less contribution to the overall response. If J corresponds to the highest mode used, the modal truncation can be expressed as (Chopra 2013):

$$\mathbf{u}(t) = \sum_{i=1}^J q_i(t) \Phi_i \quad (2.8)$$

2.4 Forced harmonic vibration

When a dynamic system is exposed to a forced harmonic load the response varies depending on the frequency of the load, ω , and eigenfrequencies of the system. The response for a SDOF system can be expressed in complex form as (Chopra 2013):

$$u^* = \frac{p_0}{k} \frac{1}{1 - \left(\frac{\omega}{\omega_n}\right)^2 + 2i\zeta \left(\frac{\omega}{\omega_n}\right)} = (u_{st})_0 R_d^* \quad (2.9)$$

$$R_d = |R_d^*| = \left| \frac{u^*}{(u_{st})_0} \right| = \left| \frac{1}{1 - \left(\frac{\omega}{\omega_n}\right)^2 + 2i\zeta \left(\frac{\omega}{\omega_n}\right)} \right| \quad (2.10)$$

The response factor, R_d , as a function of the frequency ratio ω/ω_n is plotted in Figure 2.1. As can be seen in the figure, the response is amplified at the fundamental frequency of the SDOF system and depends largely on the damping. If no damping is present, the amplitude would go to infinity at $\omega = \omega_n$. This means that the response is amplified when a vehicle excites a bridge with frequencies that are close to the bridge eigenfrequencies.

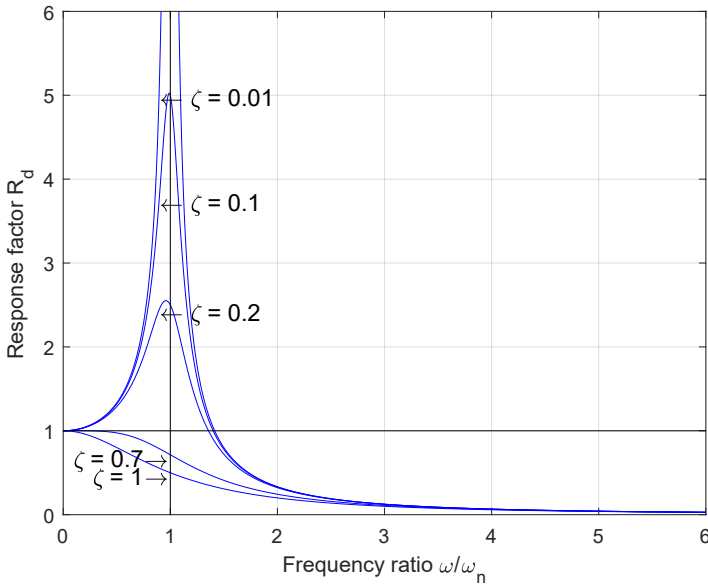


Figure 2.1: Response factor, R_d , as a function of the frequency ratio ω/ω_n .

2.5 Damping

In order to model energy dissipation in structures damping coefficients, c (Ns/m), are used. The damping is assumed to be proportional to the velocity according to:

$$f_D = c\dot{u} \quad (2.11)$$

The energy loss when a vehicle is traversing a bridge is mainly due to material strain, friction in bearings/joints, soil-structure interaction and vehicle-bridge interaction (Svedholm 2017).

Damping in a structure can be expressed with classical damping matrices according to the Rayleigh or Caughey method. These methods are well adjusted for structures that exhibit similar damping behaviour throughout the structure, e.g. a bridge with similar properties along its length. Rayleigh damping is determined based on two parts; mass and stiffness proportional damping:

$$\mathbf{C} = a_0\mathbf{M} + a_1\mathbf{K} \quad (2.12)$$

The damping ratio for the n :th mode can be determined as:

$$\zeta_n = \frac{a_0}{2\omega_n} + \frac{a_1\omega_n}{2} \quad (2.13)$$

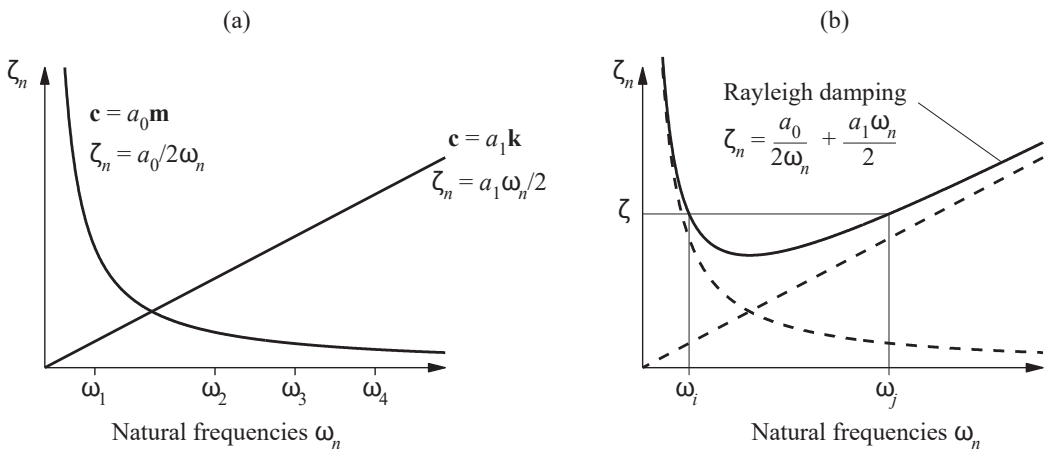


Figure 2.2: (a) Mass and stiffness proportional damping. (b) Rayleigh damping. (Chopra 2013).

If two damping ratios have been determined, e.g. with the half-bandwidth method or by assuming recommended values from national codes, values of a_0 and a_1 can be determined and the damping matrix \mathbf{C} can thereafter be constructed. A graphical illustration of Rayleigh damping can be seen in Figure 2.2. Subfigure (a) shows the mass and stiffness proportional damping. Subfigure (b) shows the Rayleigh damping based on these two parts (Chopra 2013).

2.6 Newmark- β

The Newmark- β method is commonly used as an iterative procedure in the time-domain. Other iteration schemes are available e.g. the Runge-Kutta (Y. B. Yang, J. D. Yau, and Wu 2004) or Wilson- θ method (Lou and Au 2013). The Newmark method include the constant average and linear acceleration method, where the former is used mainly for stability reasons. A sufficiently small time step for the iterations is determined as:

$$\frac{\Delta t}{T_n} \leq \frac{1}{\pi\sqrt{2}} \frac{1}{\sqrt{\gamma - 2\beta}} \quad (2.14)$$

where T_n is the time period for the eigenfrequency. Using J amount of modes and noting that the constant average acceleration method has values of $\gamma = 0.5$ and $\beta = 0.25$ the condition becomes:

$$\frac{\Delta t}{T_J} < \infty \quad (2.15)$$

This means that the solution is an unconditionally stable procedure since Δt can be set to any value. A small time-step is however usually needed and it is normally set to (Chopra 2013):

$$\frac{\Delta t}{T_J} \leq 0.1 \quad (2.16)$$

In this thesis the Nyquist-Shannon criteria of a sampling rate of $f_S = 2f_J$ is used which corresponds to a time-step of:

$$\Delta t \leq \frac{1}{2f_J} = 0.5T_J \quad (2.17)$$

The direct time integration scheme can be seen in Figure 2.3.

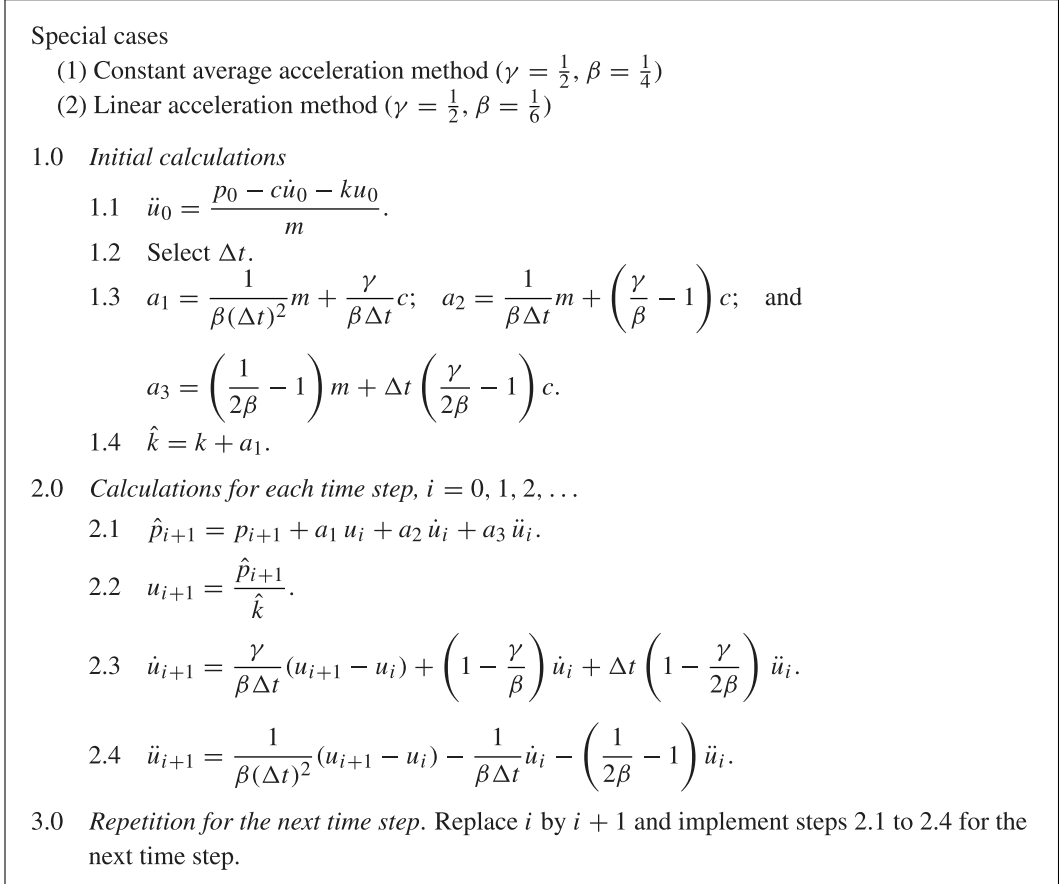


Figure 2.3: Newmark- β integration scheme for the constant average and linear acceleration method (Chopra 2013).

2.7 Bernoulli dynamic beam

The equation of motion for a Bernoulli beam element is given by:

$$\frac{\partial^2}{\partial x^2} \left(EI \frac{\partial^2 v}{\partial x^2} \right) + m \frac{\partial^2 v}{\partial t^2} = p \quad (2.18)$$

A 6-DOF beam element with modulus of elasticity (E), area (A), second moment of area (I), mass per unit length (m) and length (L) can be seen in Figure 2.4. By using the Galerkin and C-matrix method and thereafter expressing the equation in weak form, the finite element formulation can be derived. Assuming evenly distributed mass along the beam the consistent mass matrix for the beam element can be expressed as:

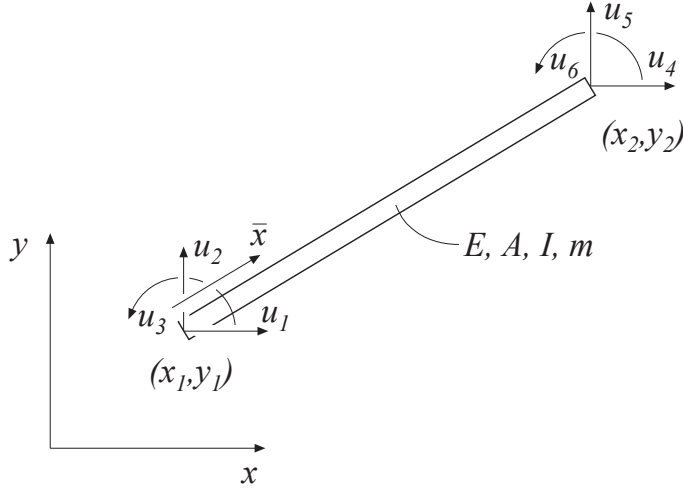


Figure 2.4: Degrees of freedom and properties for a dynamic Bernoulli beam element (Austrell et al. 2004).

$$\mathbf{M}^e = \frac{mL}{420} \begin{bmatrix} 140 & 0 & 0 & 70 & 0 & 0 \\ 0 & 156 & 22L & 0 & 54 & -13L \\ 0 & 22L & 4L^2 & 0 & 13L & -3L^2 \\ 70 & 0 & 0 & 140 & 0 & 0 \\ 0 & 54 & 13L & 0 & 156 & -22L \\ 0 & -13L & -3L^2 & 0 & -22L & 4L^2 \end{bmatrix} \quad (2.19)$$

The stiffness matrix for a 4-DOF beam element, i.e. neglecting the axial displacements at the element nodes, can be expressed as:

$$\mathbf{K}^e = \frac{EI}{L^3} \begin{bmatrix} 12 & 6L & -12 & 6L \\ 6L & 4L^2 & -6L & 2L^2 \\ -12 & -6L & 12 & -6L \\ 6L & 2L^2 & -6L & 4L^2 \end{bmatrix} \quad (2.20)$$

For a 6-DOF Bernoulli element the term EA/L is included in positions (1,1) and (4,4) and the term $-EA/L$ is included in positions (1,4) and (4,1) for $[\mathbf{K}^e]_{6 \times 6}$. Derivations of the matrices can be found in Paz and Y. H. Kim (2019). The damping matrix can thereafter be expressed as a function of the assembled global matrices \mathbf{M} and \mathbf{K} according to Rayleigh damping in equation 2.13.

Chapter 3

Dynamic amplification factor

When designing and evaluating bridges the effect of moving loads on bridges must be taken into account. To determine the effects, a dynamic amplification factor or DAF is commonly used. The DAF states the ratio between the total, i.e. the dynamic and static load effect, and static load effect according to (Deng et al. 2014):

$$\text{DAF} = \frac{R_{dyn}}{R_{stat}} \quad (3.1)$$

The total and static effect can be taken as the total strain ε_T and the static strain ε_S (C. C. Caprani et al. 2012; Paeglite and Paeglitis 2013). Other load effects such as bending moment and shear force is also commonly used (Mohammed, Gonzalez, and Cantero 2018). These quantities can be used when elastic behaviour is assumed. In non-linear analysis other quantities must be used such as energy ratio (Ludescher and Brühwiler 2009). The DAF differs depending on country and code used, and in many standards a dynamic impact factor (IM) is used:

$$\text{IM} = \text{DAF} - 1 = \frac{R_{dyn} - R_{stat}}{R_{stat}} \quad (3.2)$$

The total load effect, P_{dyn} , is retrieved from the static load effect, P_{stat} , according to:

$$P_{dyn} = \text{DAF} \cdot P_{stat} = (1 + \text{IM}) P_{stat} \quad (3.3)$$

The dynamic load effect depends on the road surface irregularities and the properties of the bridge. The factor also depends on the amount of lanes of the bridge as well as the speed, properties and numbers of vehicles traversing the bridge (Deng et al. 2014).

3.1 DAF in national codes

The DAF differs depending on national code. In Sweden, Japan, New Zealand and in the Eurocode, the DAF is defined as a function of the span length of the bridge. In other codes such as the Swiss and Canadian the DAF depends on the fundamental frequency. Other nations such as the US, the UK and Australia apply constant values, where the latter provides different values depending on the vehicle type (Deng et al. 2014). The French, German and Iranian national codes all use a function of the length of the span, but also include the thickness of the bridge deck (Mohseni et al. 2018). The following sections provide some examples of the DAF in various national codes, with a special emphasis on the Swedish.

3.1.1 Trafikverket

Bridges in Sweden are divided into four bearing capacity classes by Trafikverket (TRVR) in order to specify the maximum load allowed on the bridge. When determining the class the dynamic impact factor D is used, which is applied to axle loads in 14 vehicle scenarios. The following sections describes this in greater depth.

Bearing capacity class

After the Government's decision to introduce the new bearing capacity class BK4 (Regeringskansliet 2018), the Swedish road network is divided into four different bearing capacity classes, BK1 - BK4. The new bearing capacity class means that the road network can be loaded by vehicles with a maximum gross weight of 74 tonnes (Trafikverket 2019a). This means that fewer transports can be carried out with the same amount of goods, which has a positive environmental and cost effect. In addition, heavier trucks also emits more fuel per truck than lighter trucks, but less fuel per tonnes, which is environmentally beneficial (Lumsden 2004). The maximum gross weight of trucks can be seen in Table 3.1. For smaller distances between the axles, smaller values of the maximum gross weight is applied (Transportstyrelsen 2018).

Table 3.1: Bearing capacity class for state roads (Transportstyrelsen 2018).

Bearing capacity class	Max. gross weight (t)	Minimum distance between first and last axle (m)
BK1	64	20.2
BK2	51.4	18.5
BK3	37.5	22.0
BK4	74	20.2

Vehicle scenarios

14 different types of vehicle scenarios are used in the bearing capacity calculations. An example can be seen in Figure 3.1 where the values of axle loads A (not present in the current vehicle scenario) and B must be determined in order to determine the bearing capacity class of the bridge (Trafikverket 2019b).

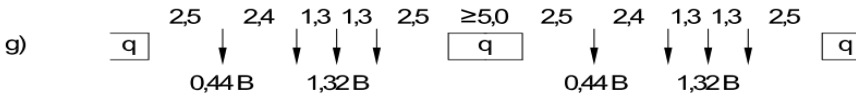


Figure 3.1: Vehicle load scenario (g) (Trafikverket 2019b).

Dynamic impact factor

When determining axle loads A and B in the Swedish standards, the impact factor D , see equation 3.4, should be added to the load. D can be set to a maximum of 35 % (Trafikverket 2019b):

$$D = \min \left\{ \begin{array}{l} \frac{180 + 8(v - 10)}{20 + L} \text{ [%]} \\ 35 \end{array} \right. \quad (3.4)$$

L Determining length, see Table 3.2

v Set to 80 km/h

The determining length depends on the type of bridge and if it is simply supported or continuous. The value of L for slab, girder and integral concrete bridges can be seen in Table 3.2.

Table 3.2: Determining length, L , for slab, girder and integral bridges. $l_{leg,i}$ is the i :th leg of the integral bridge. 1l_m is the mean value of the five connected spans that provide the lowest value (Trafikverket 2019b).

Type of bridge	L					
Simply supported girder/slab	The span length					
Continuous girder/slab	$n =$	2	3	4	5	span
$l_m = \frac{1}{n}(l_1 + \dots + l_n)$	$L =$	1.2	1.3	1.4	1.5	$\cdot l_m > l_{max}$
	$n \geq 6$	$L = 1.5 \cdot l_m^1$				
Integral	$n = 1$	$1.3(l_{leg,1} + l_{span} + l_{leg,2})/(n + 2)$				
	$n = 2$	$1.4(l_{leg,1} + l_{span,1} + l_{span,2} + l_{leg,2})/(n + 2)$				
	$n > 2$	$1.5(l_{leg,1} + l_{span,1} + \dots + l_{span,n} + l_{leg,2})/(n + 2)$				

3.1.2 Eurocode

Eurocode (EC) specifies a DAF depending on if shear force or bending moment is considered. The factor is included in the load values specified in SS-EN 1991-2 Part 2: Traffic loads on bridges. The factor depends on the length and number of lanes of the bridge. For one-lane bridges (Deng et al. 2014):

$$DAF_{moment} = \begin{cases} 1.7 & L \leq 5 \text{ m} \\ 1.85 - 0.03L & 5 \text{ m} < L < 15 \text{ m} \\ 1.4 & L \geq 15 \text{ m} \end{cases} \quad (3.5)$$

$$DAF_{shear} = \begin{cases} 1.4 & L \leq 5 \text{ m} \\ 1.45 - 0.01L & 5 \text{ m} < L < 25 \text{ m} \\ 1.2 & L \geq 25 \text{ m} \end{cases} \quad (3.6)$$

For both moment and shear for two-lane bridges:

$$DAF = \begin{cases} 1.3 - 0.004L & L \leq 50 \text{ m} \\ 1.1 & L > 50 \text{ m} \end{cases} \quad (3.7)$$

The value 1.1 is applied for four-lane bridges for both shear and moment. Note that the DAF for multi-lane is lower than for one-lane bridges.

3.1.3 AASHTO

In the American Association of State Highway and Transportation Officials (AASHTO) "Standard Specification for Highway Bridges" from 1992, the IM was determined as a function of the span length as (Hernandez and Myers 2017):

$$\text{IM} = \frac{15.24}{L + 38.10} \leq 0.30 \quad (3.8)$$

The IM was changed to a dynamic load allowance (DLA) in 1994 in the LRFD Bridge Design Specifications, and the value was changed to a constant value of 33 %, see Table 3.3. This value remain unchanged as of the "LRFD Bridge Design Specifications" from 2014 (Transportation Federal Highway Administration 2015). The value can also be lowered if the quality of the road surface is good (Deng et al. 2014).

Table 3.3: Dynamic load allowance (DLA) in the LRFD Bridge Design Specifications (Transportation Federal Highway Administration 2015).

Limit state	DLA (%)
Deck joints: All limit states	75
All other components: Fatigue and fracture limit state	15
All other limit states	33

3.1.4 British standard

In the British Standard (BS) the IM is set to a constant value of 25 % (British Standard Institution 2003).

3.1.5 New Zealand

In New Zealand (NZ) the DAF is set as a function of the bridge length (NZ Transport Agency 2013). For shear and reaction forces this value is set to a constant value of 1.3. When determining moment in simply supported or continuous bridges, it is set to a constant value for spans below 12 m and a function of the bridge length above 12 m (Deng et al. 2014):

$$\text{DAF} = \begin{cases} 1.30 & L \leq 12 \text{ m} \\ 1 + \frac{15}{L + 38} & L > 12 \text{ m} \end{cases} \quad (3.9)$$

3.1.6 Summary

A summary of the DAF in various national codes that depend on the bridge span can be seen in Figure 3.2.

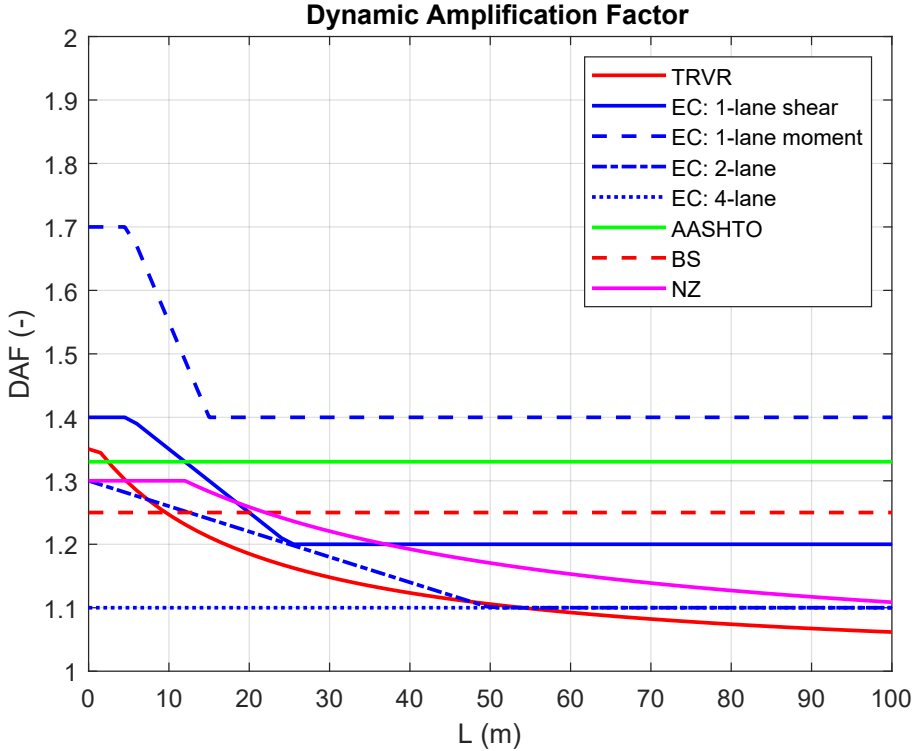


Figure 3.2: A summary of the DAF based on the bridge span in various national codes.

A comparison of the DAF based on frequency can be seen in Figure 3.3. The codes which depends on the span have been transformed based on the expression for the fundamental frequency, $f_1 = 82L^{-0.9}$, in section 4.3.1. The dashed and dash-dotted black coloured lines are for lane (SIA-L) and single truck loading (SIA-T) respectively in the Swiss code. The Canadian norm (OHBD) is based on single truck loading (Jung, G. Kim, and Park 2013).

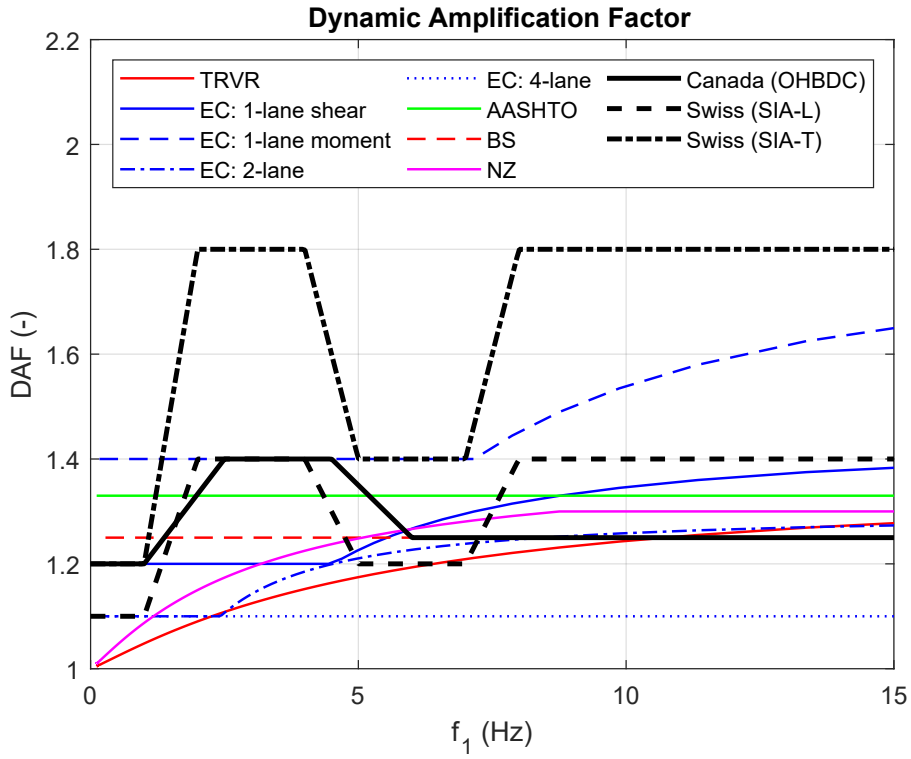


Figure 3.3: A summary of the DAF based on the fundamental frequency in various national codes.

Chapter 4

Vehicle-bridge interaction

The first sections in this chapter describe how the VBI can be solved using coupled and uncoupled equations. The sections after that describe the prerequisites for the VBI such as road modelling and bridge considerations as well as vehicle dynamics, suspensions, models and properties.

4.1 Solving VBI

The VBI can be solved with several methods. An analytical solution can be provided for simple systems such as simply supported beams and simple load cases. When solving more complicated systems the finite element method (FEM) is useful. Two methods that are solved with FEM is mentioned in this thesis; the uncoupled and coupled equations of motion for the vehicle and bridge.

4.1.1 Load models

Load models that can be used for calculations of vehicles on bridges include a moving force (MF), moving mass (MM) and moving sprung-mass (SM) system, see Figure 4.1. The most commonly used load models are the moving force and sprung-mass system, where the latter gives rise to vehicle-bridge interaction and can be modified in order to properly account for the vehicle system in question. The solutions can be solved analytically, but that is mainly for simple systems such as simply supported beams with simple load cases (Frýba 1972).

An effect that is included in the VBI is centripetal acceleration due to the curvature of the bridge. The so called Coriolis effect is also included which

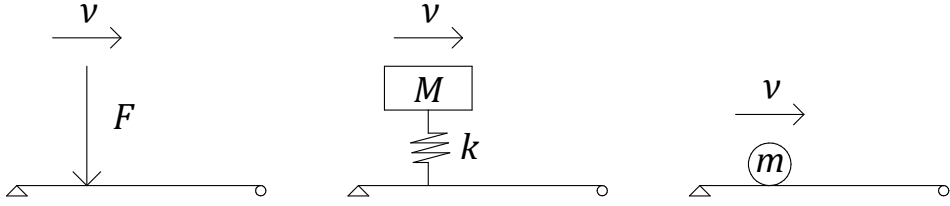


Figure 4.1: Left: Moving force. Middle: Moving sprung-mass. Right: Moving mass.

corresponds to the inertial effects of a moving wheel. The wheel is assumed to always be in contact with the bridge (Frýba 1972). These effects can usually be neglected for massive and stiff bridges and when the bridge is assumed to have a smooth surface (Cantero, Arvidsson, et al. 2016). When road irregularities are accounted for, these effects are included (Lou and Au 2013).

4.1.2 Coupled equations

The VBI can be solved with coupled equations of motion. The wheel DOF's, e.g. u_w for the 2-DOF vehicle in Figure 4.2, can be expressed entirely with the bridge element DOF's that the wheel is in contact with.

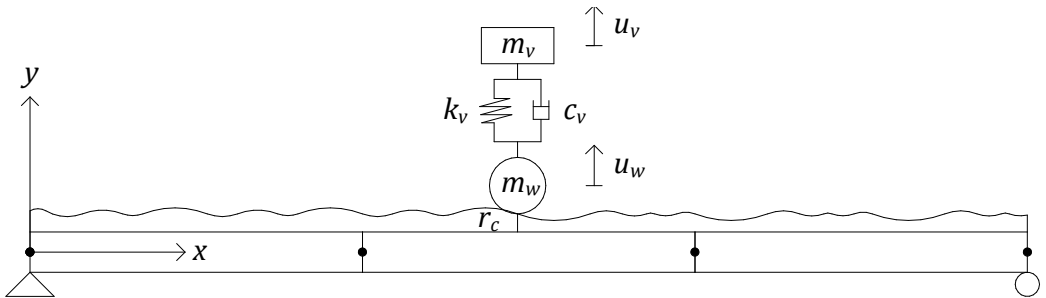


Figure 4.2: 2-DOF vehicle model with a sprung mass, m_v , and unsprung mass, m_w . The bridge is divided into three beam elements as an illustrative example.

The equation of motion for a vehicle, and denoting \mathbf{k} and \mathbf{c} according to which linear equations it corresponds to and which DOF's it is multiplied

with, can be expressed as:

$$\begin{bmatrix} \mathbf{m}_v & 0 \\ 0 & \mathbf{m}_w \end{bmatrix} \begin{bmatrix} \ddot{\mathbf{u}}_v \\ \ddot{\mathbf{u}}_w \end{bmatrix} + \begin{bmatrix} \mathbf{c}_v & -\mathbf{c}_{v,w} \\ -\mathbf{c}_{w,v} & \mathbf{c}_w \end{bmatrix} \begin{bmatrix} \dot{\mathbf{u}}_v \\ \dot{\mathbf{u}}_w \end{bmatrix} + \begin{bmatrix} \mathbf{k}_v & -\mathbf{k}_{v,w} \\ -\mathbf{k}_{w,v} & \mathbf{k}_w \end{bmatrix} \begin{bmatrix} \mathbf{u}_v \\ \mathbf{u}_w \end{bmatrix} = \begin{bmatrix} \mathbf{p}_v \\ \mathbf{p}_w \end{bmatrix} + \begin{bmatrix} \mathbf{0} \\ \mathbf{f}_c \end{bmatrix} \quad (4.1)$$

where the forces \mathbf{p}_v and \mathbf{p}_w are gravitational and external forces acting on the vehicle and \mathbf{f}_c denotes the dynamic contact forces between the wheels and bridge. The bridge EOM at an element in contact with a wheel and adding the contact forces from the vehicle can be expressed as:

$$\mathbf{M}_b \ddot{\mathbf{u}}_b + \mathbf{C}_b \dot{\mathbf{u}}_b + \mathbf{K}_b \mathbf{u}_b = \mathbf{f} - \mathbf{N} f_{c,i} \quad (4.2)$$

where $[\mathbf{N}]_{1 \times 4}$ is the shape function for a beam element which transforms the contact force on the beam to the corresponding element forces. \mathbf{f} are the external forces acting on the beam element and $f_{c,i}$ is the contact force for the i :th wheel. The wheel DOF in contact with the bridge, u_w , can be expressed in terms of the bridge element DOF's that the wheel is in contact as:

$$\begin{cases} u_w = \mathbf{N} \mathbf{u}_b + r_c & (4.3a) \end{cases}$$

$$\begin{cases} \dot{u}_w = \mathbf{N} \dot{\mathbf{u}}_b + v \mathbf{N}_x \mathbf{u}_b + v r_{c,x} & (4.3b) \end{cases}$$

$$\begin{cases} \ddot{u}_w = \mathbf{N} \ddot{\mathbf{u}}_b + 2v \mathbf{N}_x \dot{\mathbf{u}}_b + a \mathbf{N}_x \mathbf{u}_b + v^2 \mathbf{N}_{xx} \mathbf{u}_b + a r_{c,x} + v^2 r_{c,xx} & (4.3c) \end{cases}$$

The notations \mathbf{N}_x and \mathbf{N}_{xx} are the first and second derivatives with respect to x respectively. The time derivative of the shape function can namely be expressed as:

$$\frac{d\mathbf{N}}{dt} = \frac{d\mathbf{N}}{dx} \cdot \frac{dx}{dt} = v \mathbf{N}_x \quad (4.4)$$

r_c is the road irregularity at the contact point between wheel and bridge. $r_{c,x}$ and $r_{c,xx}$ are the first and second derivatives with respect to x and are derived similarly as the shape function derivatives. If the acceleration, a , is set to 0, those terms are omitted. The wheel DOF's can be replaced in equation 4.1 and $f_{c,i}$ can be solved for each wheel. $f_{c,i}$ can thereafter be replaced in the

EOM of the bridge in equation 4.2. By doing this the transformed matrices for the wheels can be expressed as:

$$\begin{cases} \mathbf{M}_{w,i} = m_{w,i} \mathbf{N} \mathbf{N}^T & (4.5a) \\ \mathbf{C}_{w,i} = 2m_{w,i} v \mathbf{N}^T \mathbf{N}_x + c_{w,i} \mathbf{N}^T \mathbf{N} & (4.5b) \\ \mathbf{K}_{w,i} = m_{w,i} a \mathbf{N}^T \mathbf{N}_x + m_{w,i} v^2 \mathbf{N}^T \mathbf{N}_{xx} + c_{w,i} v \mathbf{N}^T \mathbf{N}_x + k_{w,i} \mathbf{N}^T \mathbf{N} & (4.5c) \end{cases}$$

By replacing the wheel DOF's with equations 4.3a - 4.3c in the first line of equation 4.1 and additional terms from the previous derivation yields:

$$\begin{cases} \mathbf{c}_{v,b,i} = -\mathbf{c}_{v,w} \mathbf{N}_V^T \mathbf{N} & (4.6a) \\ \mathbf{c}_{b,v,i} = -\mathbf{N}^T \mathbf{N}_V \mathbf{c}_{w,v} & (4.6b) \\ \mathbf{k}_{v,b,i} = -(\mathbf{k}_{v,w} \mathbf{N}_V^T \mathbf{N} + \mathbf{c}_{v,w} v \mathbf{N}_V^T \mathbf{N}_x) & (4.6c) \\ \mathbf{k}_{b,v,i} = -\mathbf{N}^T \mathbf{N}_V \mathbf{k}_{w,v} & (4.6d) \end{cases}$$

Where $[\mathbf{N}_V]_{1 \times n}$ is the vehicle shape function relating the i :th wheel with the suspended vehicle body DOF's. The total system, i.e. vehicle and bridge, can thereafter be expressed as:

$$\begin{bmatrix} \mathbf{m}_v & 0 \\ 0 & \mathbf{M}_w + \mathbf{M}_b \end{bmatrix} \begin{bmatrix} \ddot{\mathbf{u}}_v \\ \ddot{\mathbf{u}}_b \end{bmatrix} + \begin{bmatrix} \mathbf{c}_v & \mathbf{c}_{v,b} \\ \mathbf{c}_{b,v} & \mathbf{C}_b + \mathbf{C}_w \end{bmatrix} \begin{bmatrix} \dot{\mathbf{u}}_v \\ \dot{\mathbf{u}}_b \end{bmatrix} + \begin{bmatrix} \mathbf{k}_v & \mathbf{k}_{v,b} \\ \mathbf{k}_{b,v} & \mathbf{K}_b + \mathbf{K}_w \end{bmatrix} \begin{bmatrix} \mathbf{u}_v \\ \mathbf{u}_b \end{bmatrix} = \begin{bmatrix} \mathbf{0} \\ \mathbf{f} \end{bmatrix} + \begin{bmatrix} \mathbf{f}_v \\ \mathbf{f}_b \end{bmatrix} \quad (4.7)$$

where the forces $\mathbf{f}_{v,i}$ and $\mathbf{f}_{b,i}$ are expressed as:

$$\begin{cases} \mathbf{f}_{v,i} = \mathbf{p}_v + (\mathbf{c}_{v,w} v r_{c,x} + \mathbf{k}_{v,w} r_c) \mathbf{N}_V^T & (4.8a) \\ \mathbf{f}_{b,i} = \mathbf{N}^T [p_{w,i} - m_{w,i} (a r_{c,x} + v^2 r_{c,xx}) - c_{w,i} v r_{c,x} - k_{w,i} r_c] & (4.8b) \end{cases}$$

The terms that include a , v and v^2 corresponds to the Coriolis and centripetal effects (Yeong-Bin Yang and Bing-Houng Lin 1995; Arvidsson 2014; Cantero, Arvidsson, et al. 2016; Lou and Au 2013). The procedure can be summed up for each time-step in the Newmark- β scheme as:

1. For the first step: Calculate initial static force(s) and displacement(s) for the vehicle(s) from gravity and the road surface. The static force(s) due to gravity can be saved and used for each time-step since it does not change.
2. Locate the position, $x(t)$, of the vehicle wheel(s) on the bridge and determine the force(s) from the road profile, i.e. the terms that include r_c in equations 4.8a - 4.8b.
3. Construct the matrices in equations 4.5a - 4.5c and 4.6a - 4.6c.
4. Insert the matrices into equation 4.7 and solve the equation system according to the Newmark- β integration scheme.
5. Solve equations 4.3a - 4.3c if information of wheel deformations is desirable.
6. Repeat until $t \geq t_{end}$.

The same procedure can be performed with a modal analysis. The equation 4.7 is then transformed into a modal reduced system, see equation 2.7, in step (4) in order to achieve a more time efficient solution.

4.1.3 Uncoupled equations

Solving the VBI for uncoupled equations is based on solving the two sub-systems, i.e. bridge and vehicle, separately. Geometric constraints, $u_{w,i}$, and contact forces, $f_{c,i}$ where the wheels are in contact with the bridge should be in equilibrium for each time-step in the iterative procedure. The condition $f_{c,i} > 0$ should be used in order for the vehicle to always stay in contact with the bridge. For each time-step the vehicle equations are solved and contact forces obtained. Initial assumptions for the vehicle equations can be displacements from the road surface irregularities. The contact force(s) are then used to determine the bridge response. To retrieve the element forces for the element in contact with the wheel(s) the shape function can be used:

$$\mathbf{f}^e = \mathbf{N}f_{c,i} \quad (4.9)$$

The response in form of displacements, velocity and acceleration are then inserted into the vehicle equations and the procedure is repeated. The process is repeated for each time-step until the error for the total displacement $u_{tot}(x, t)$ between two time-steps converges to a small value (Gonzalez 2010)

(Y. Yang and J. Yau 2017) (Mohammed and Arturo González 2017) (Mohammed, Gonzalez, and Cantero 2018).

The general outline for the iterative procedure can be seen in Figure 4.3. The data preparation can consist of determining parameters for the Newmark- β iteration scheme, generating a road surface and performing a FEM model of the bridge and vehicle (Y. Yang and J. Yau 2017).

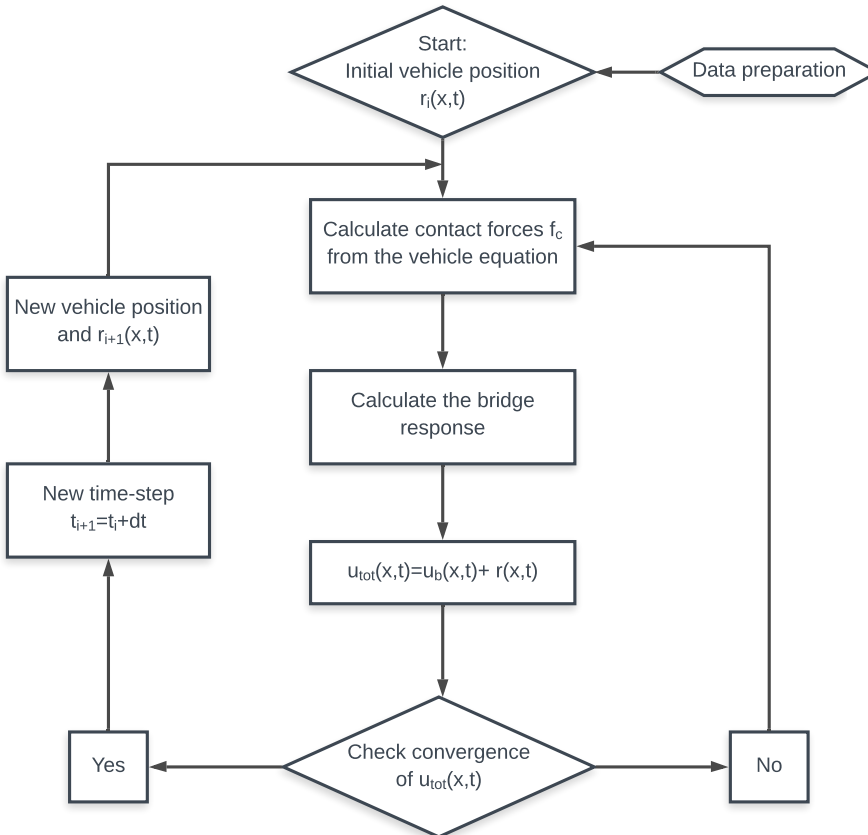


Figure 4.3: Flowchart for the uncoupled equations iterative procedure (Gonzalez 2010).

4.2 Road

An important factor to take into account in the VBI calculations is modelling of the road before the bridge and during the bridge traversal. The following sections provide information of how to simulate surface irregularities and presents requirements of the International Roughness Index (IRI)

in the Swedish road network.

4.2.1 Road irregularities

Road irregularities are usually modeled using Power Spectral Density (PSD) functions. The functions represent a statistical variation of displacements as a function of (angular) spatial frequency or wavelength. Irregularities shall be modeled according to ISO 8608:2016 when performing computer simulations. The road profiles are classified from A-H in decreasing order of the surface quality. The PSD function can be expressed with the spatial frequency as (ISO 2016):

$$G_d(\Omega) = G_d(\Omega_0) \left(\frac{\Omega}{\Omega_0} \right)^{-w} \quad (4.10)$$

where w is usually set to 2 in order to get a constant velocity PSD. Ω_0 is the reference value of 1 rad/m and Ω is a value set between approximately 0.01 and 100 rad/m. $G_d(\Omega_0)$ is a value between $1 \cdot 10^{-6}$ and $16384 \cdot 10^{-6} \text{ m}^3$, corresponding to road class A and H respectively. By performing an inverse fast Fourier transform (IFFT) the displacements can be expressed as a function of longitudinal position x :

$$r(x) = \sum_{i=1}^N \sqrt{G_d(\Omega_i) \frac{\Delta\Omega}{\pi}} \sin(\Omega_i x - \varphi_i) \quad (4.11)$$

where φ is a random phase shift between 0 and 2π , $\Delta\Omega$ is set to the increment between two points and N is set to the maximum number of increments (Tyan et al. 2009). An example of a PSD function and randomly generated road irregularities for a road surface of class A can be seen in Figure 4.4.

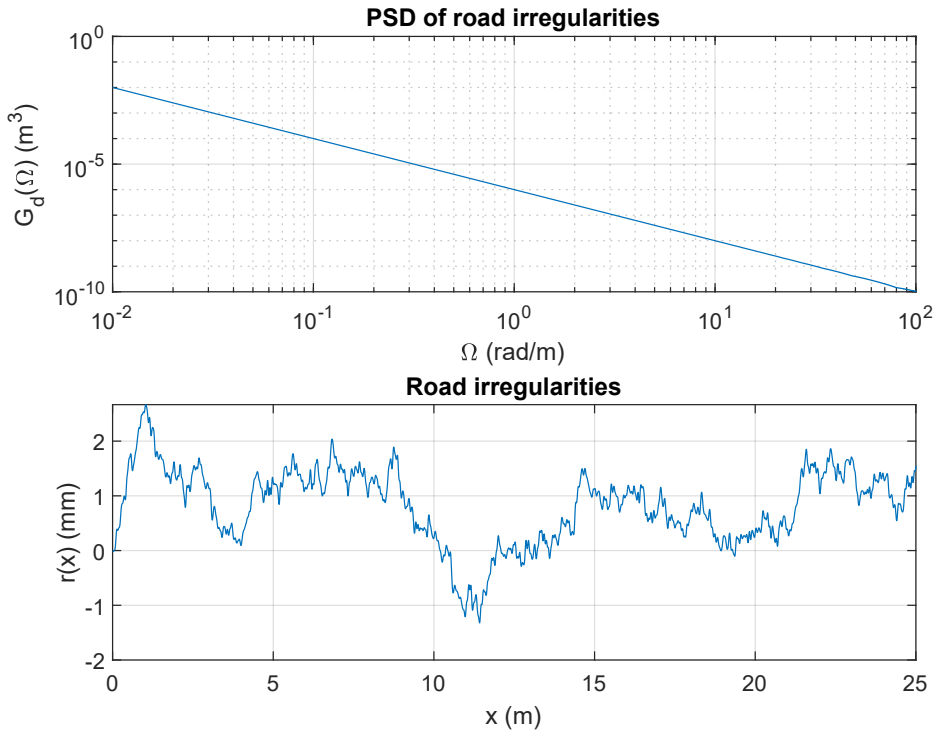


Figure 4.4: Example of a class A road surface. Top: PSD function. Bottom: Road irregularities.

4.2.2 Swedish road network

The Swedish road network has requirements on the International Roughness Index (IRI), which is a measurement of road irregularities measured in mm/m. It is measured as a mean value of the vertical profile over a distance of at least 100 m and is measured in the right wheel track. Requirements are based on the traffic flow and speed limit, and is presented in Table 4.1 (Trafikverket 2012).

Table 4.1: Requirements of IRI (mm/m) according to Trafikverket (2012).

Traffic (vehicles/day)	Speed limit (km/h)							
	120	110	100	90	80	70	60	50
0-250		≤ 4.3	≤ 4.7	≤ 5.2	≤ 5.9	≤ 6.7	≤ 6.7	≤ 6.7
250-500		≤ 4.0	≤ 4.4	≤ 4.9	≤ 5.5	≤ 6.3	≤ 6.3	≤ 6.3
500-1000		≤ 3.7	≤ 4.1	≤ 4.5	≤ 5.1	≤ 5.8	≤ 5.8	≤ 5.8
1000-2000		≤ 3.0	≤ 3.3	≤ 3.7	≤ 4.2	≤ 4.8	≤ 5.2	≤ 5.2
2000-4000	≤ 2.4	≤ 2.6	≤ 2.9	≤ 3.2	≤ 3.6	≤ 4.1	≤ 4.9	≤ 4.9
4000-8000	≤ 2.4	≤ 2.6	≤ 2.9	≤ 3.2	≤ 3.6	≤ 4.1	≤ 4.9	≤ 4.9
>8000	≤ 2.4	≤ 2.6	≤ 2.9	≤ 3.2	≤ 3.6	≤ 4.1	≤ 4.9	≤ 4.9

4.2.3 Road modeling

The road can be modeled as an Euler-Bernoulli or Timoshenko beam resting on a linear or non-linear elastic or viscoelastic Pasternak or Winkler foundation. These types of models are used when determining the load effect on roads to get an accurate model that coincides with experimental results and for evaluating road damage (S. Yang, Chen, and Li 2015). When analyzing the VBI such models are computationally non-efficient and is not necessary for the bridge evaluation.

In order to obtain a computationally efficient and dynamic response of the vehicle before the bridge, a distance with road irregularities can be simulated. The studies by Mohammed, Gonzalez, and Cantero (2018) and Hester and Arturo González (2015) both simulate 100 m of road irregularities before the vehicle reaches the bridge when evaluating the response of heavy vehicles on short-span highway bridges. In the study by Mohammed, Gonzalez, and Cantero (2018) troughs are also modelled which simulates the dynamic effect of protruding expansion joints. In this thesis only surface irregularities before the bridge is taken into consideration, see Figure 4.5.

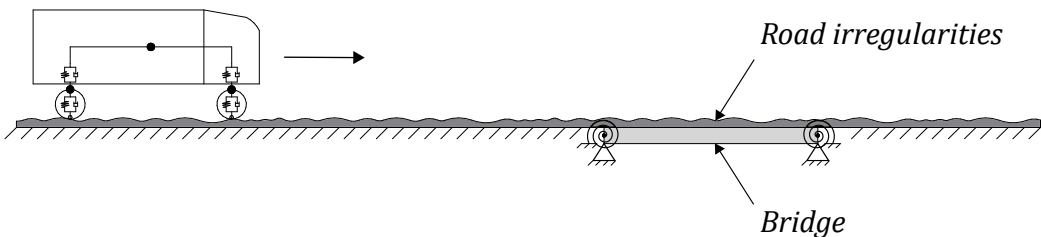


Figure 4.5: Simulated road irregularities (highly exaggerated) before the vehicle reaches the bridge.

4.3 Bridge

The following sections describes considerations for bridges such as eigenfrequencies, resonance and cancellation.

4.3.1 Eigenfrequencies

The eigenfrequencies, f_n , of a bridge depends on its bending stiffness EI (Nm^2), length L (m) and mass per unit length m (kg/m). For a simply supported beam or continuous beam with equivalent span length the eigenfrequencies can be determined as (Y. B. Yang, J. D. Yau, and Wu 2004):

$$\omega_n = \frac{n^2\pi^2}{L^2} \sqrt{\frac{EI}{m}} \quad \text{and} \quad f_n = \frac{\omega_n}{2\pi} \quad (4.12)$$

A study made by the RILEM Committee 65 MDB of 200 European bridges gives an expression for the fundamental frequency as $f_1 = 82L^{-0.9}$, see Figure 4.6, where L is the length of the largest span (Paultre, Chaallal, and Proulx 1992). Studies made by Cantieni (1983) shows similar relationships such as $f_1 = 95.4L^{-0.9}$. Similar studies can be found in other literature such as Jung, G. Kim, and Park (2013).

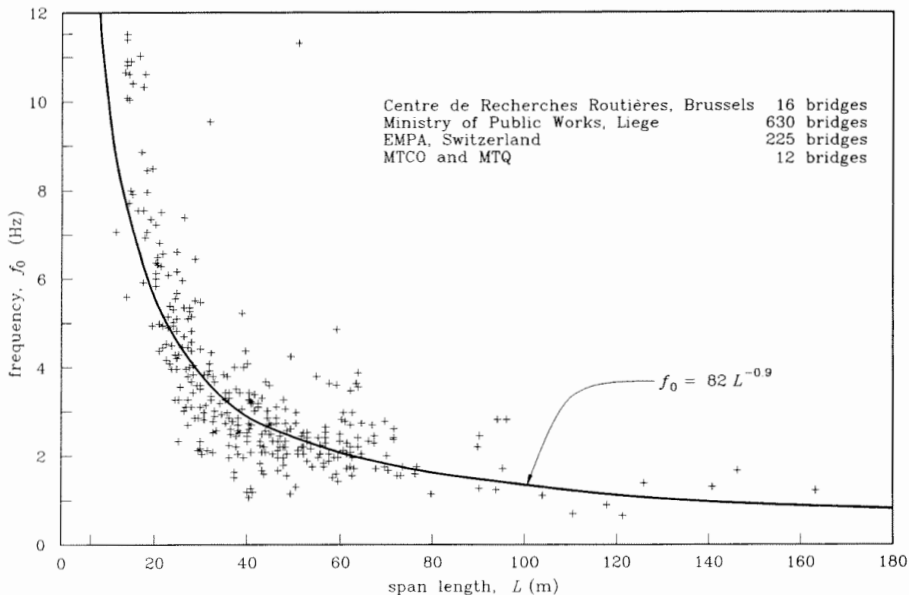


Figure 4.6: The fundamental frequency as a function of the maximum span length according to a study by Paultre, Chaallal, and Proulx (1992).

Several parameters can change f_n such as temperature, relative humidity, creep and cracks in concrete structures (Hester and Arturo González 2015), and an additional mass added to the bridge such as a heavy vehicle. Figure 4.7 show the change in frequency when a vehicle is traversing a bridge in the study by Cantero, Arvidsson, et al. (2016). It is shown that adding mass lowers the frequency, which can be verified by analyzing equation 4.12. f_n will therefore change substantially if the vehicle to bridge mass ratio, m_v/m_b , is large. This is shown in Figure 4.8. Recent studies also shows that f_n changes depending on the fundamental frequency of the vehicle traversing the bridge. The eigenmodes also change in this case (Cantero, Patrick McGetrick, et al. 2019).

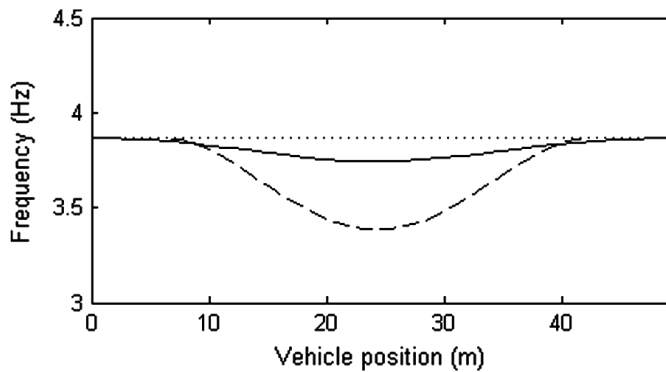


Figure 4.7: The change in frequency depending on vehicle position on a train bridge (Cantero, Arvidsson, et al. 2016). Dotted line: No vehicle. Solid line: Vehicle. Dashed line: Approximate expression according to Frýba (1996).

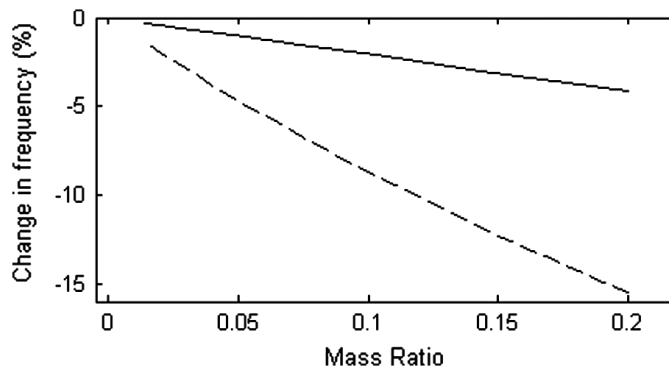


Figure 4.8: The change in frequency depending on the vehicle to bridge mass ratio (Cantero, Arvidsson, et al. 2016). Solid: Coupled VBI. Dashed line: Approximate expression according to Frýba (1996).

4.3.2 Resonance

Having determined the fundamental frequency, i.e. the first frequency f_1 , for a beam it is possible to determine the speeds of the vehicle that create resonance with the function:

$$v_{res} = \frac{f_1 L_v}{i} \quad \text{for} \quad i = 1, \dots, \infty \quad (4.13)$$

where L_v is the length between the axles of the vehicle (Johansson, Pacoste, and R. Karoumi 2013). The same applies for a succession of vehicles traversing the beam at equal distance. The resonance effect is higher for lower modes than higher modes. Derivations to retrieve the formula can be found in Y. B. Yang, J. D. Yau, and Wu (2004).

4.3.3 Cancellation

The opposite effect of resonance is the phenomena of cancellation. The formula for a simply supported beam can be expressed as:

$$v_{canc} = \frac{2f_1 L_v}{(2i - 1)} \quad \text{for} \quad i = 1, \dots, \infty \quad (4.14)$$

where f_1 is the first eigenfrequency of the beam and L_v is the length between the axles of the vehicle. The derivations of the formula can be found in Y. B. Yang, J. D. Yau, and Wu (2004).

4.4 Vehicles

The following sections describe vehicle dynamics, suspension and presents the vehicle models and properties used during the simulations.

4.4.1 Vehicle dynamics

Motions that are included for a regular two axle car/truck in vehicle dynamics are (Guglielmino et al. 2008):

- Vertical translations:
 - Bounce and wheel hop.
- Horizontal translations:

- Longitudinal forward and backward motion.
- Lateral side-slip.
- Rotational motions:
 - Pitch, roll and yaw.

This thesis focuses on a 2D-model of the VBI and the vehicle velocity is constant. The motions that are included are therefore only vertical translations and pitch. The response varies due to suspension properties, mass distribution and geometry of the vehicle (Jacobsson n.d.). The motions for a regular two axle car/truck can be seen in Figure 4.9 and 4.10. Typical heavy trucks have frequencies between 1-3 Hz and light trucks fall within the range of 2-5 Hz (Gonzalez 2010).

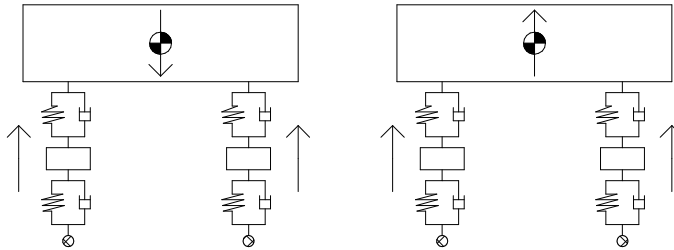


Figure 4.9: Left: Wheel hop. Right: Bounce.

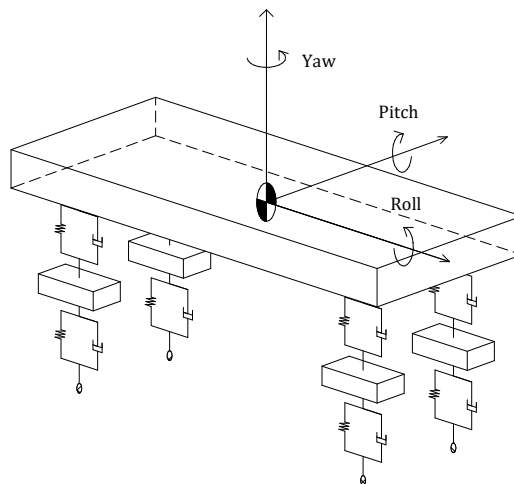


Figure 4.10: Rotational motions.

4.4.2 Suspension

Suspension types that exist are passive, semi-active and active suspensions, see Figure 4.11. This thesis only includes passive suspension but the following sections describe the principles for each suspension system further.

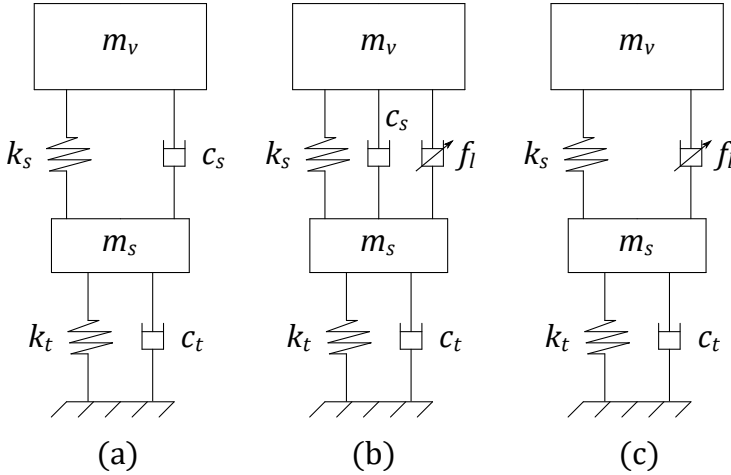


Figure 4.11: (a) Passive suspension. (b) Semi-active suspension. (c) Active suspension. m_v and m_s denotes the vehicle and suspension mass. k_s and c_s denotes the suspension stiffness and viscous damping. k_t and c_t denotes the tire stiffness and viscous damping. f_l is the active or semi-active damping (Kashem, Ektesabi, and Nagarajah 2018).

Passive suspension

A passive suspension contains a spring, a damper (viscous, viscoelastic or friction shock-absorbers) and anti-roll bars (cancels out roll motion) that connects tires to the vehicle body. Springs used for vehicles include steel coils as well as air and leaf springs, where leaf springs are typically stiffer than air springs (Guglielmino et al. 2008). Passive indicates that no energy is added to the system. Soft springs gives better ride characteristics, whereas a stiffer spring gives better road handling. In order to achieve both characteristics a combination is desirable; which can be achieved with active and semi-active suspension (Kashem, Ektesabi, and Nagarajah 2018).

Active and semi-active suspension

Vehicle suspension optimization such as active and semi-active suspension gives better ride comfort and induces less damage to the road. This is especially important for heavy trucks that contribute far more to road damage

than lighter vehicles (Guglielmino et al. 2008). When a suspension is electronically controlled the terms active and semi-active suspension is applied. The output data for the vehicle response can be body acceleration (ride comfort) and tire deflection (road handling). Active suspension uses an energy input, such as viscous flow, into the suspension whereas semi-active suspension is entirely electronically controlled which changes the damping ratio appropriately (Sergio M. Savaresi et 2010). The essence is to have a controllable damper which gives a non-linear response in order to control the vehicle dynamics (Guglielmino et al. 2008).

4.4.3 Vehicle models

Four types of trucks are described in the following sections. The name of the truck vehicle model is based on the amount of bodies and axles the model consists of as:

$$\text{Truck} + \text{No. of axles body 1} + \dots + \text{No. of axles of body } i \quad (4.15)$$

Studies have shown that neglecting the unsprung mass, i.e. the wheel, gives almost the same response as adding mass to the wheel during simulations (Jacobsson n.d.). In this thesis the wheel mass is included in the suspension mass and the Coriolis effect, i.e. the effect of a rotating body, is included in the derivation of the coupled solution, see section 4.1.2. Since no acceleration in the longitudinal direction is considered, only vertical and rotational motions are included.

Truck 2

A common truck is the vehicle model shown in Figure 4.12 and has been used in numerous studies such as Arturo González, O'Brien, and P. McGetrick (2010) and Patrick McGetrick et al. (2013). The vehicle consists of a rigid body with a front and rear axle. The rigid body has a mass, m_S , and rotational moment of inertia, I_S , and has two motions; vertical translation, y_S , and pitch, θ_S . The body is connected to suspension units. The suspension and tires are modeled as spring-dashpot units with stiffness, $k_{s,i}$ and $k_{t,i}$, and viscous damping, $c_{s,i}$ and $c_{t,i}$. The axle and wheel mass are lumped together, m_i , and has vertical translation, y_i .

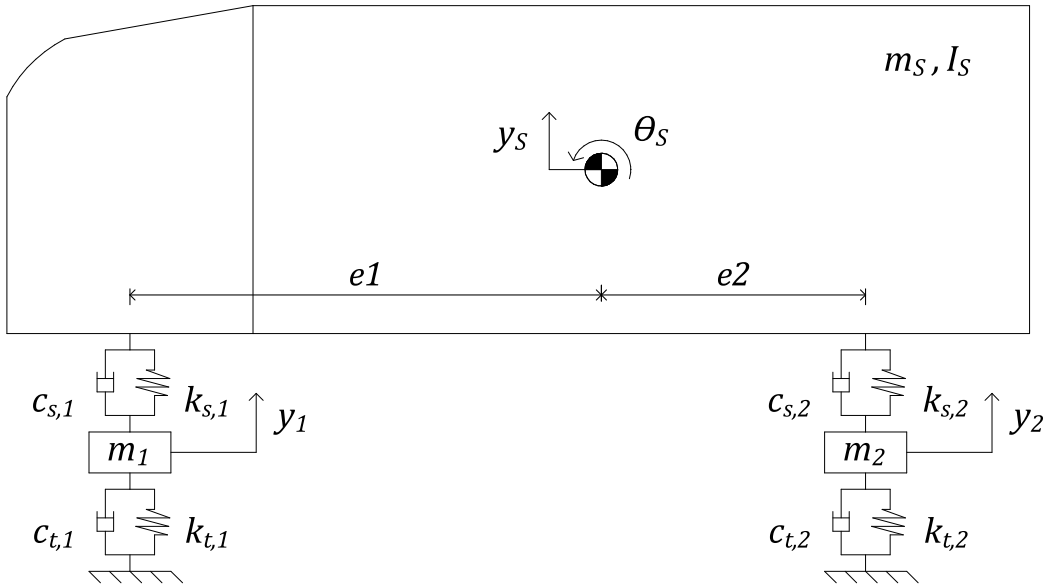


Figure 4.12: Vehicle model Truck 2.

Truck 2-3 and 3-3

Two of the most common trucks on European roads are shown in Figure 4.13 and 4.14. Numerous studies have been made with Truck 2-3 such as Harris, E.J. O'Brien, and A. González (2007) and Cantero, Gonzalez, and Eugene O'Brien (2011). The vehicle consists of two rigid bodies that connect to the suspension units, tractor and semi-trailer with mass m_T and m_S respectively. Both bodies have pitch motion, θ_S and θ_T , and vertical translation, y_S and y_T . The pitch motions include rotational moment of inertia, I_T and I_S . The trailer connection on the truck is modelled as a hinge without friction, and the vehicle model is usually said to be "articulated" when a trailer is hitched to the tractor (Cantero, Gonzalez, and Eugene O'Brien 2011). The suspension and tires are modeled as spring-dashpot units with stiffness, $k_{s,i}$ and $k_{t,i}$ and viscous damping $c_{s,i}$ and $c_{t,i}$. The axle and wheel mass are lumped together, m_i , and has vertical translation, y_i .

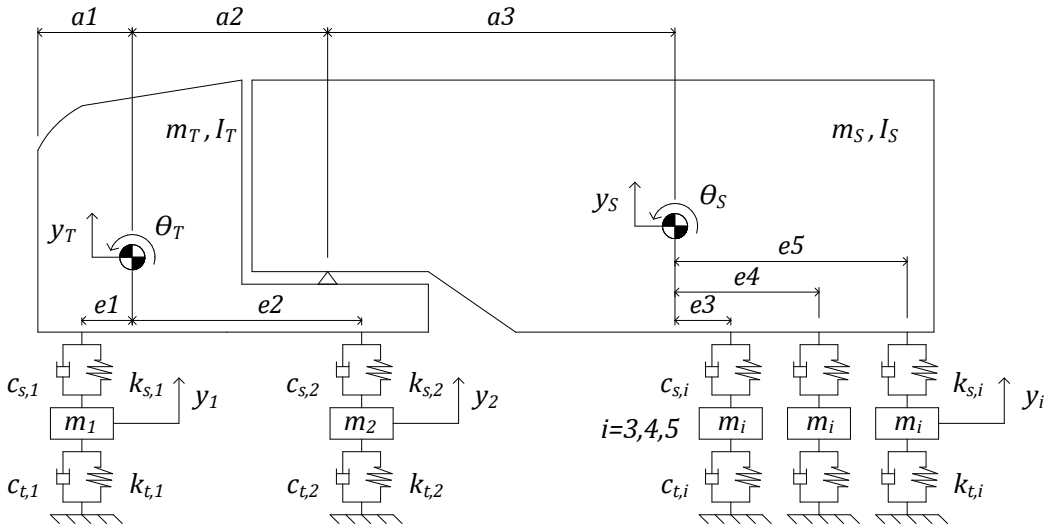


Figure 4.13: Vehicle model Truck 2-3. Standard European truck with a tractor and semi-trailer.

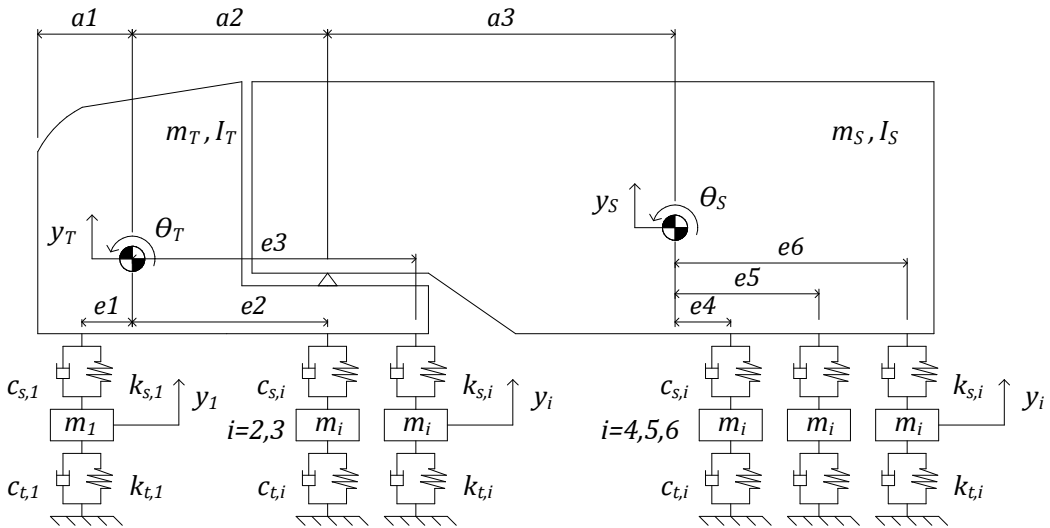


Figure 4.14: Vehicle model Truck 3-3. Standard European truck with a tractor and semi-trailer.

Truck 3-3-3

In order to retrieve a vehicle model to study the effects of a heavier truck, the vehicle model Truck 3-3-3 in Figure 4.15 is used. The truck is similar to Truck 3-3 and the only difference is that another semi-trailer is added to the configuration.

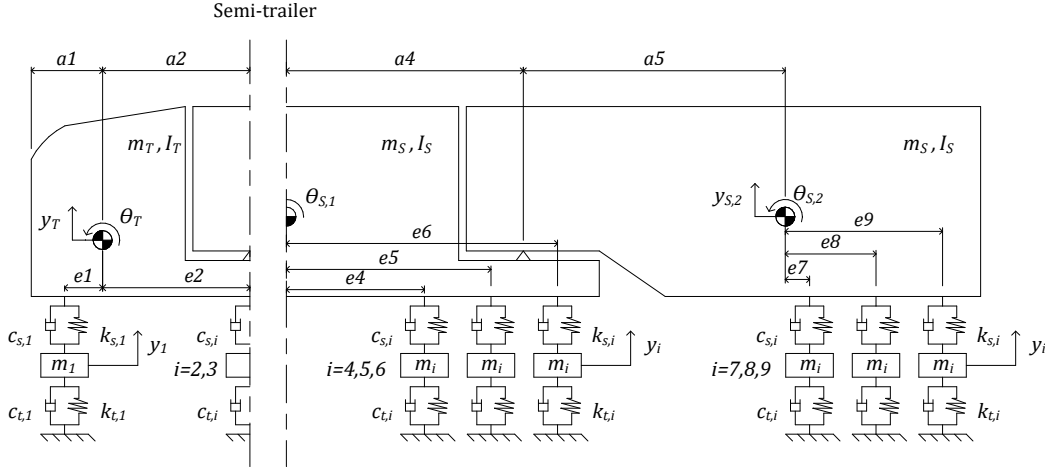


Figure 4.15: Vehicle model of Truck 3-3-3.

4.4.4 Vehicle properties

The vehicle properties for Truck 2 can be seen in Table 4.2 and the properties for Truck 2-3, 3-3 and 3-3-3 can be seen in Table 4.3. Both air and leaf suspension is retrieved in order to study the difference of the DAF. The vehicle properties and geometric data for the vehicle models is obtained from previous studies made by Cantero, Gonzalez, and Eugene OBrien (2011), Harris, E.J. OBrien, and A. González (2007), Mohammed, Gonzalez, and Cantero (2018) and Arturo González, O'Brien, and P. McGetrick (2010) and Patrick McGetrick et al. (2013).

The tire stiffness for the semi-trailer and tractor rear wheels for the vehicles are twice as large since they usually have a double wheel configuration (Cantero, Gonzalez, and Eugene OBrien 2011). The properties and geometry for the second trailer in the Truck 3-3-3 model is assumed to be the same as for the first trailer. The geometric data can be seen in Table 4.4. Assumptions for the geometric data of the second and third wheel position on the tractor for Truck 3-3 is based on existing data for Truck 2-3. The midpoint between the two wheels are set to the second wheel position of Truck 2-3, i.e. e_2 , and the wheels are assumed to be 1.1 m apart, the same as for the semi-trailer wheels.

Table 4.2: Vehicle properties for Truck 2. ¹ Center of gravity.

Parameters		Notation	Value
Mass parameters (kg)	Body mass	m_S	16600
	Axle mass, front	m_1	700
	Axle mass, rear	m_2	700
Inertia parameters (kg m ²)	Body pitch moment of inertia	I_S	64598
	Suspension parameters		
Leaf suspension stiffness (kN/m)	Front	$k_{s,1}$	400
	Rear	$k_{s,2}$	1000
Air suspension stiffness (kN/m)	Front	$k_{s,1}$	400
	Rear	$k_{s,2}$	400
Suspension viscous damping (kNs/m)	Front	$c_{s,1}$	10
	Rear	$c_{s,2}$	10
Tire parameters			
Tire stiffness (kN/m)	Front	$k_{t,1}$	1750
	Rear	$k_{t,2}$	3500
Tire viscous damping (kNs/m)	Front	$c_{t,1}$	6
	Rear	$c_{t,2}$	6
Distance from axle to C.O.G ¹ (m)	Front	e_1	1.875
	Rear	e_2	1.875

Table 4.3: Vehicle properties for Truck 2-3, 3-3 and 3-3-3.

Parameters		Notation	Value
Mass parameters (kg)	Tractor mass	m_T	4500
	Trailer mass	m_S	31450
	Tractor axle mass, front	m_1	700
	Tractor axle mass, rear	m_2	m_{2-3} 1100
	Trailer axle mass	m_{3-5}	m_{4-6} 750
Inertia parameters (kg m ²)	Tractor pitch moment of inertia	I_T	4875
	Trailer pitch moment of inertia	I_S	123000
Suspension parameters			
Leaf suspension stiffness (kN/m)	Tractor, front	$k_{s,1}$	400
	Tractor, rear	$k_{s,2}$	$k_{s,2-3}$ 2000
	Trailer	$k_{s,3-5}$	$k_{s,4-6}$ 1500
Air suspension stiffness (kN/m)	Tractor, front	$k_{s,1}$	400
	Tractor, rear	$k_{s,2}$	$k_{s,2-3}$ 1000
	Trailer	$k_{s,3-5}$	$k_{s,4-6}$ 750
Suspension viscous damping (kNs/m)	Tractor, front	$c_{s,1}$	10
	Tractor, rear	$c_{s,2}$	$c_{s,2-3}$ 10
	Trailer	$c_{s,3-5}$	$c_{s,4-6}$ 10
Tire parameters			
Tire stiffness (kN/m)	Tractor, front	$k_{t,1}$	1750
	Tractor, rear	$k_{t,2}$	$k_{t,2-3}$ 3500
	Trailer	$k_{t,3-5}$	$k_{t,4-6}$ 3500
Tire viscous damping (kNs/m)	Tractor, front	$c_{t,1}$	6
	Tractor, rear	$c_{t,2}$	$c_{t,2-3}$ 6
	Trailer	$c_{t,3-5}$	$c_{t,4-6}$ 6

Table 4.4: Geometric data for Truck 2-3, 3-3 and 3-3-3. All values are in metres (m).

Truck	a_1	a_2	a_3	a_4	a_5	e_1	e_2	e_3	e_4	e_5	e_6	e_7	e_8	e_9
2-3	1.50	2.15	4.15	-	-	0.50	2.50	1.30	2.40	3.50	-	-	-	-
3-3	1.50	2.15	4.15	-	-	0.50	1.95	3.05	1.30	2.40	3.50	-	-	-
3-3-3	1.50	2.15	4.15	2.15	4.15	0.50	1.95	3.05	1.30	2.40	3.50	1.30	2.40	3.50

4.4.5 Truck 2: Eigenmodes

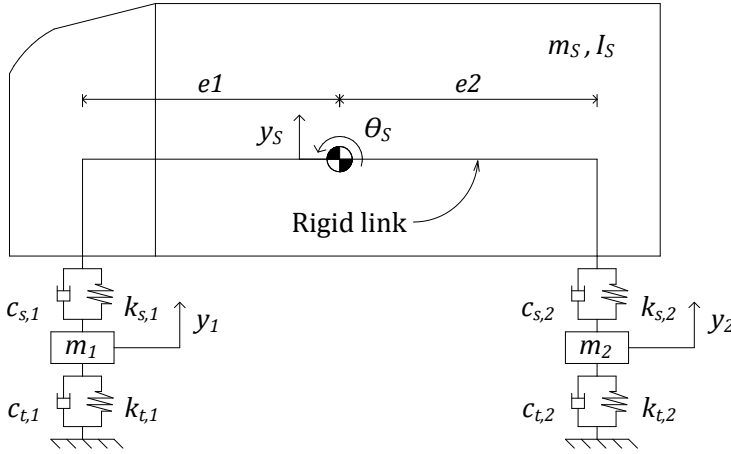


Figure 4.16: Model of Truck 2 illustrating the rigid link connecting the truck body to the suspension units.

A reminder of the vehicle model for Truck 2 can be seen in Figure 4.16. The truck body connects to the suspension units via a rigid link. The vehicle displacement vector, \mathbf{y}_v , is written as:

$$\mathbf{y}_v^T = [y_s \quad \theta_s \quad y_1 \quad y_2]^T \quad (4.16)$$

The vehicle matrices are determined by setting up a force equivalence, i.e. that external and internal (spring and dashpot forces as well as inertia forces) should be equivalent, for the vertical translation DOF's. Since no external forces are present, the internal forces should add up to zero. An example of a force equivalence for y_1 and y_2 is written as:

$$\sum f_i = m_i \ddot{y}_i + k_{s,i}(y_i - y_s) + c_{s,i}(\dot{y}_i - \dot{y}_s) - e_i(k_{s,i}\theta_s + c_{s,i}\dot{\theta}_s) + k_{t,i}y_i + c_{t,i}\dot{y}_i = 0 \quad (4.17)$$

For θ_S a moment equivalence is determined, where the internal forces from the suspension dashpots acting on the truck body should be equal to the body inertial force $I_S\ddot{\theta}_S$. Note that the term e_1 is defined as negative and e_2 is defined as positive relative to the center of the vehicle, i.e. at m_S . In order to retrieve the displacement and velocity at the connection of the rigid link and suspension unit the term e_i is multiplied with θ_S (since it is a right angled triangle) and $\dot{\theta}_S$ (compare with the angular velocity $\omega = v/r$, where v is the velocity at the distance r from the center of a circle). The moment equivalence is written as:

$$\sum M = I_S\ddot{\theta}_S + \sum_{i=1}^2 f_i e_i = I_S\ddot{\theta}_S + \sum_{i=1}^2 e_i [k_{s,i}(y_S - y_i) + c_{s,i}(\dot{y}_S - \dot{y}_i)] + e_i^2 [k_{s,i}\theta_S + c_{s,i}\dot{\theta}_S] = 0 \quad (4.18)$$

The vehicle mass and stiffness matrices, \mathbf{M}_v and \mathbf{K}_v , for Truck 2 is given in equations 4.19 and 4.20. The damping matrix \mathbf{C}_v is identical to \mathbf{K}_v by just changing the stiffness constants $k_{s,i}$ and $k_{t,i}$ to $c_{s,i}$ and $c_{t,i}$.

$$\mathbf{M}_v = \begin{bmatrix} m_S & 0 & 0 & 0 \\ 0 & I_S & 0 & 0 \\ 0 & 0 & m_1 & 0 \\ 0 & 0 & 0 & m_2 \end{bmatrix} \quad (4.19)$$

$$\mathbf{K}_v = \begin{bmatrix} k_{s,1} + k_{s,2} & e_1 k_{s,1} + e_2 k_{s,2} & -k_{s,1} & -k_{s,2} \\ e_1 k_{s,1} + e_2 k_{s,2} & e_1^2 k_{s,1} + e_2^2 k_{s,2} & -e_1 k_{s,1} & -e_2 k_{s,2} \\ -k_{s,1} & -e_1 k_{s,1} & k_{s,1} + k_{t,1} & 0 \\ -k_{s,2} & -e_2 k_{s,1} & 0 & k_{s,2} + k_{t,2} \end{bmatrix} \quad (4.20)$$

By performing an eigenvalue analysis according to section 2.2 the modes and eigenfrequencies can be obtained. The modes for Truck 2 with air suspension can be seen in Figure 4.17. The tire and suspension dashpots are dashed and the rigid link is solid in the figure. The vehicle in an undeformed state is coloured black, whereas the deformed state is coloured red. The modes are not symmetrical due to the tire stiffness being different for $k_{t,1}$ and $k_{t,2}$. The normalized values for the modes can be seen in Table 4.5. As can be seen

mode 1 is a suspension pitch mode, mode 2 is a suspension hop mode whereas mode 3 and 4 are tire hop modes.

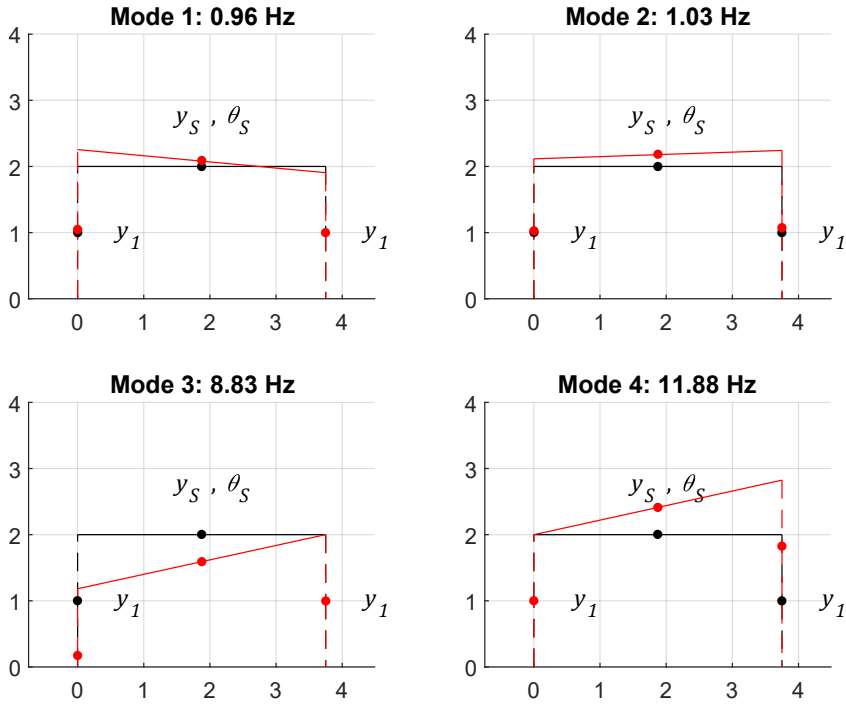


Figure 4.17: Eigenmodes for Truck 2 with air suspension.

Table 4.5: Modes for Truck 2 according to Figure 4.17.

DOF	Mode			
	1	2	3	4
y_S	0.582	0.964	0.008	-0.004
θ_S	-0.723	0.200	-0.004	-0.002
y_1	0.365	0.111	-1.000	0
y_2	-0.080	0.138	0	1.000

If the tire stiffness would be equal for both wheels, i.e. if equation 4.20 would be symmetric, the modes would be symmetrical, see Figure 4.18. Mode 1 would be a suspension pitch mode, mode 2 a suspension hop mode, mode 3 a tire pitch mode and mode 4 a tire hop mode.

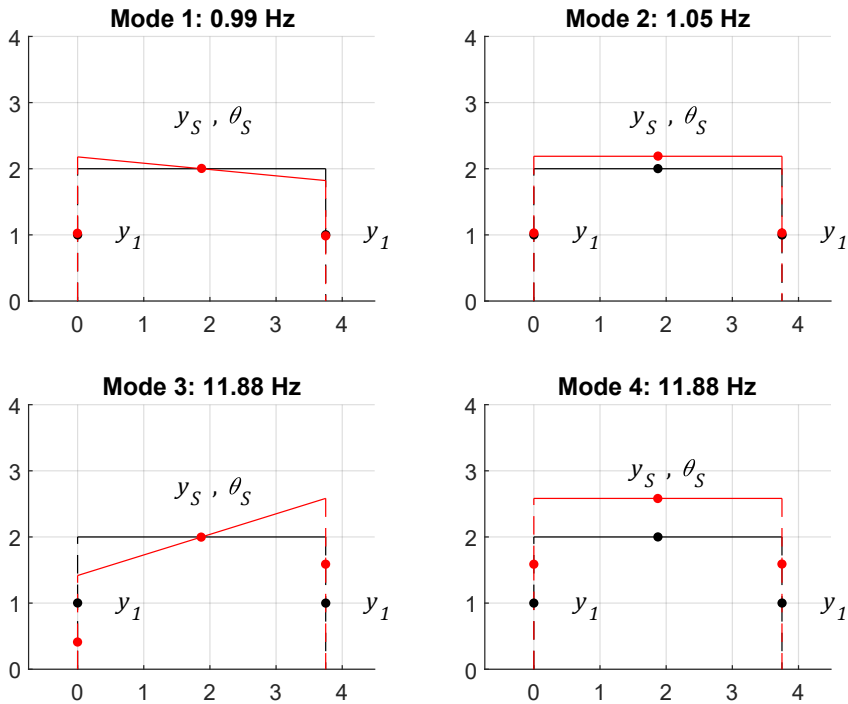


Figure 4.18: Eigenmodes for Truck 2 with a symmetric stiffness matrix \mathbf{K}_v with air suspension.

4.5 Frequency and mass

The DAF depends largely on the frequency ratio between vehicle and bridge, see Figure 4.19. If a vehicle eigenfrequency and bridge fundamental frequency are the same the DAF tends to increase (McLean et al. 1998). The bridge to vehicle mass ratio also affects the DAF largely. A lighter vehicle gives a larger DAF than a heavier vehicle (Ludescher and Brühwiler 2009). The reason being that the static load effect increases faster than the dynamic load when increasing the weight of the vehicle. The maximum DAF is also said to be found at a bridge fundamental frequency at around 2-5 Hz (McLean et al. 1998).

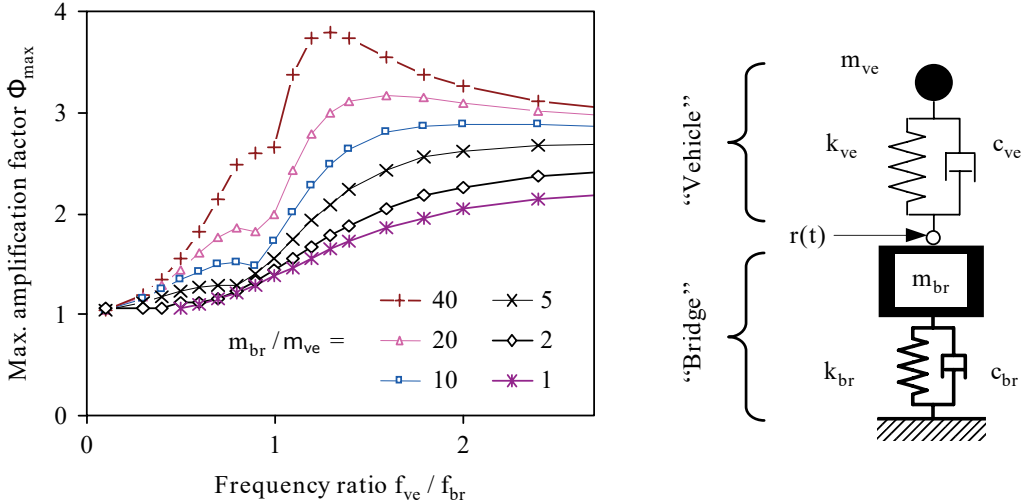


Figure 4.19: Left: The response due to different vehicle to bridge mass and frequency ratios. Right: Modal load model used to produce the plot. (Ludescher and Brühwiler 2009).

4.6 Vehicle events

Previous studies shows that a single truck event gives a higher DAF than multiple trucks crossing the bridge (Zhu and Law 2002). The same is stated in Ghosn et al. (2003) and McLean et al. (1998). The main reason to the lower DAF when several vehicles are traversing the bridge simultaneously is said to be that vehicles are usually out of phase with one another, which cancels out some of the dynamic response.

4.7 Suspension

Several studies have been conducted on the area of suspension type, i.e. leaf and air, and its effect on bridges. The studies include Cantero, Gonzalez, and Eugene OBrien (2011) and Raid Karoumi and Andersson (2006), and both studies show that air suspension with its softer characteristics, see section 4.4.2, induces a smaller load effect on bridges compared to leaf suspension. A figure from the study by Cantero, Gonzalez, and Eugene OBrien (2011) can be seen in Figure 4.20. As can be seen, the DAF tends to be larger when increasing the stiffness of the suspension. Several other papers mentions the same effect such as McLean et al. (1998), Deng et al. (2014), Gonzalez (2010), and Ludescher and Brühwiler (2009). The only time air suspension gives a

larger DAF is when the bridge and vehicle frequencies are the same (McLean et al. 1998).

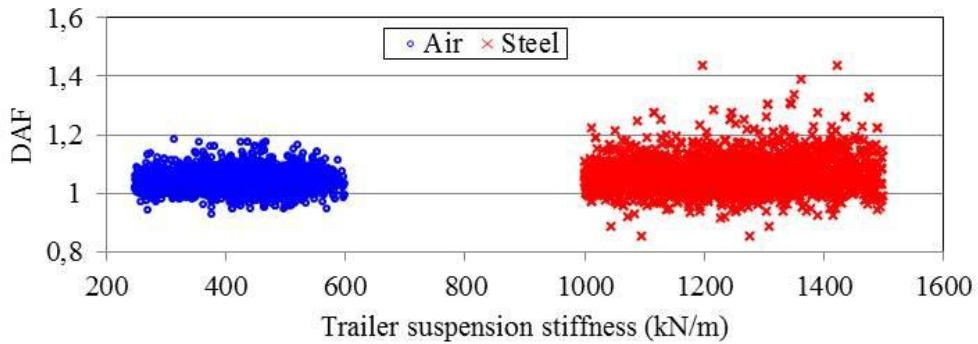


Figure 4.20: A study on the difference between air and leaf suspension in Cantero, Gonzalez, and Eugene OBrien (2011).

Studies made by Bhise et al. (2016) show that a semi-active suspension induce less acceleration of the sprung mass in a quarter-car model. Harris, E.J. OBrien, and A. González (2007) mentions previous studies that have shown that the bridge response is lowered when a vehicle with semi-active suspension, or bridge friendly suspension, is traversing a bridge. Harris also implements a method where the generated road profile is used to find an optimal constant damping coefficient for the vehicle during a bridge passage. This shows that the DAF can be lowered if the road irregularities are known beforehand. The natural frequency of the bridge and vehicle also changes due to a variation of the vehicle properties (Cantero, Patrick McGetrick, et al. 2019).

Chapter 5

Soil-structure interaction

The following sections describe soil-structure interaction where the dynamic stiffness of the soil is presented and descriptions of how it can be modelled with simplified methods.

5.1 Dynamic stiffness

Consideration of the soil surrounding the bridge foundations can provide more accurate results when modelling the VBI. The soil can be modelled in the frequency domain with impedance functions using the dynamic stiffness, $\mathbf{S}(\omega)$. $\mathbf{S}(\omega)$ depends on the shear wave velocity (V_s), Poisson ratio (ν), shear modulus (G) and density (ρ) of the soil. The shear or secondary wave (S-wave) velocity is determined as (Svedholm 2017):

$$V_s = \sqrt{\frac{G}{\rho}} \quad (5.1)$$

The pressure or primary wave (P-wave) velocity is typically faster than the S-wave and is determined as (Sieffert and Cevaer 1995):

$$V_p = \sqrt{\frac{2(1-\nu)}{1-2\nu} \cdot \frac{G}{\rho}} \quad (5.2)$$

$\mathbf{S}(\omega)$ is also highly dependent on the amount of soil layers and the distance to the bedrock. Several motions can be included such as vertical, horizontal,

rocking and torsional motion (Ibsen and Liingaard 2006). A massless foundation resting on an elastic half-space, which represents a homogenous soil strata, can be seen in Figure 5.1 (Svedholm 2017).

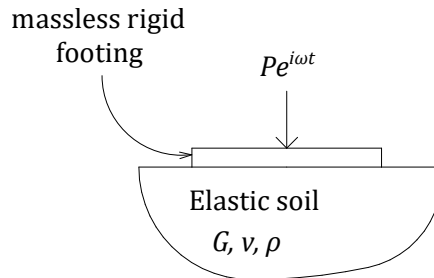


Figure 5.1: A massless footing resting on an elastic half-space.

The reaction forces for the foundation can be expressed as a function of the dynamic stiffness, $\mathbf{S}(\omega)$, and displacements, \mathbf{u} , for a MDOF system as:

$$\mathbf{R}(\omega) = \mathbf{S}(\omega)\mathbf{u} \quad (5.3)$$

where $\mathbf{S}(\omega)$ can be expressed as:

$$\mathbf{S}(\omega) = \mathbf{K}(\omega) + i\omega\mathbf{C}(\omega) \quad (5.4)$$

$\mathbf{S}(\omega)$ can be seen to depend on the frequency dependent stiffness, $\mathbf{K}(\omega)$, and damping, $\mathbf{C}(\omega)$, of the soil (Ibsen and Liingaard 2006). The damping consists of two parts; material and geometrical damping. The material damping consists of energy loss from heat, friction etc. within the material whereas the geometrical damping is attributed to the radiating waves into the soil (Möller et al. 2000). Often times the dimensionless frequency, a_0 , is used instead of the angular frequency ω (Sieffert and Cevaer 1995):

$$a_0 = \frac{\omega r}{V_s} \quad (5.5)$$

where r is the radius of a circular footing or the equivalent radius of a rectangular or square footing. The equivalent radius for a rectangular footing,

with B and L being the width and length of the footing, is set to (Sieffert and Cevaer 1995):

$$r_{eq} = \sqrt{\frac{4BL}{\pi}} \quad (5.6)$$

Since the VBI is determined in the time domain, a frequency dependent stiffness and damping can not be modelled. One solution is therefore to use lumped parameter models which are constructed in order to retrieve an equivalent response (Svedholm 2017). Several other methods exists, such as the boundary element method (BEM) which is used to provide more accurate solutions (Zangeneh Kamali 2018). The simplest way of modelling the soil is with a standard lumped parameter model which consists of a mass and a spring-dashpot, see subfigure (b) in Figure 5.2. To get a more refined result a monkey-tail model can be used where one or several masses and dampers are added (Wolf 1998; Svedholm 2017), see subfigure (c). More advanced configurations of lumped parameter models can be used in order to get even more accurate solutions (Ibsen and Liingaard 2006), see Figure 5.3.

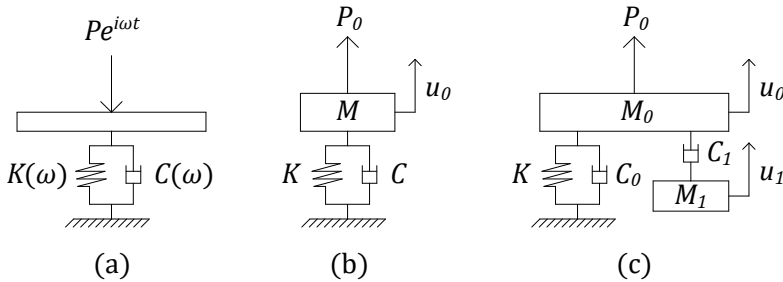


Figure 5.2: A mass-less footing on an elastic half-space. (a) Massless footing with the soil modelled as an impedance function. (b) Standard lumped parameter model. (c) Monkey-tail arrangement.

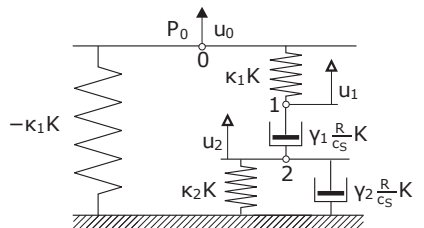


Figure 5.3: An advanced lumped parameter model with two internal degrees of freedom (Ibsen and Liingaard 2006).

5.2 Standard lumped parameter model

The standard lumped parameter model is the easiest way to model the soil and consists of a mass, spring and damper. The model is best used for low frequencies since the deviation from the real behaviour varies for higher frequencies. $S(\omega)$ for the SDOF system can be expressed as:

$$S(\omega) = K - \omega^2 M + i\omega C \quad (5.7)$$

The dynamic stiffness can be expressed in the terms of the dimensionless frequency a_0 as:

$$S(a_0) = K[k(a_0) + ia_0 c(a_0)] \quad (5.8)$$

where $k(a_0)$ and $c(a_0)$ are the dimensionless dynamic stiffness and damping, and K is the static stiffness. The vertical static stiffness for a circular footing resting on a foundation can be set to:

$$K = \frac{4Gr}{1 - \nu} \quad (5.9)$$

The values of the M and C is expressed as a function of the static stiffness as:

$$C = \frac{r}{V_s} \gamma K \quad (5.10)$$

$$M = \frac{r^2}{V_s^2} \mu K \quad (5.11)$$

where γ and μ is set to 0.85 and 0.27 respectively for a mass resting on an elastic half-space, for the case of a circular footing. Inserting the expressions for C and M as well as expressing ω in terms of a_0 in equation 5.7, the dimensionless dynamic stiffness and damping for the single degree of freedom system can be expressed as (Ibsen and Liingaard 2006):

$$k(a_0) = 1 - \mu a_0^2 \quad (5.12)$$

$$c(a_0) = \gamma \quad (5.13)$$

Comparisons of the standard lumped parameter model with solutions presented in Sieffert and Cevaer (1995) for a rectangular footing with ratio L/B of 4 and a Poisson ratio of $1/3$ can be seen in Figure 5.4. γ is in this case set to approximately 1.81 and μ to 0 in order to get a similar response. The damping coefficient $c(a_0)$ increases almost linearly with the ratio L/B (Sieffert and Cevaer 1995), and 1.81 is therefore a safe-sided value to use when the ratio of L/B is higher than 4.

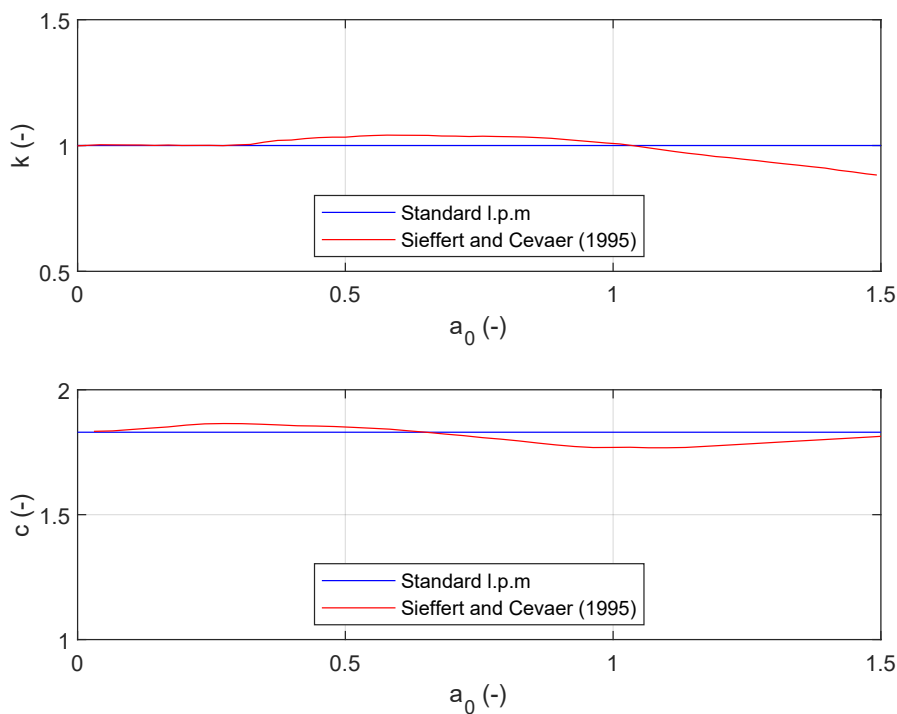


Figure 5.4: Comparisons of the standard lumped parameter model, with coefficients $\gamma = 1.81$ and $\mu = 0$, with the rigorous solution in Sieffert and Cevaer (1995) for a rectangular footing with $L/B = 4$ and $\nu = 1/3$.

Chapter 6

Traffic

The following sections describe the concept of platooning which might induce resonance in bridges. Furthermore, information of how traffic composition can be obtained and how traffic flow can be simulated is presented.

6.1 Platooning

In an effort to reduce emissions from traffic several projects have been ongoing the last couple of years which evaluate the possibility of vehicle platooning. The reduction in emission is largely due to a reduction of wind resistance and a more continuous driving pattern. The reduction in emission when varying the amount of vehicles and the vehicle distance can be seen in Figure 6.1 (Dávila and Nombela 2011). The concept is to have a leader vehicle where other vehicles can connect to the leader via wireless connection. The accompanying vehicles thereafter follow the leader automatically through radar, lidar and camera sensors (NyTeknik 2017). Some projects worth mentioning include SARTRE ¹ (European Commission 2017b) and COMPANION ² which are all commissioned by the European Commission (European Commission 2017a). The concept of platooning is quite far in development and may be present on future roads in 10 years according to NyTeknik (2017).

¹Safe Road Trains for the Environment; developing strategies and technologies to allow vehicle platoons to operate on normal public highways with significant environmental, safety and comfort benefits.

²Cooperative dynamic formation of platoons for safe and energy-optimized goods transportation.

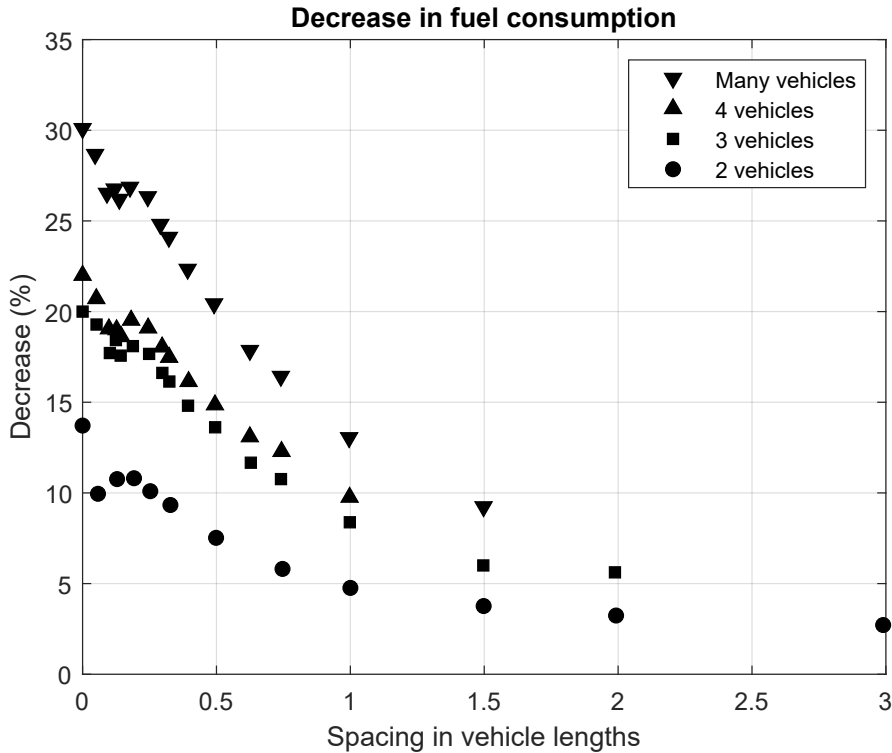


Figure 6.1: Reduction of emission depending on number of vehicles and spacing in a platoon. The figure is reproduced from Dávila and Nombela (2011).

6.1.1 Vehicle distance

The accompanying vehicles all have an approximately equivalent distance between each other. The smaller the distance the more fuel efficiency is guaranteed (Tobar and Martinez 2019). If a car squeezes in between two trucks in a platoon, the distance is doubled between the vehicles (NyTeknik 2017). Since the trucks drive with equal distance, future platoons can induce the phenomena of resonance in bridges, see section 4.3.2, and an evaluation of the DAF to equidistant heavy trucks is therefore relevant. The required distance between vehicles is defined in either seconds or meters between vehicles according to Tobar and Martinez (2019). The distance for platoons was between 1-0.3 s (10-20 m at a speed of 80 km/h) in the ENSEMBLE³ project. In the ETPC⁴ the permitted distance between trucks was set to 0.5 s at the maximum speed limits of 80-90 km/h (Tobar and Martinez

³ENabling Safe Multi-Brand pLatooning for Europe

⁴European Truck Platooning Challenge 2016

2019).

6.2 Traffic

When simulating traffic on bridges some means of generating a statistical flow is necessary. The main method when investigating the traffic flow and load effects on bridges is made by weigh-in-motion (WIM) data collection. This method is the basis to the traffic loads in Eurocode (Grave 2002). To simulate vehicle distances probability density functions (PDF) can be used. In this thesis the shifted exponential distribution is used. The following sections describes these methods further.

6.2.1 WIM measurements

The WIM system uses sensors underneath the bridge which register the bridge strain. From this data several parameters can be gathered such as gross vehicle weight (GVW), axle loads, axle distances, velocities etc. The WIM measurements also give information of type of vehicle as well as percentage of the traffic flow in both directions of the road. The Swedish road administration, Trafikverket (former Vägverket), uses WIM measurements and results from 2004-2005 can be found in Vägverket (2006).

6.2.2 Headway

One main focus when modelling traffic flow is the principle of headway, i.e. the distance between trucks. The distance is defined from the front of the leading vehicle to the front of the following vehicle. One common way to define headway is to use a Poisson distribution. The negative exponential distribution is a PDF of the intervals in time between events and is expressed as (Luttinen 1996):

$$F(t) = \begin{cases} 1 - e^{-\gamma t} & \text{if } t \geq 0 \\ 0 & \text{otherwise} \end{cases} \quad (6.1)$$

This distribution model does not account for a minimum distance between vehicles, and adjustments such as the minimum gap criterion is therefore commonly used. The shifted exponential distribution is expressed as:

$$F(t) = \begin{cases} 1 - e^{-\gamma(t-t_0)} & \text{if } t \geq t_0 \\ 0 & \text{otherwise} \end{cases} \quad (6.2)$$

The function intersects the x -axis at t_0 which is why it is called the shifted exponential distribution and is only valid for $t \geq t_0$. The parameter γ is defined as:

$$\gamma = \frac{Q}{Qt_0 - 1} \quad (6.3)$$

where t_0 (s) is the minimum headway and Q (veh/h) is the traffic flow rate. Other ways to define headway can be achieved with the gamma distribution model, driver behaviour models, the normalized headway model (C. Caprani 2005), log-normal distribution etc. (Luttinen 1996).

Part II

Results

Chapter 7

Verification of VBI

7.1 Toolbox in MATLAB

The toolbox in MATLAB made by Daniel Cantero at NTNU that solves the VBI using the coupled approach is verified with examples from Y. B. Yang, J. D. Yau, and Wu (2004) of a moving force and a moving 1-DOF sprung-mass system. The 1-DOF system is used as a verification of the VBI and the moving force is used as a comparison. The input data can be seen in Table 7.1. Gravity is set to 9.81 m/s^2 . Modelling aspects for the toolbox is described in Chapter 8.

Table 7.1: Beam and vehicle properties for the verification of the MATLAB toolbox.

Beam parameters	Notation	Unit	Value
Length	L	m	25
Mass distribution	m	kg/m	2303
Modulus of elasticity	E	GPa	2.87
Area	A	m^2	1
Second moment of area	I	m^4	2.9
Damping	ζ	%	0
Vehicle parameters	Notation	Unit	Value
Sprung mass	M_v	kg	5750
Spring stiffness	k_v	kN/m	1595
Speed	v	km/h	100

The MATLAB model has 100 beam elements and the time-step is set to 10^{-3} s. The sprung-mass deflection in Y. B. Yang, J. D. Yau, and Wu (2004) is

obtained digitally from a graph, whereas the deflection from the moving force is solved analytically using only the first mode of vibration ($n = 1$) in the expression:

$$u(x, t) = \frac{2pL}{EI\pi^4} \sum_{n=1}^{\infty} \frac{1}{n^4} \sin \frac{n\pi x}{L} \left(\frac{\sin \Omega_n t - S_n \sin \omega_n t}{1 - S_n^2} \right) \quad (7.1)$$

where p is the moving force, ω_n is determined according to equation 4.12 and $x = L/2$. The parameters Ω_n and S_n are expressed as:

$$\left\{ \begin{array}{l} \Omega_n = \frac{n\pi v}{L} \\ S_n = \frac{\Omega_n}{\omega_n} \end{array} \right. \quad (7.2a)$$

$$\left\{ \begin{array}{l} \Omega_n = \frac{n\pi v}{L} \\ S_n = \frac{\Omega_n}{\omega_n} \end{array} \right. \quad (7.2b)$$

The verification of the VBI can be seen in Figure 7.1.

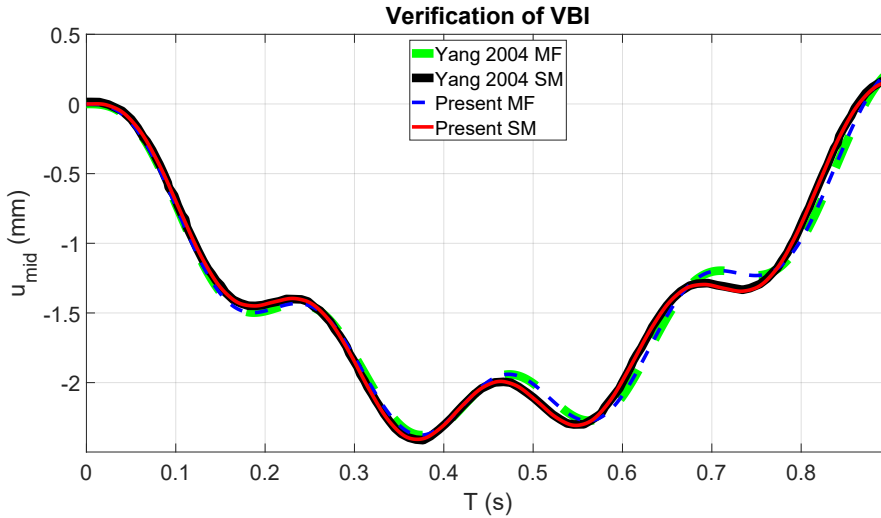


Figure 7.1: Verification of the VBI. The present solutions are compared with examples from Y. B. Yang, J. D. Yau, and Wu (2004). MF: Moving force. SM: Sprung-mass.

Chapter 8

Modelling aspects

The following sections describe the modelling aspects that are used in the MATLAB toolbox during the parameter studies. The aspects include the static systems of the bridges, its properties and appropriate size of the bridge mesh. Simulation aspects such as minimum frequency considered, number of vehicle events, length of a platoon and generated road surfaces is also presented. The retrieval of the maximum DAF is also mentioned.

8.1 Finite element modelling

The finite element modelling of the bridges is made by using Bernoulli beam elements with 4 DOF's; vertical translation and rotation. No horizontal translation is therefore possible. Consistent mass matrices and stiffness matrices according to section 2.7 are used. The damping matrix is based on the Rayleigh method using the first two modes of the bridge and the same damping ratio, ζ , is used for both modes. The values of ζ according to Table 8.3 are used. The Newmark- β iteration scheme is performed according to section 2.6 during the solution of the coupled equations.

8.2 Maximum DAF

The DAF is evaluated at the mid-span for bending moment (BM). The largest BM is retrieved and divided by the value of the maximum static BM. The DAF is evaluated at the boundary nodes for shear. The maximum shear force is retrieved and divided by the maximum static shear force. The largest value of the DAF of the two boundary nodes is thereafter determined. See an example of the maximum total and static BM and shear in Figure 8.1.

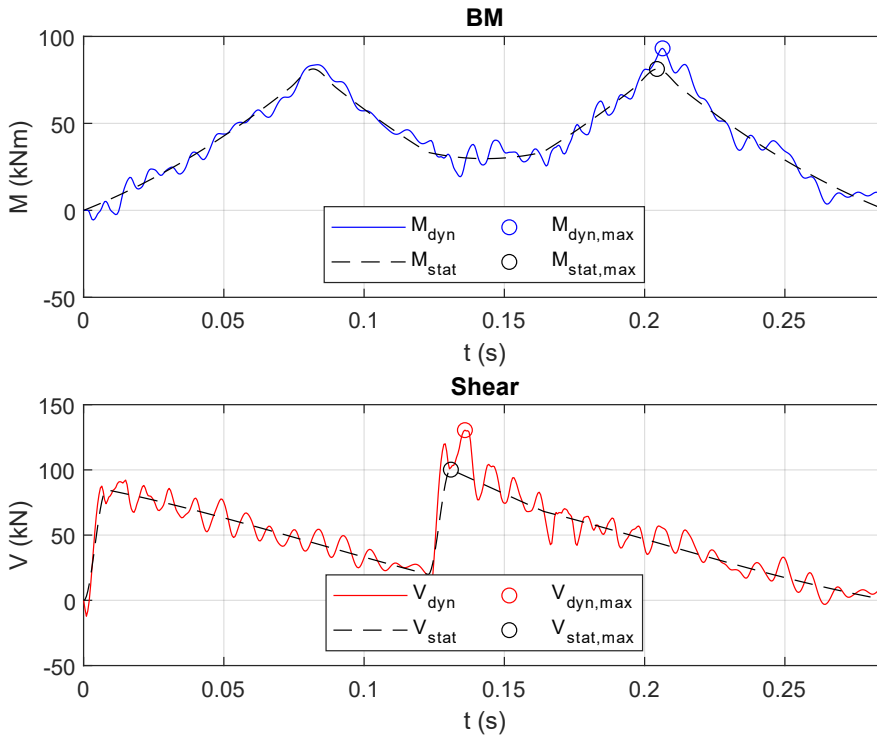


Figure 8.1: Example of the retrieval of the maximum DAF for BM and shear. Both the total (dyn) and static (stat) BM and shear is plotted for a vehicle traversing a bridge.

8.3 Static systems

The following sections describe the static systems of the bridges that are to be analyzed, i.e. slab and integral bridges as well as integral bridges with an incorporated SSI model.

8.3.1 Slab bridge

The static system of the slab bridge can be seen in Figure 8.2 and consists of pin supports at the boundary nodes. No roller support is modelled since horizontal translations are neglected in the MATLAB toolbox.

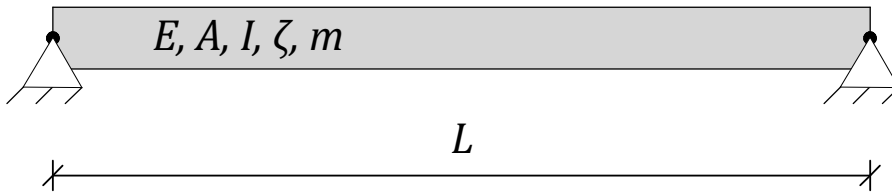


Figure 8.2: Static system for a slab bridge.

8.3.2 Integral bridge

The static system for the integral bridge in the MATLAB toolbox is modelled with pin supports and rotational springs at the boundaries, where $k_r = 4EI/L$ see \mathbf{K}^e in equation 2.20. The rotational mass from the integral legs at the boundary DOF's are also included, where $m_r = 4A\rho L^3/420$ see \mathbf{M}^e in equation 2.19. The vertical stiffness from the integral legs is neglected since the stiffness is quite large and therefore no vertical mass is needed at the boundary nodes. The system can be seen in Figure 8.3.

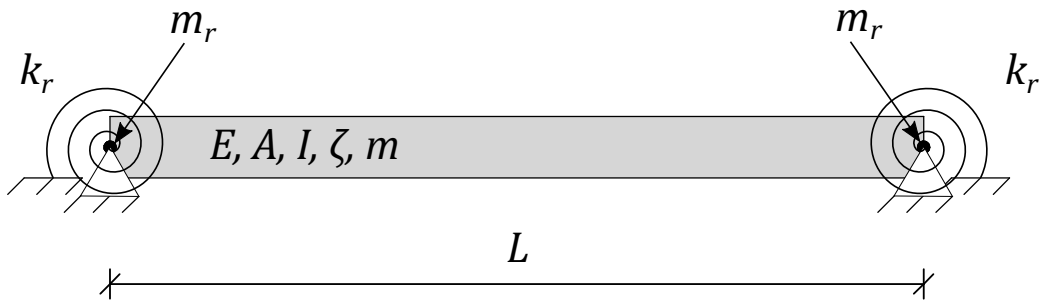


Figure 8.3: Static system for an integral bridge.

In order to study the difference of the DAF when including the influence of the soil, a standard lumped parameter model is modelled at the boundaries, see Figure 8.4. The mass of the integral legs at the boundary DOF's are included, where m_l is the total mass of the integral legs. The mass from the soil, M , is also included as well as the static stiffness, K , and damping, C .

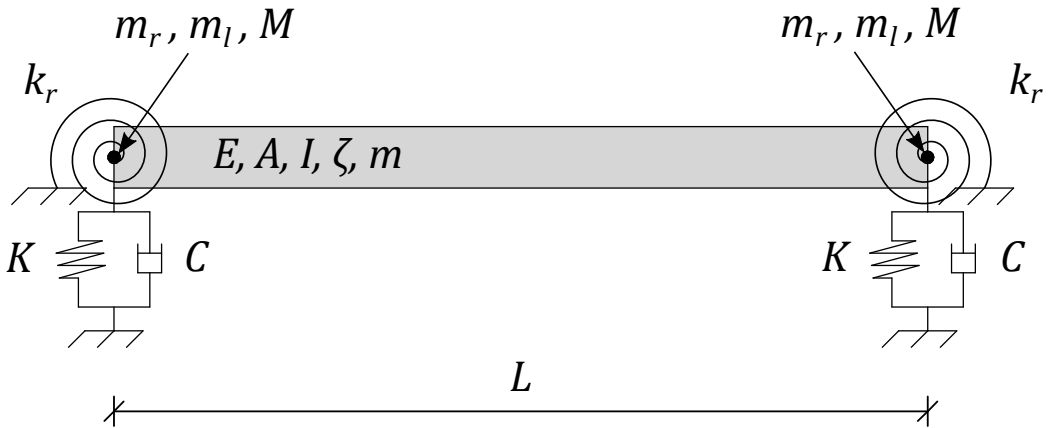


Figure 8.4: Static system for an integral bridge when including the soil.

8.4 Bridge properties

Bridge properties – i.e. length (L), modulus of elasticity (E), area (A) and second moment of area (I) – are gathered from construction drawings provided by ELU Konsult. The material weight is unknown and gathered from literature. The products $A\rho$ and EI are used since these are the only values needed in the matrices in equations 2.19 and 2.20. All of the bridges are of reinforced concrete with pavement and railings. The reinforcement is however neglected and the cross-section is assumed to consist solely of concrete.

8.4.1 Material weight

The assumed weight for the construction material can be seen in Table 8.1. The pavement thickness is not always provided in the drawings and a standard value of 100 mm is set when it is unknown, since this is common value. The railing weight varies depending on the producer and values between 20-40 kg/m can be found in product catalogues from Tibnor (2019) for a standard W-profile. Since a larger value on the mass of the bridge gives a larger DAF during calculations and to take higher railings and median barriers into consideration, the weight is set to 100 kg/m. See Figure 4.19 where the DAF increases when m_b/m_v and f_v/f_b increases.

Table 8.1: Assumed material weight for the bridges. The weight of the concrete is found in Mosley, Hulse, and Bungey (2012) and the weight of the pavement in *Projektarbetet "vägen till vägen"* (n.d.).

Material	Weight
Reinforced concrete	2500 kg/m ³
Pavement	2400 kg/m ³
Railing	100 kg/m

8.4.2 Integral bridge

The parameters for the integral bridges are gathered from the project "Norra länken" in Umeå and for "Road 50" between Motala and Mjölby. The span lengths vary from approximately 5-40 m. Typical cross-sections can be seen in Figure 8.5 and 8.6.

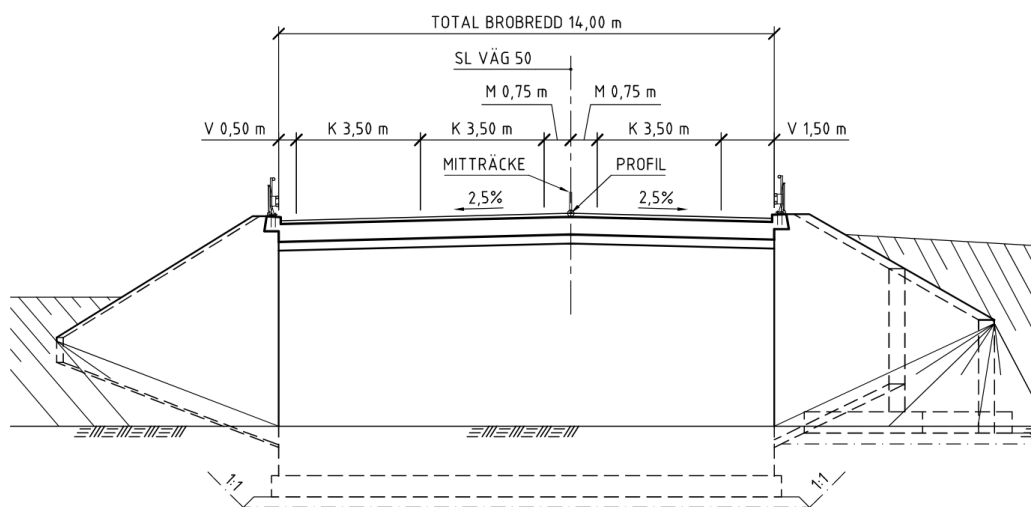


Figure 8.5: Typical example of a cross-section for an integral bridge of 5-25 m.

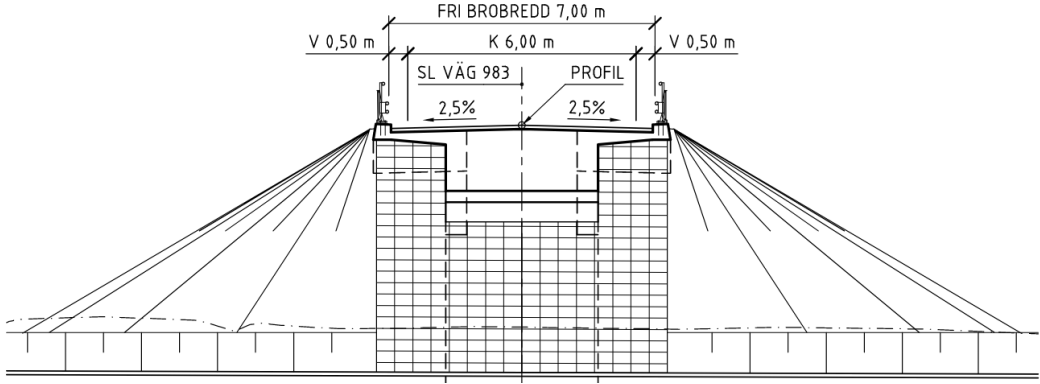


Figure 8.6: Typical example of a cross-section for an integral bridge above 30 m.

Span

The fundamental frequency for the bridges are determined with a FEM analysis using CALFEM (Austrell et al. 2004). Bridge parameters EI and $A\rho$ are used for the beam elements. All translational DOF's at the bridge foundations are assumed to be fixed but rotation is allowed. The length of the beam elements are arbitrarily set to approximately 0.25 m. The data points depending on lane are plotted alongside the fundamental frequency, f_1 , as a function of the bridge length in Figure 8.7. The equation for the fitted curve of f_1 is:

$$f_1(L) = 334.9L^{-1.4} \quad (8.1)$$

The red dashed line is f_1 assuming the bridge to be simply supported which shows that the frequency is higher for the stiffer integral bridge. Note that higher values on EI in equation 4.12, i.e. including the rotational stiffness at the integral legs, gives a stiffer structure and thus larger frequency. The equation for the simply supported case is:

$$f_1(L) = 443.0L^{-1.7} \quad (8.2)$$

The two equations is compared with the study made by the RILEM Committee 65 MDB of 200 European bridges, see section 4.3.1, which states the expression $f_1 = 82L^{-0.9}$, where L is the length of the largest span. The curves can be seen to be quite similar. As can be seen, the fundamental frequency can be well fitted to the integral bridges even if the number of lanes varies.

This is due to the fact that I and A , used in the numerator and denominator when calculating the eigenfrequency in equation 4.12, varies linearly since it is mainly the width b that affects both values.

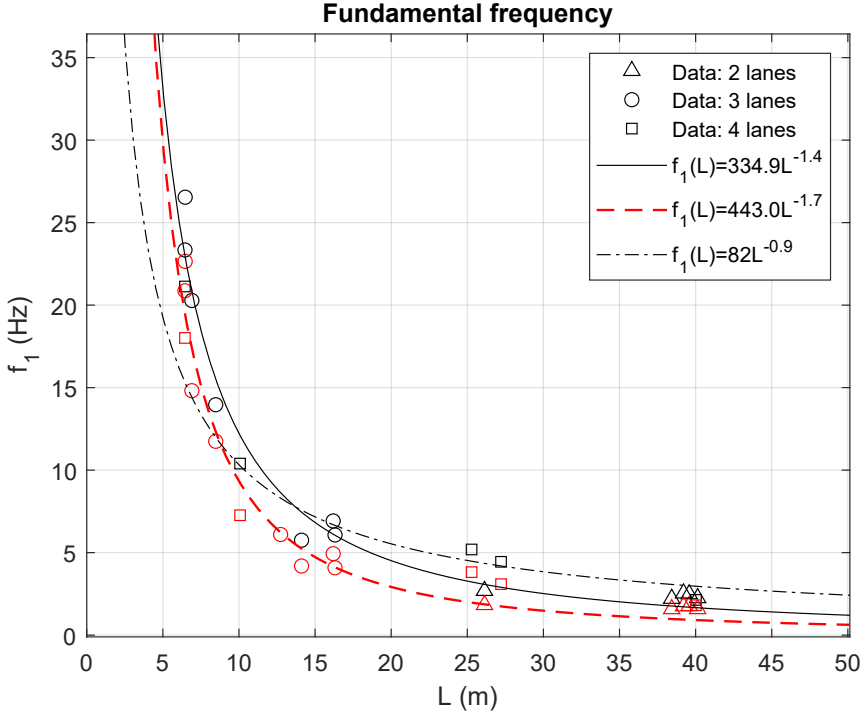


Figure 8.7: The fundamental frequency as a function of the bridge length. The data points are for 2, 3 and 4 lanes. The red line and data points is when assuming the bridge to be simply supported.

In order to use the function in equation 8.1 when extracting values during simulations, an expression that includes the relevant parameters for the fundamental frequency must be determined. This can be achieved by performing a variable analysis of f_1 according to:

$$f_1(L, k, m) = CL^a k^b m^c \quad (8.3)$$

where C is a constant, L is the length, k is the stiffness (EI) and m is the weight per unit length ($A\rho$). Inserting the dimensions of each variable, i.e. k ($\text{kg m}^3/\text{s}^2$), m (kg/m) and L (m) and solving the equality for each dimension

provides a value for the constants a , b and c :

$$\underbrace{f_1}_{s^{-1}} = \underbrace{C}_1 \cdot \underbrace{L^a}_{m^a} \cdot \underbrace{kg^b \cdot m^{3b} \cdot s^{-2b}}_{k^b} \cdot \underbrace{kg^c \cdot m^{-c}}_{m^c} \quad (8.4)$$

$$\begin{cases} -1 = -2b \\ 0 = b + c \\ 0 = a + 3b - c \end{cases} \Rightarrow \begin{cases} b = 0.5 \\ c = -0.5 \\ a = -2 \end{cases} \quad (8.5)$$

Using the solved values from the system of equations in 8.5 and performing a linear regression of the data points f_1 and $(\sqrt{k/m})/L^2$ for the bridges, provides a value of the constant C , see Figure 8.8 where $x = (\sqrt{k/m})/L^2$. The equation can therefore be expressed as (compare with equation 4.12 for a simply supported beam):

$$f_1(L, k, m) = \frac{1.9}{L^2} \sqrt{\frac{k}{m}} \quad (8.6)$$

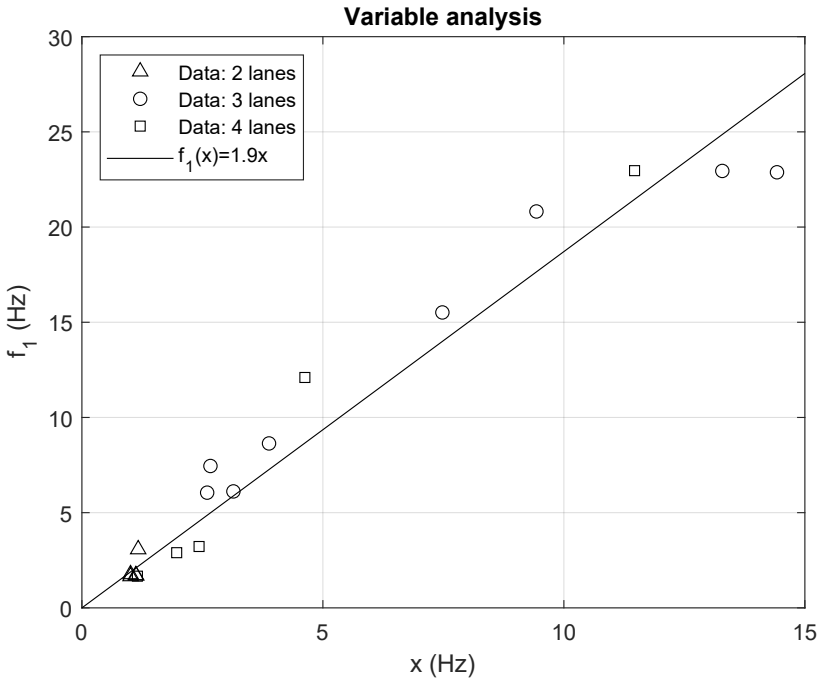


Figure 8.8: Linear regression of the function f_1 for the variable analysis in equation 8.3 in order to retrieve a value on the constant C .

One additional equation is needed in order to determine the parameters during simulations. Analysis shows that an expression for $A\rho(L)$ is best suited, since an approximation for $EI(L)$ can have negative values for short bridge lengths. The curve fitting can be seen in Figure 8.9 and the values for 2 and 3 lanes are multiplied with 2 and $4/3$ respectively in order to fit the data points to the ones for 4 lanes. When the ratio m_b/m_v increases the DAF also increases, see Figure 4.19, which is why 4 lanes is chosen. The thickness of the bridge is assumed to vary much less than the width and it is therefore assumed to be a valid approximation. The curve fitting gives the equation for $m(L)$:

$$m(L) = A\rho(L) = 0.8L + 21.2 \pm 7.8 \text{ t/m} \quad (8.7)$$

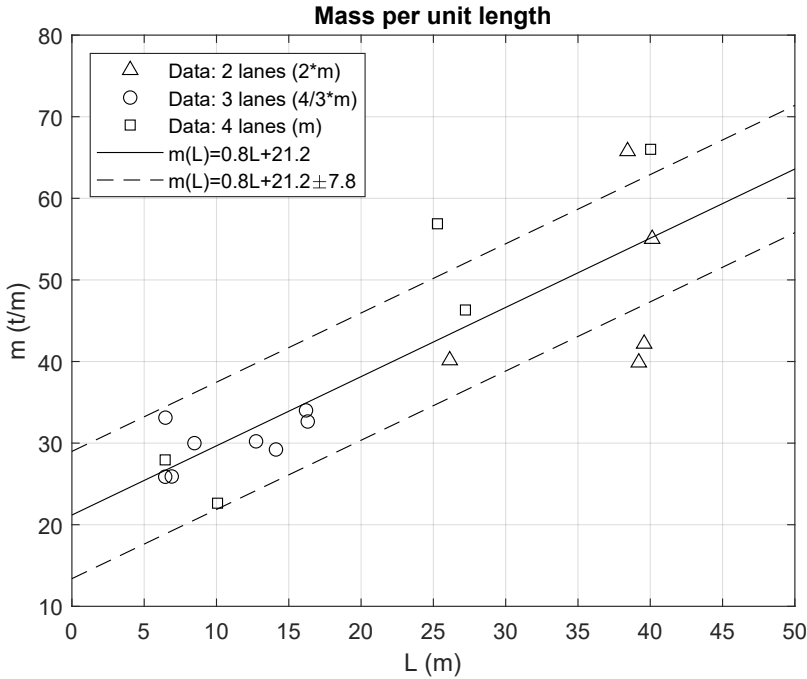


Figure 8.9: Variation of m as a function of the bridge length.

When performing simulations, relevant parameters can be retrieved using the following steps:

1. Determine the fundamental frequency, $f_1(L)$, in equation 8.1.
2. Determine the mass per unit length, $m(L)$, in equation 8.7.

3. Insert $f_1(L)$ and $m(L)$ into equation 8.6 in order to retrieve $k(L)$.

Leg

The rotational stiffness $k_r(L)$ for the integral legs are determined in the same way as for $m(L)$ for the span using curve fitting and the values for 2 and 3 lanes are multiplied with 2 and 4/3 respectively to correspond to 4 lanes. The approximation can be seen in Figure 8.10. The equation for $k_r(L)$ is determined as:

$$k_r(L) = 1.8L - 6.7 \pm 18.5 \text{ GNm} \quad (8.8)$$

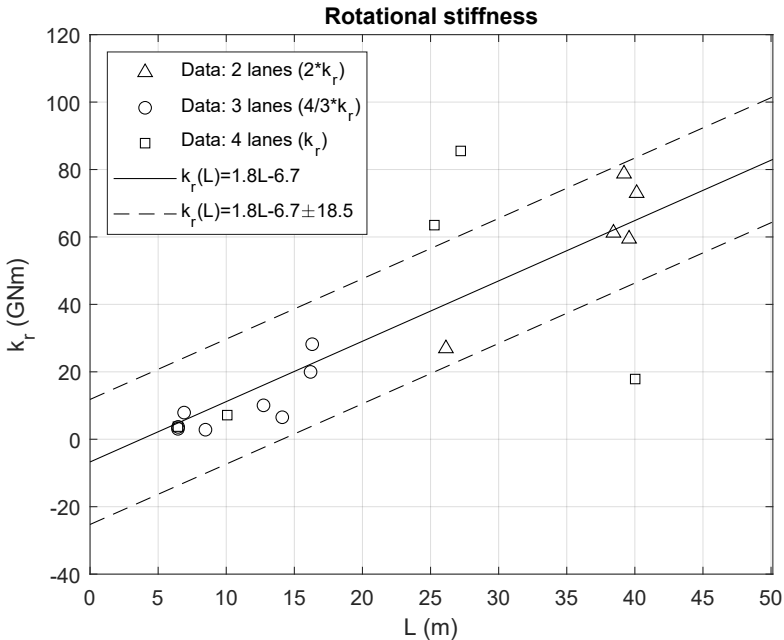


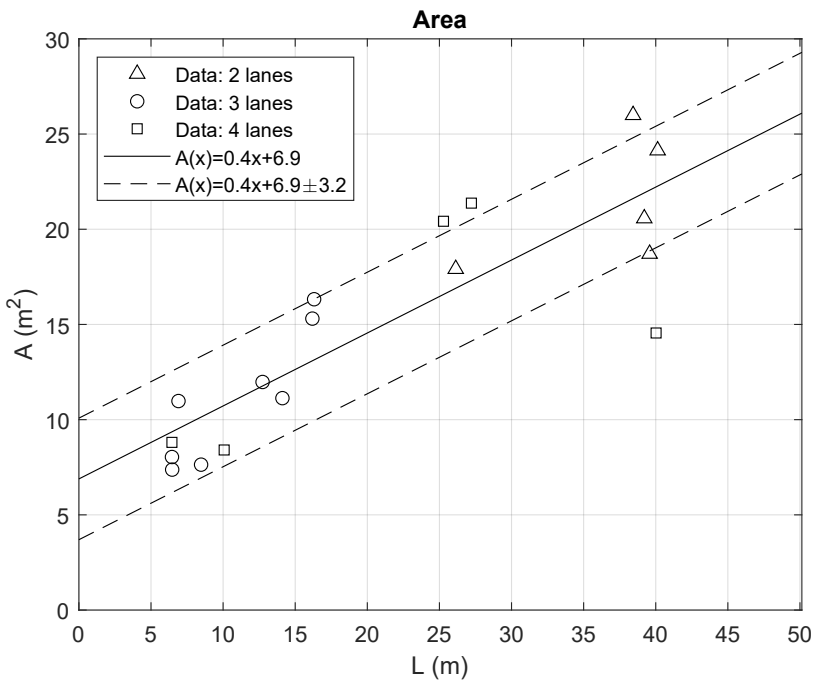
Figure 8.10: Variation of k_r as a function of the bridge length.

The height of the integral legs can not be determined as a function of the bridge length. It varies based on requirements of the free height beneath the bridge. The data of the integral legs are therefore determined as a mean value with a standard deviation, see Table 8.2, in order to retrieve a lower and upper limit on the Swedish DAF, see Table 3.2.

Table 8.2: Mean value and standard deviation for the integral leg length.

Integral leg	
μ (m)	σ (m)
6.0	1.2

In order to retrieve values on the mass of the integral legs, the area as a function of the bridge length is required which can be seen in Figure 8.11. The density of the concrete in Table 8.1 is used.

Figure 8.11: Variation of A as a function of the bridge length.

8.4.3 Slab bridge

The slab bridge parameters are based on the same properties as for the integral bridges as a simplification. However, the parameters are multiplied with a factor of approximately 1.32 for $A\rho$ and 2.32 for EI . This is based on a gross simplification of a point load at the mid-span. By first determining the ratio between the moment for the two bridge types, a relationship between the cross-sectional thickness can be determined and thereafter inserted into

the expression for $A\rho$ and EI for the integral bridges. Determining the transformation of the deck thickness, h , can be seen in equation 8.9.

$$\left\{ \begin{array}{l} M_{ratio} = \frac{M_{slab}}{M_{int}} \\ M = Wf = \frac{bh^2}{6}f \end{array} \right. \Rightarrow h_{slab} \approx h_{int} \sqrt{M_{ratio}} \quad (8.9)$$

8.4.4 Damping

Damping in bridges can be measured experimentally and a study presented in (McLean et al. 1998) of 213 concrete bridges in Switzerland, Great Britain and Belgium with span lengths 10-85 m had an average damping of 7.9 % and lowest value of 2 %. A similar study in McLean et al. (1998) presents values in the range of 2-10 % for concrete bridges.

Eurocode gives general guidelines in terms of approximate damping ratios for different types of bridges, such as pedestrian and train bridges. The damping for bridges is very arbitrary, and safe-sided assumptions is to set the damping ratio to 0 %. The values for train bridges can be set according to guidelines provided by Swedish Standards Institute (2019), see Table 8.3. With a minimum span length of 5 m, see section 8.4, this gives a maximum damping ratio of 2.55 % for bridges made of reinforced concrete, which is close to the lowest value found in McLean et al. (1998). The values in Table 8.3 are therefore assumed to also be applicable for road bridges.

Table 8.3: Damping according to Swedish Standards Institute (2019).

Type of bridge	Damping (%)	
	$L < 20$ m	$L \geq 20$ m
Steel and composite	$\zeta = 0.5 + 0.125(20 - L)$	$\zeta = 0.5$
Pre-stressed concrete	$\zeta = 1.0 + 0.07(20 - L)$	$\zeta = 1.0$
Reinforced concrete	$\zeta = 1.5 + 0.07(20 - L)$	$\zeta = 1.5$

8.5 Soil properties

A parameter study based on the effect of the soil will be made where the purpose is to study the difference on the DAF based on the soil stiffness and damping. Some typical values on S-wave and P-wave velocities, V_s and V_p , as well as the density for various soils is presented in Table 8.4 and 8.5. Some

typical values on the Poisson ratio found in Rajapakse (2008) is presented in Table 8.6.

Table 8.4: P- and S-wave velocities (Möller et al. 2000) and density for various soils (Larsson 2008).

Soil	P-wave (m/s)	S-wave (m/s)	Density (t/m ³)
Saturated moraine	1400-2300	200-700	2.1-2.3
Moraine	700-1500	200-700	2-2.3
Saturated Sand and Gravel	1300-1700	200-400	2-2.2
Sand and Gravel	300-700	200-400	1.8-1.9
Saturated Clay	1300-1600	10-250	1.7
Clay, Silt	400-700	10-250	1.7

Table 8.5: P- and S-wave velocities (Zangeneh Kamali 2018) and density for various soils (Larsson 2008).

Soil	P-wave (m/s)	S-wave (m/s)	Density (t/m ³)
Moraine	1400-2000	300-600	2-2.3
Saturated Sand and Gravel	1400-1800	100-300	2-2.2
Dry Sand and Gravel	500-800	150-350	1.8-1.9
Clay below GW level	1480-1520	40-100	1.7
Organic soils	1480-1520	30-50	1.1-1.4

Table 8.6: Poisson ratio, ν , for various soil types (Rajapakse 2008). ¹ For undrained clay.

Soil	Gravel	Sand	Silt	Clay ¹
ν (-)	0.2-0.4	0.2-0.35	0.3-0.35	0.4-0.5

A study of the difference on the DAF is made for different soils with the upper and lower limits of the soil properties found in Table 8.4 and 8.5. In order to get results with no deviation due to the bridge properties, these are set to the mean values according to section 8.4. Upper and lower values from constructional drawings are used on the foundation dimensions as a width of 2.5 and 0.6, with a constant approximate length of 15 m. The damping is set according to Table 8.3. All vehicle models are used in the analysis and the mean value on the DAF based on all vehicles are gathered. The vehicle speed is set to 100 km/h. Only moraine as well as sand and gravel

are analyzed, since it is assumed that foundations on clay and organic soils are usually piled which would have a different dynamic stiffness than the one described in section 5.1. The Poisson ratio is set to $1/3$, in order to comply with the conditions in section 5.2, which is a reasonable assumption based on Table 8.6. The results can be seen in Figure 8.12. Since moraine is the most common soil in Sweden (SGU 2000) this soil is used in further analysis.

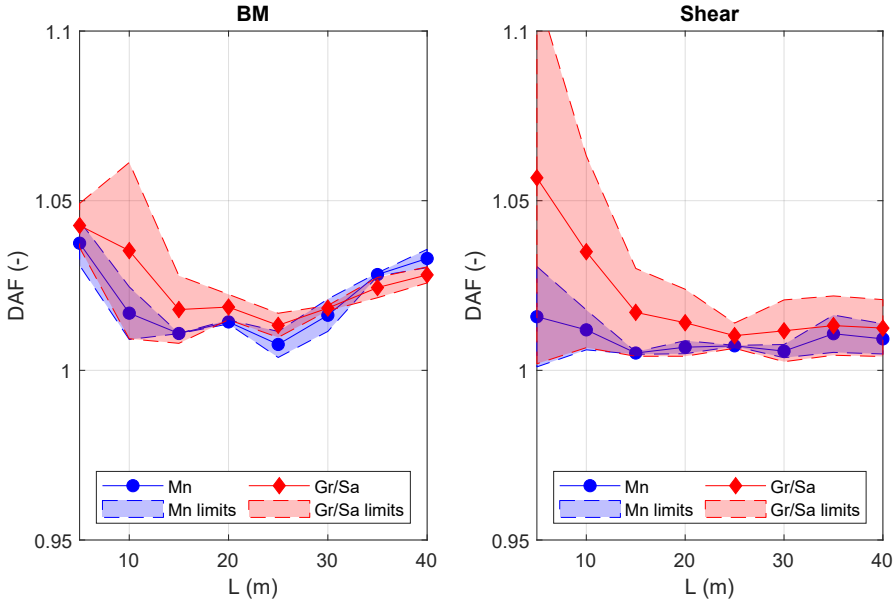


Figure 8.12: Upper and lower limits of the DAF for moraine (Mn) as well as sand and gravel (Sa/Gr) as a function of the bridge length.

The stiffness K and damping C can be expressed as, see section 5.1:

$$K = \frac{4Gr}{1-v} = \frac{4V_s^2 \rho r_{eq}}{1-v} = \frac{4V_s^2 \rho}{1-v} \sqrt{\frac{4BL}{\pi}} \quad (8.10)$$

$$C = \frac{r_{eq}}{V_s} \gamma K = \sqrt{\frac{4BL}{V_s^2 \pi}} \gamma K \quad (8.11)$$

Since μ is set to 0 in section 5.1 for a rectangular footing, the mass from the soil is set to 0. The properties for moraine used in the parameter study can be seen in Table 8.7.

Table 8.7: Properties for moraine (Mn) used in the parameter study.

Property	Notation	Unit	Max	μ	Min
S-wave	V_s	m/s	700	450	200
Density	ρ	kg/m ³	2300	2150	2000
Width	B	m	2.5	1.55	0.6
Stiffness	K	GN/m	46.7	14.2	1.6
Damping	C	MNs/m	834.8	311.0	49.8

8.6 Vehicle properties

Vehicle properties are set according to section 4.4.4.

8.7 Vehicle velocity

On the Swedish road network the maximum speed limit for heavy trucks (above 3.5 tonnes) is set to 90 km/h on highways and 80 km/h on all other roads (Transportstyrelsen 2013). The velocity on a number of Swedish roads based on data gathered from WIM measurements of bridges by Trafikverket is presented in Björnsson, Thelandersson, and Carlsson (2013) and can be seen in Figure 8.13.

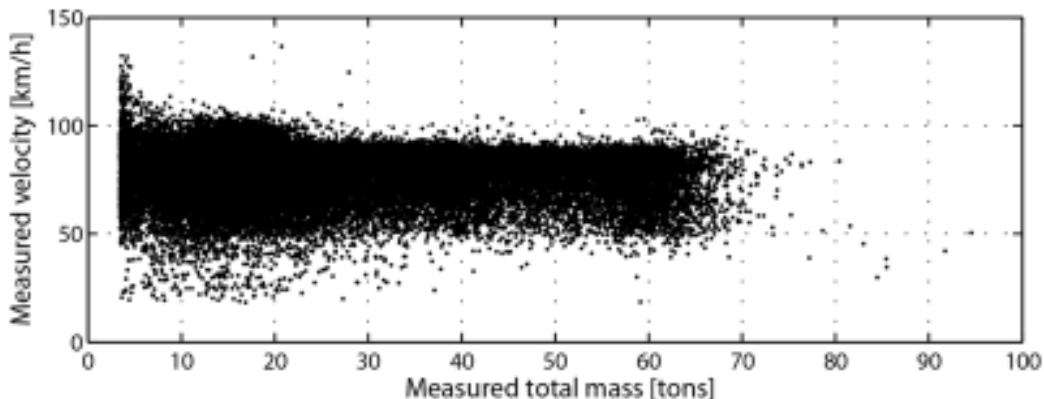


Figure 8.13: Velocity depending on vehicle weight based from WIM measurements on Swedish roads.

A study on the influence of vehicle speed on the DAF can be seen in Figure 8.14. The same bridge properties as in Table 7.1 is used and the road surface

is set to smooth. It can be shown that the DAF increases with larger velocity, see Figure 8.14.

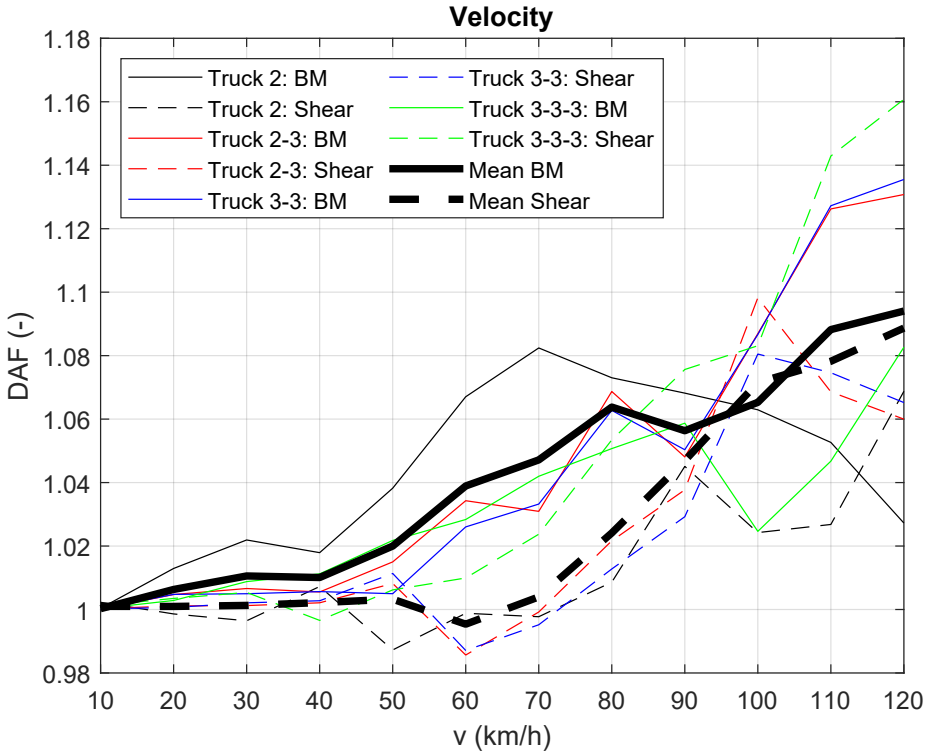


Figure 8.14: DAF as a function of velocity for the different vehicle models.

Since the DAF gets larger values at higher velocities, an upper limit of 110 km/h is used for the parameter studies due to the fact that the DAF mainly gets lower values below this speed. It corresponds well to the upper values for vehicles above 20 tonnes in Figure 8.13.

For the STE, the speed is varied between 100 and 110 km/h, in one step, during the simulations and the maximum value on the DAF is retrieved from each truck event. The variation in velocity is to make sure that possible cancellations, see section 4.3.3, does not influence the result. If a resonance speed for the first mode between 100 and 110 km/h exists, that value is used instead of 110 km/h.

For the MTE, the velocity is assumed to follow a log-normal distribution, $N(\mu, \sigma^2)$, as $N(100, 10^2)$. An upper and lower limit of 90 and 110 km/h is however used, see section 8.10 for more information.

Platoons are assumed to consist of a variety of heavy vehicles in practice, and a constant velocity of 100 km/h is therefore used which corresponds well to heavy vehicles above 20-30 tonnes in Figure 8.13. The upper value is chosen in order to retrieve safe-sided results and the value of 110 km/h is not used since it is assumed to be unrealistic for platoons.

In order to study the difference of the DAF due to soil-structure interaction, the velocity is varied between 100 and 110 km/h in steps of 2.5 km/h and the maximum value of the DAF for these steps is retrieved. No resonance speed is determined as for the single truck event since the bridges will have varying eigenfrequencies. The preconditions for the vehicle velocity for the parameter studies can be seen in table 8.8.

Table 8.8: Vehicle velocity for the parameter studies.

Parameter study	Velocity (km/h)	Conditions
STE	100-110	Varied in one step. If a resonance speed v_{res} is found between 100-110 km/h this value is used instead of 110 km/h.
MTE	$N(100, 10^2)$	Upper and lower limit of 90 and 110 km/h.
Platooning	100	Constant.
SSI	100-110	Varied in steps of 2.5 km/h.

8.8 Convergence

Convergence studies are presented in the following sections for the beam mesh, number of vehicle events needed in order to retrieve the upper and lower limit for the DAF as well as the minimum amount of modes needed.

8.8.1 Mesh

In order to retrieve sufficiently accurate results with regards to the bridge FE mesh, a convergence study is made. Figure 8.15 shows the convergence with the same bridge properties and vehicle speed as in Table 7.1, except the number of beam elements vary. The convergence is determined based on the relative error for the maximum BM and shear. The vehicle models all have air suspension properties according to section 4.4.4. The suspension type is unimportant at this stage. The road surface is set to smooth in order to not have deviations due to random generated profiles for each event. When changing the beam length the amount of time-steps varies proportionally and therefore other beam lengths does not have to be studied, i.e. the element length should remain constant. The convergent length is approximately 0.25

m, which corresponds to 100 elements for the beam length of 25 m. In order to guarantee accuracy, an element length of 0.25 m is therefore used. The vehicle speed is irrelevant since the time-step is constant and no road profile is used, see section 8.8.3.

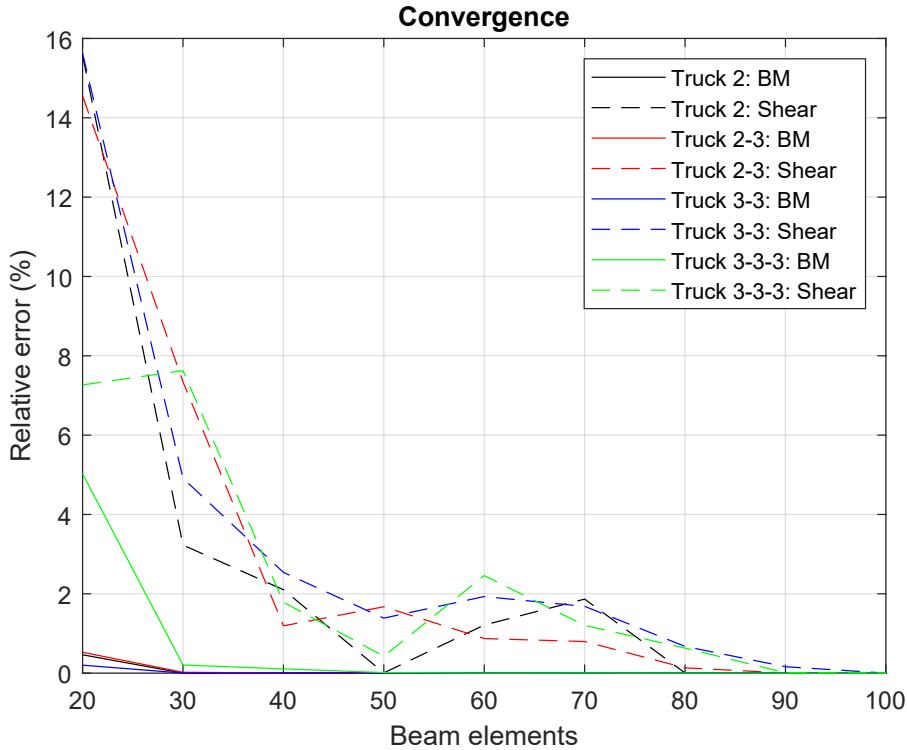


Figure 8.15: Convergence rate of the solution when varying the amount of beam elements

8.8.2 Vehicle events

During simulations of the STE and MTE, an upper and lower limit is retrieved for the DAF since a new profile of the road irregularities is generated for each vehicle event. A convergence study is made for a single vehicle traversing a bridge in order to choose a sufficient number of vehicle events to retrieve both the upper and lower limit. This will ensure that as accurate results as possible will be retrieved during simulations. The vehicle properties is set to leaf suspension according to Table 4.2 and 4.3, which gives larger peaks due to its stiffer properties. The road surface is set to class A since this profile is used, see section 8.11. For time efficient reasons an upper limit of the maximum bridge frequency considered is set to 20 Hz. The same

bridge properties as in Table 7.1 is used and the vehicle speed is set to 100 km/h.

The results of the convergence study for BM and shear can be seen in Figure 8.16 and 8.17. The DAF converges when the number of vehicle events is around 8000 for BM and 6000-7000 for shear, and it is assumed that a larger amount of vehicle events would generate a minor increase of the DAF. In order to provide accurate results during simulations for the parameter studies, a similar study could be made for each bridge beforehand but that would prove very computationally inefficient and this is assumed to be a good approximation. The same number of vehicle events is used for the different scenarios, i.e. when evaluating the STE and MTE. Since the number of events is time-consuming, a value much less than the required amount for convergence is chosen, which is 1000 vehicle events. However, this should give reasonable values since the DAF does not see a large increase after this.

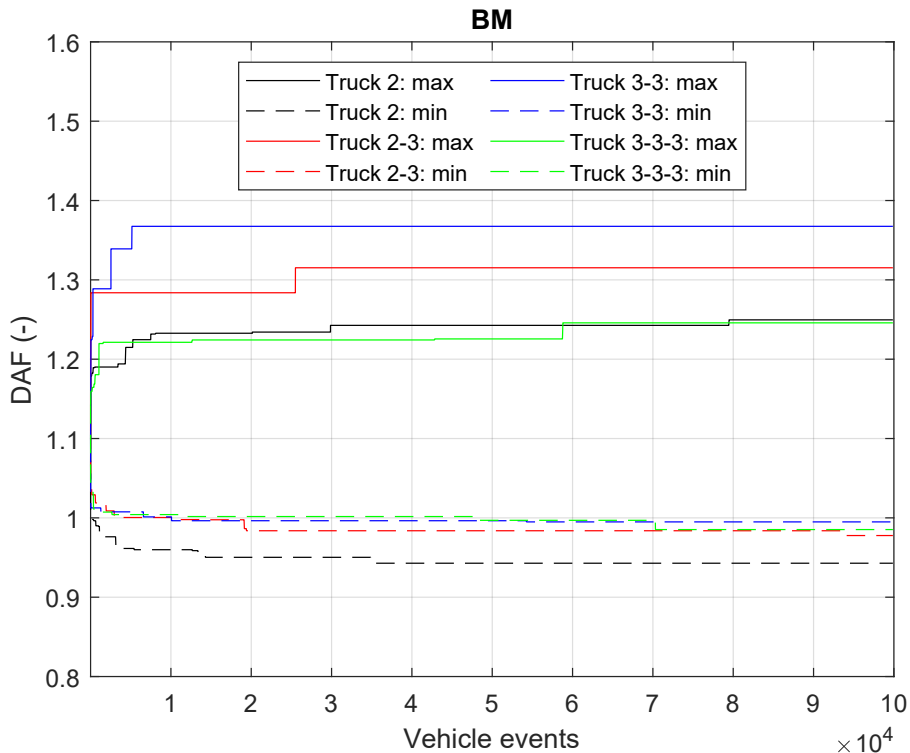


Figure 8.16: Convergence rate for the upper and lower limit of the DAF for BM when varying the number of vehicle events.

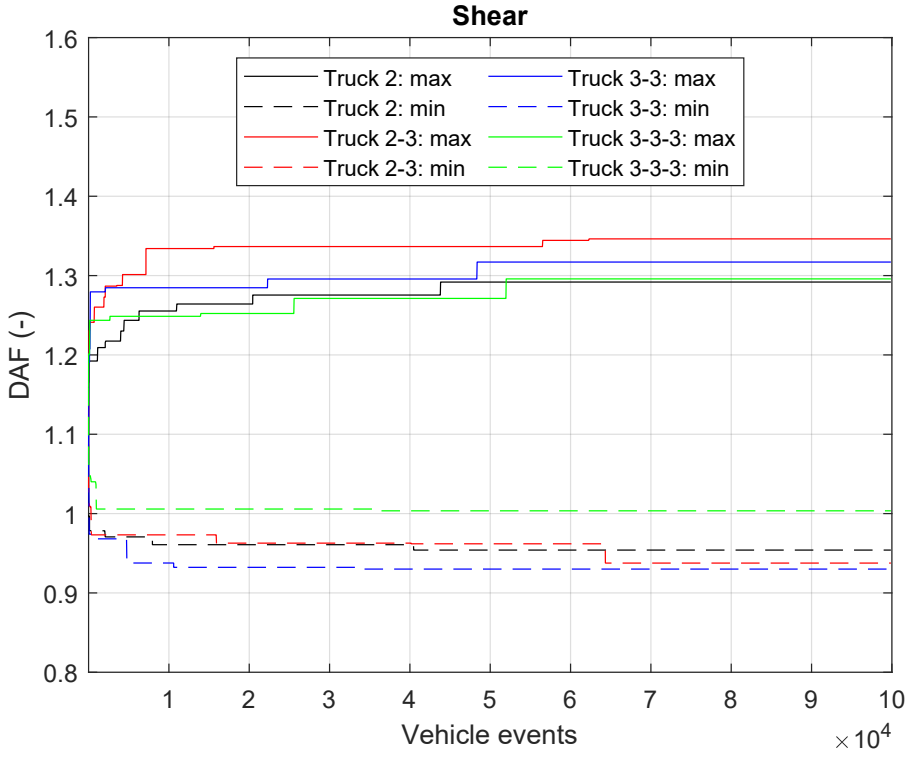


Figure 8.17: Convergence rate for the upper and lower limit of the DAF for shear when varying the number of vehicle events.

8.8.3 Frequency

The amount of time-steps in the MATLAB toolbox is set to the largest value based on 3 criterion; the maximum frequency of the vehicle, the maximum bridge mode considered and the maximum frequency of the ISO road profile. All criterion are based on the Nyquist-Shannon where the sampling rate for the first two criterion are set to $f_s = 2f_{max}$, whereas the third is also based on the vehicle velocity as $f_s = 2vf_{max}$ ($m \cdot s^{-1} \cdot m^{-1}$). In order to guarantee an accurate result based on the amount of modes of the bridge that contribute to the solution, a convergence study is made. The other criterion are automatically applied when these are larger than the largest beam mode considered. The principle can be compared with modal truncation, see section 2.3, where an appropriate amount of modes are used to give the smallest error possible.

The beam and vehicle properties with leaf suspension according to section 8.4 and 4.4.4 are used. Mean values on the bridge properties are used in

order to have no deviation based on these parameters. The road profile is set to smooth and the vehicle speed is set to 100 km/h. The result of the convergence study can be seen in Figure 8.18. The DAF converges at around 500 and 300 Hz for lengths of 5 and 40 m. However, an FFT analysis for a frequency span of 1 kHz shows that the largest contribution to BM and shear occurs at frequencies below 200 Hz, see Figure 8.19. A cut-off limit for the frequency could therefore be set to around 200-300 Hz, but in order to retrieve an accurate result similar studies are made for lengths between 5 to 40 m and reasonable cut-off frequencies are presented in Table 8.9. The same results when SSI is included is also presented in the table. Since an elastic spring is added at the supports the frequency content is larger than if the vertical translations are fixed, and thus a higher cut-off frequency is used between 10 and 20 m. The cut-off frequencies does not only produce more accurate results, but also gives more time-efficient simulations.

Table 8.9: Cut-off frequencies for integral and slab bridges depending on bridge length. Frequencies depending on if SSI is considered or not is also presented.

No SSI	Length (m)	$L \leq 10$	$10 < L \leq 40$
	Cut-off frequency (Hz)	500	300
SSI	Length (m)	$L \leq 20$	$20 < L \leq 40$
	Cut-off frequency (Hz)	500	300

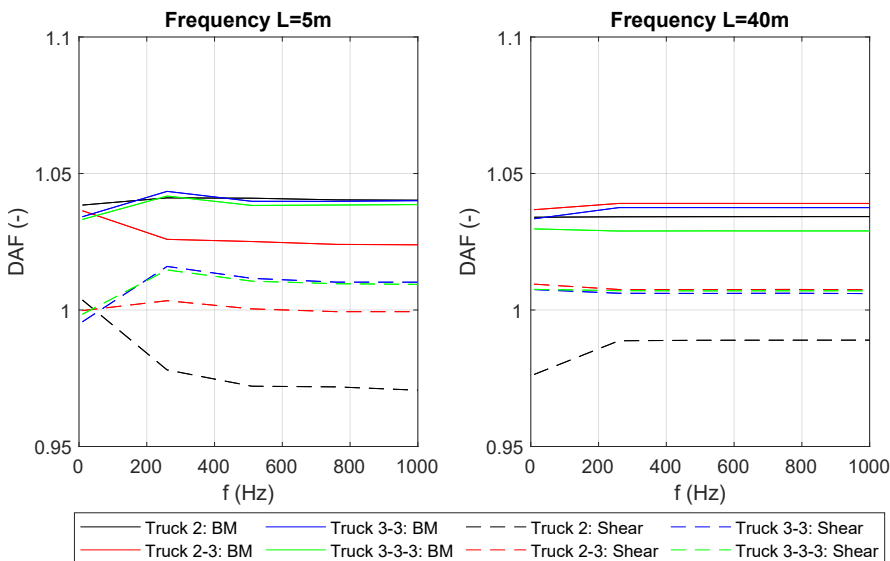


Figure 8.18: Convergence rate for the DAF depending on frequency for integral bridges.

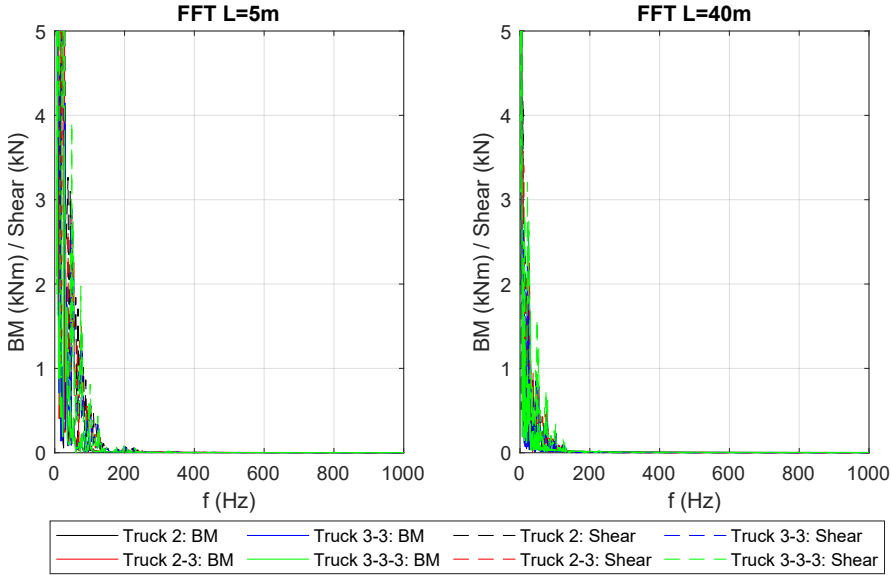


Figure 8.19: FFT plots of the response for BM and shear for integral bridges.

8.9 Platooning

The following sections determine the number of vehicles in a platoon and an appropriate distance between the vehicles based on the vehicle distances for platoons in section 6.1 and the axle distance to induce resonance in section 4.3.2.

8.9.1 Resonance distance

Since truck platooning uses equal distances between the vehicles, resonance might occur in the bridges. The condition for the distance between axles that induces resonance is derived from equation 4.13:

$$L_v = \frac{v_{res}^i}{f_1} \quad \text{for} \quad i = 1, \dots, \infty \quad (8.12)$$

The first mode, f_1 , gives the highest resonant response, see section 4.3.2, and is therefore only used. The distance between vehicles in a platoon is around 10-20 m from the literature, see section 6.1.1. The distance between vehicles during simulations is therefore set to the first resonant distance L_v , see figure

8.20, that fall between 10-20 m in addition to the axle length:

$$L_{v,ax} + 10 \leq L_v \leq L_{v,ax} + 20 \quad (8.13)$$

where $L_{v,ax}$ is the distance between a vehicle's first and last axle.

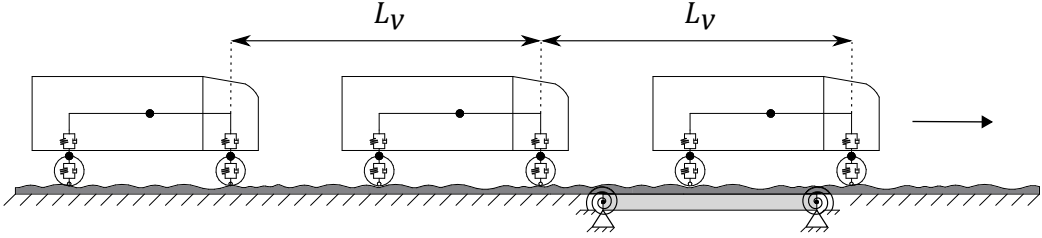


Figure 8.20: A truck platoon with distance L_v between vehicles.

8.9.2 Number of vehicles

No exact number of vehicles in a platoon is found from the literature. Increasing the amount of vehicles reduces the emission and it is reasonable to assume that future platoons will be as long as possible, but still have a set limit. The study on platooning is therefore set to a specific number of vehicles which gives the largest possible DAF in order to show the difference for equal and random distances. Figure 8.21 shows the increase of DAF when increasing the number of vehicles in a platoon and also shows the effect of having random distances between the vehicles. The figure confirms the effect of resonance in the bridge. The same bridge properties as in Table 7.1 have been used and the vehicle properties is set to air suspension, see Table 4.2 and 4.3. The vehicle properties is unimportant at this stage since the deviation is quite small between air and leaf suspension. The road surface is set to a smooth profile and the speed to 100 km/h.

Another study is made with the same conditions as previously mentioned, but the bridge properties in section 8.4 is used in order to set an appropriate value on the number of vehicles in a platoon based on the length of the bridge. The mean values on the properties for integral bridges are used for this purpose. A study on the increase of the DAF based on vehicle and bridge length is conducted and the result can be seen in Figure 8.22. The number of vehicles in further evaluations is set to the values according to Table 8.10, since the largest number of vehicles needed for convergence for all vehicle models occur around these values. The number of vehicles is assumed to be a good approximation also for slab bridges.

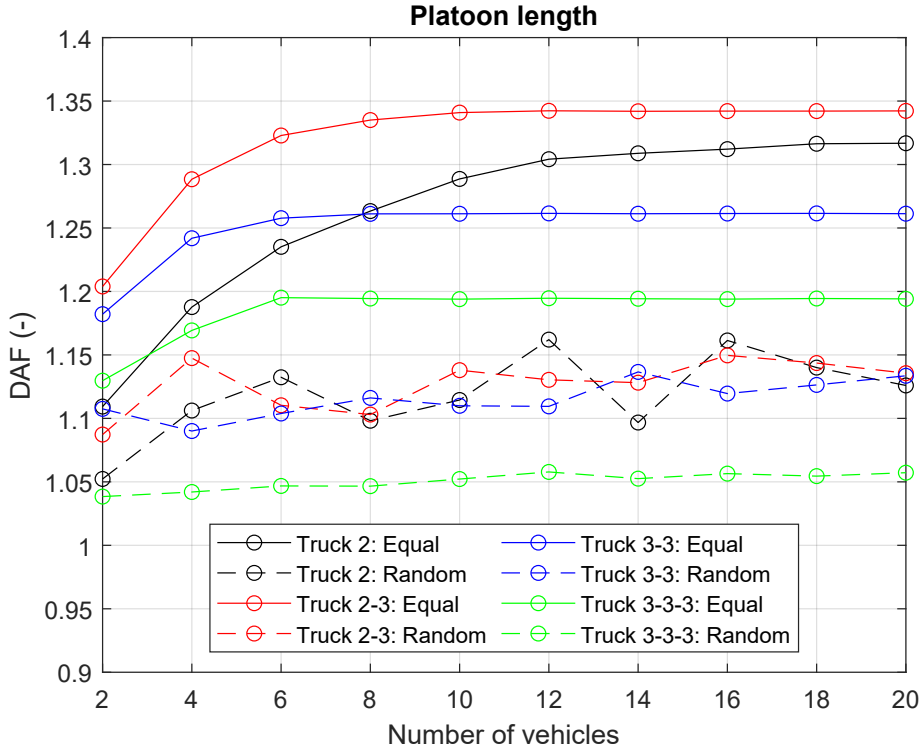


Figure 8.21: DAF based on BM as a function of number of vehicles in a platoon with equal and random distance for the bridge properties found in Table 7.1.

Since a value of L_v does not always exist between 10-20 m, an iterative procedure is also implemented where the distance between vehicles is increased to 5-40 and the velocity is changed to values between 90 and 110 km/h in order to always find a value for L_v . If it is not found, the first resonant length is used.

Table 8.10: Amount of vehicles required in order to capture the maximum increase of the DAF depending on the bridge length.

Length (m)	$L \leq 10$	$10 < L \leq 20$	$20 < L \leq 40$
Number of vehicles	8	16	20

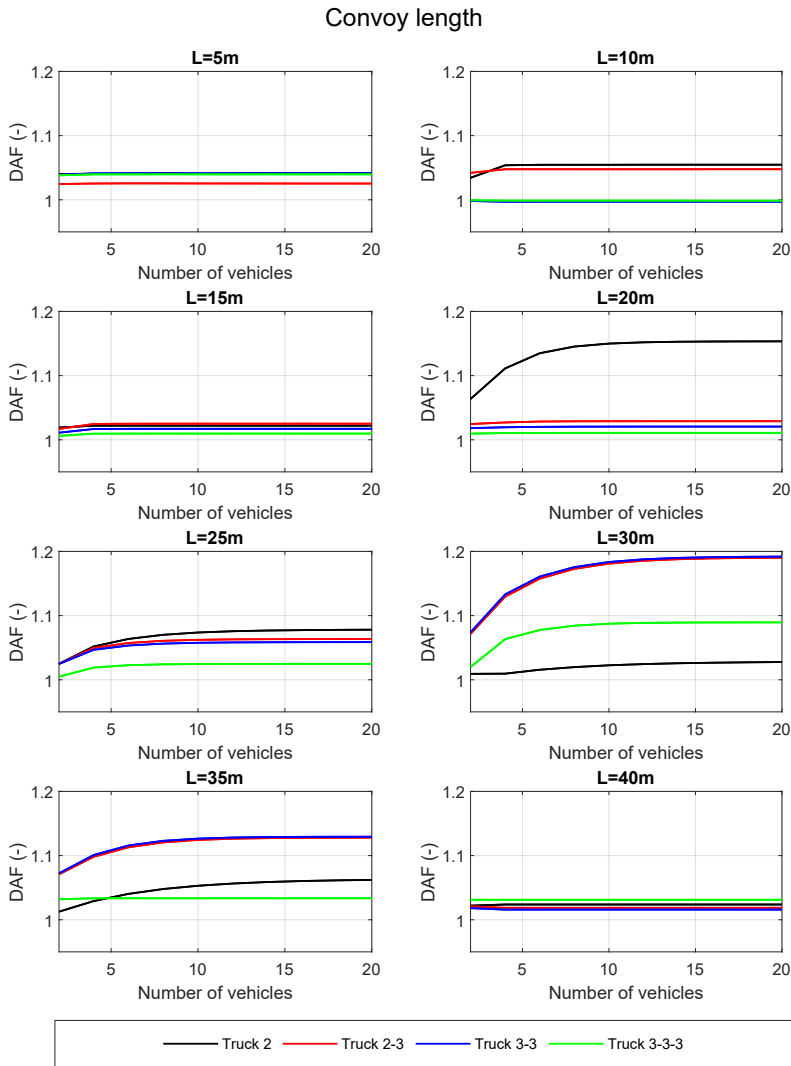


Figure 8.22: DAF based on BM as a function of number of vehicles in a platoon for different bridge lengths.

8.10 Multiple truck event

Gross simplifications are made when estimating the traffic from multiple heavy vehicles traversing the bridges. The WIM measurements from 2002-2003 in Vägverket (2004) provides an estimate of the maximum hourly heavy vehicle flow rate and is set to 200 veh/h. Generalizations of percentages of each vehicle model can be found from the same measurements. Truck 2

is assumed to consist of 25-35 % and the semi-trailers, i.e. Truck 2-3, 3-3 and 3-3-3, to 10-15 % of the traffic. Type of semi-trailer is randomly generated. However, the traffic consists of buses and other types of heavy vehicles, therefore only the truck models mentioned in this thesis are used as a basis of the total flow rate.

The statistical expression according to the shifted exponential distribution for headway in section 6.2.2 is used and the minimum gap is assumed to be 5 m (C. Caprani 2005). The vehicle velocity is assumed to be log-normally distributed (C. C. Caprani et al. 2012) with a mean of 100 km/h and standard deviation of 10 km/h. The upper and lower limits are set to 110 and 90 km/h. The velocity is assumed to not be correlated to type of vehicle model and following vehicles can not be faster than the leading vehicle, i.e. no overtaking can occur. The built-in functions `exprnd` and `normrnd` in MATLAB are used for the headway and velocity. These functions generate random numbers in an exponential and normal distribution. Since the DAF is lower for multi-lane bridges, see section 3.1.2, no side-by-side truck events are considered. Vehicle meeting is assumed to occur at each event.

Table 8.11: Statistical assumptions for the multiple truck events based on measurements and previous studies.

Parameters	Statistics	Source
Velocity	Log-normal distribution	C. C. Caprani et al. (2012)
Vehicle model	Percentage from measurements	Vägverket (2004)
Headway	Poisson probability distribution	C. Caprani (2005)
Flow rate	Maximum veh/h from measurements	Vägverket (2004)

8.11 Road irregularities

The requirements in section 4.2.2 is used in order to determine which class to use for the generated road surfaces. 100 road surfaces with a length of 1000 m is generated for class A-C. $G_d(\Omega_0)$ is set to 1, 4 and 16 for class A-C respectively. Class A fulfills the requirements in Table 4.1 for speed limits above 100 km/h. Class B and C are however mainly above the requirements, see Table 8.12, and since these profiles are not realistic in the Swedish road network, only class A is used in the simulations.

Table 8.12: Degree of roughness, $G_d(\Omega_0)$ (m^3) and mean (μ), standard deviation (σ) and confidence interval of 95 % ($1 - \alpha$), with $\alpha = 0.05$, for surface class A-C (mm/m).

Class	$G_d(\Omega_0)$	μ	σ	$1 - \alpha$
A	1	3.37	0.68	(2.02, 4.72)
B	4	7.05	1.35	(4.37, 9.73)
C	16	13.99	2.49	(9.05, 18.93)

8.11.1 Simulated distance

Road irregularities are generated before the vehicle(s) reaches the bridge in order to get an initial dynamic response of the vehicle(s) traversing the bridge. The assumptions for the different parameter studies are presented in Table 8.13. i denotes the vehicle number in order with an individual count from left and right side. x_0 is the initial position from the bridge supports. $L_{v,ax}$ is the length from first to last axle for a vehicle and L_v is the distance to induce resonance according to equation 8.12.

The random distance, $t_{rnd,i}$, between a vehicle i and the vehicle in front $i - 1$ during the multiple vehicle events is determined with MATLAB's built-in function **exprnd** as (see section 6.2.2 for notations and the assumption of a minimum gap of 5 m in section 8.10):

$$t_{0,i} = \frac{L_{v,ax,i-1} + 5}{v_{i-1}} \quad (8.14)$$

$$t_{rnd,i} = \mathbf{exprnd}(\gamma_i) + t_{0,i} \quad (8.15)$$

γ_i is updated for each new vehicle i based on equation 6.3 in section 6.2.2. Note that t_0 is added since the shifted negative distribution is used. The sum of the individual values $t_{rnd,i}$ is determined as to not exceed the time for the first vehicle to cross the bridge entirely, t_{event} :

$$t_{event} \geq \sum_{i=1}^n t_{rnd,i} \quad (8.16)$$

Table 8.13: Simulated road irregularities for the different parameter studies where i denotes the i :th vehicle. ¹ The initial position for the first vehicle on the opposite side is set to a value of $\text{rand}(40,60)$. ² $L_{v,ax} + 10 \leq L_v \leq L_{v,ax} + 20$.

Parameter study	Simulated road irregularities before bridge	
	$i = 1$	$i = 2, 3, \dots, n$
Single truck event	50 m	
Multiple truck event	50 m ¹	$x_{0,i-1} + v_{i-1}t_{rnd,i-1}$
Platoon (equal distance)	20 m	$x_{0,i-1} + L_v$ ²
Platoon (random distance)	20 m	$x_{0,i-1} + L_{v,ax} + \text{rand}(10, 20)$

Chapter 9

Parameter study

The following sections include the studies:

1. Single truck event (STE).
2. Multiple truck event (MTE).
3. Platooning.
4. Soil-structure interaction (SSI).

Summaries for each study, except for SSI, are also made and the vehicle and bridge frequencies are presented since these values are important when evaluating the results.

9.1 Vehicle and bridge frequencies

The bridge fundamental frequencies and vehicle eigenfrequencies can be seen in Table 9.1 and 9.2. Note that air suspension has lower frequencies due to its lower stiffness properties. The slab also has lower frequencies than the integral bridge due to its lower stiffness.

Table 9.1: Bridge fundamental frequencies, f_1 .

L (m)	5	10	15	20	25	30	35	40
Slab (Hz)	36.84	13.60	7.59	5.02	3.64	2.80	2.25	1.85
Integral (Hz)	30.60	17.38	10.47	7.15	5.28	4.11	3.32	2.76

Table 9.2: Vehicle frequencies.

Frequency (Hz)	Truck							
	2		2-3		3-3		3-3-3	
	Air	Leaf	Air	Leaf	Air	Leaf	Air	Leaf
f_1	1.0	1.0	1.4	1.5	1.5	1.6	1.4	1.6
f_2	1.0	1.5	1.6	2.0	1.7	2.2	1.6	1.8
f_3	8.8	8.8	2.3	3.0	2.8	3.6	1.9	2.4
f_4	11.9	12.8	8.9	8.9	8.9	8.9	2.7	3.5
f_5			10.2	11.4	10.2	11.4	8.9	8.9
f_6			12.0	13.0	12.0	13.0	10.2	11.4
f_7			12.0	13.0	12.0	13.0	12.0	13.0
f_8			12.0	13.1	12.0	13.1	12.0	13.0
f_9					12.0	13.2	12.0	13.0
f_{10}							12.0	13.0
f_{11}							12.0	13.0
f_{12}							12.0	13.1
f_{13}							12.0	13.2

9.2 Single truck event

The following sections present results from a single truck traversing the different bridges. Each truck model is analyzed with the properties found in section 4.4.4. The bridge properties is set to mean values, see section 8.4. The amount of vehicle events simulated for each bridge length is set to 1000. The speed is varied according to section 8.7. The road surface is set to class A. The preconditions can be seen in Table 9.3.

Table 9.3: Preconditions for the parameter study. ¹ See section 8.4. ² See section 8.7. ³ See section 4.4.4.

Preconditions	
Bridge type	Slab/Integral
Bridge properties	Mean values ¹
Road surface	Class A
Velocity	100 to 110 km/h ²
Suspension	Air/Leaf ³
Vehicle events	1000

9.2.1 Slab bridges

The result for the single truck event for the slab bridges can be seen in Figure 9.1. The mean values and 95 % confidence interval (CI) for each bridge length is plotted versus the Swedish norm. As can be seen the mean values are mainly below the norm, however the CI and thus the maximum values, which are not plotted in the figure, are above the norm at several bridge lengths. Air suspension gives slightly lower values than leaf suspension, and the difference is more noticeable for longer bridges. For Truck 3-3-3, which is a much heavier vehicle, the difference is less noticeable.

As can be seen in Figure 9.1 the DAF experiences peaks at around 20-30 m for Truck 3-3 and 3-3-3. The same occur at 10-15 m for Truck 2. In order to study the reason to this phenomena the mean, maximum and minimum values of the DAF are plotted versus the bridge fundamental frequency, f_1 , see Figure 9.2. Peaks for all vehicle models occur at around 1.8-3.6 Hz, which is mainly due to coincidental frequencies, i.e. the vehicle eigenfrequencies (1-4 Hz) coincide with the bridges f_1 . Note especially that Truck 3-3 that has a large peak at 3.6 Hz (25 m) which corresponds exactly to the eigenfrequency f_3 for leaf suspension, see Table 9.2.

The Swedish norm seems sufficient for bridge f_1 above 10 Hz, i.e. for lengths below 10-15 m, except for Truck 2 which is above the norm. However, if a coincidental frequency would exist above 10 Hz it is assumed that a peak could exceed the norm. One reason to the exceeding values can not entirely be explained by coincidental frequencies. Instead it is due to the bridge to vehicle mass ratio m_b/m_v , see section 4.5, which is larger for Truck 2 since it is a much lighter vehicle. Compare for example with the lower values of the DAF for Truck 3-3-3 which is a much heavier vehicle.

It is evident that the Swedish norm is quite inaccurate for low bridge f_1 and that the Swiss norm for single truck loading (SIA-T), dotted line in the figure, is much more appropriate. The Swiss norm can therefore be seen to be well adjusted to take coincidental frequencies and m_b/m_v into consideration. It is however quite conservative for values above 10 Hz.

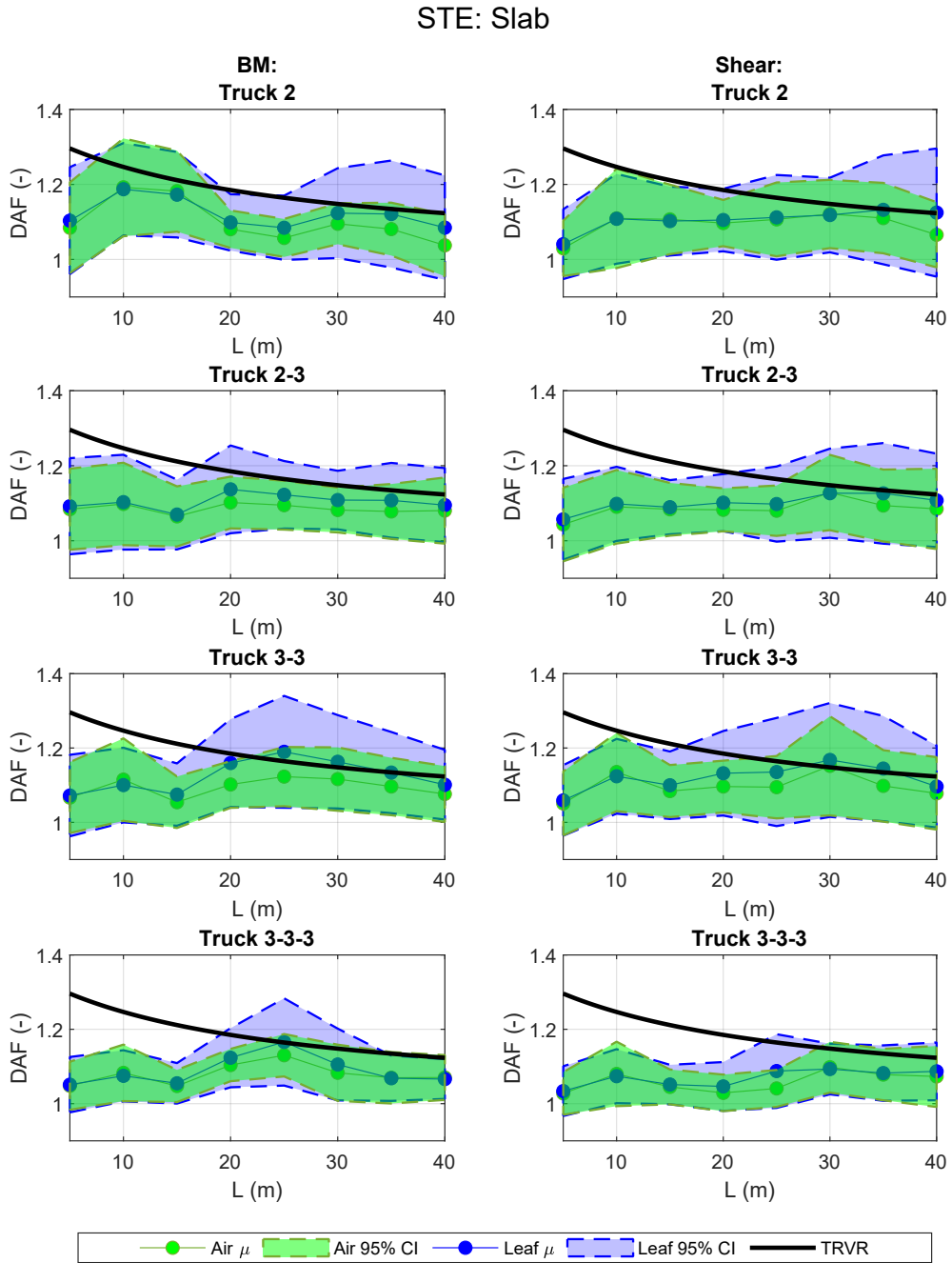


Figure 9.1: DAF for the STE depending on bridge length for the slab bridges. The values are plotted versus the Swedish norm (TRVR).

STE: Slab

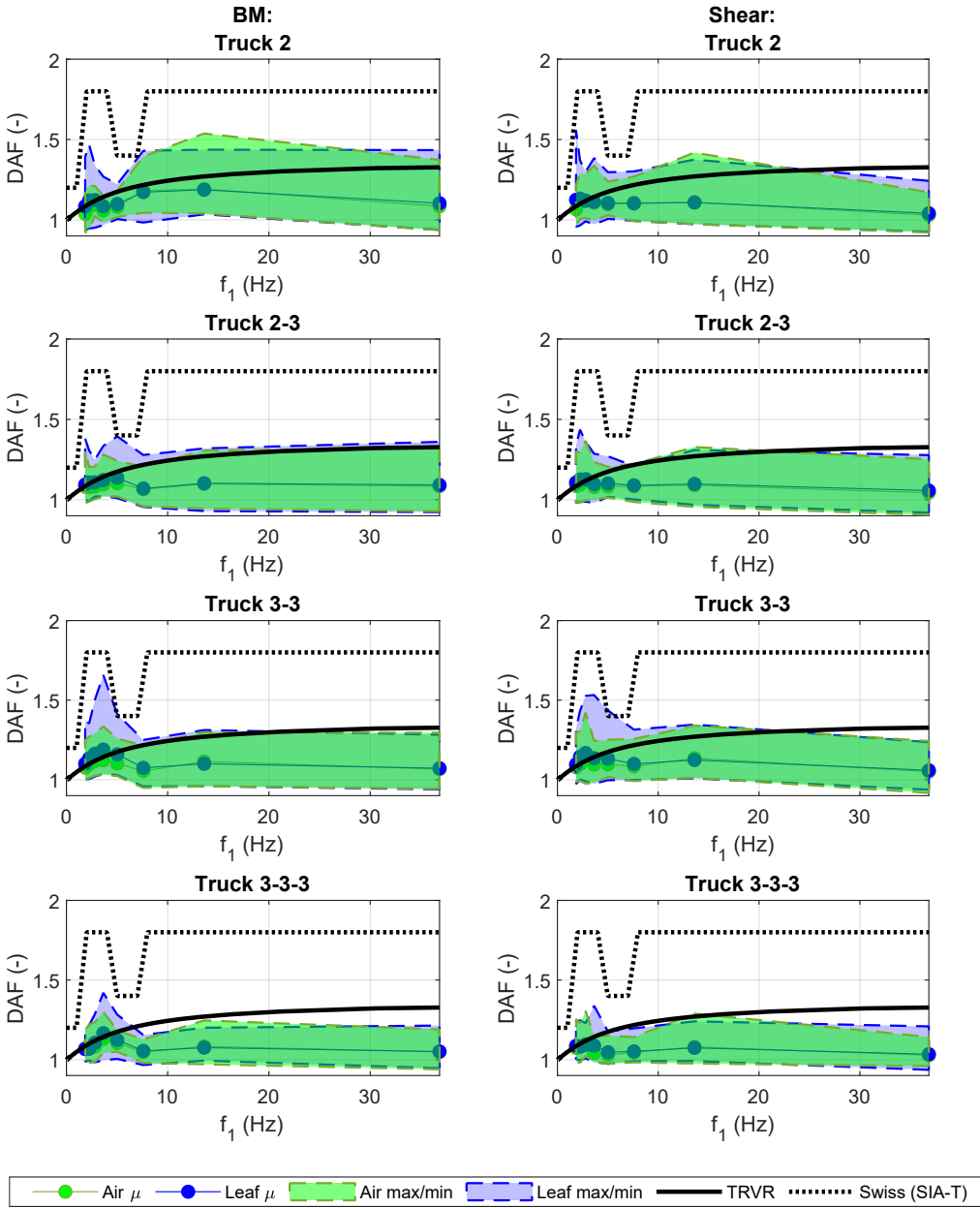


Figure 9.2: DAF for the STE depending on bridge fundamental frequency for the slab bridges. The values are plotted versus the Swedish (TRVR) and Swiss norm.

9.2.2 Integral bridges

The result for the single truck event for the integral bridges can be seen in Figure 9.3 and 9.4. The mean values and 95 % confidence interval (CI) for each bridge length is plotted versus the Swedish norm in Figure 9.3. As can be seen the mean values are below the norm, but the CI and thus the maximum values, which are not plotted in the figure, are above the norm at several bridge lengths.

As can be seen in Figure 9.3 the DAF experiences peaks at around 15 m for all vehicles. In order to study the reason to this phenomena the mean, maximum and minimum values of the DAF are plotted versus the bridge fundamental frequency, f_1 , see Figure 9.4. The peak at 15 m (10.5 Hz) is close to f_4 for Truck 2, f_5 for Truck 2-3 and 3-3 and f_6 for Truck 3-3-3. Since the eigenfrequencies for air suspension is closer to the bridge f_1 than leaf suspension, a higher peak is experienced for air suspension.

For low bridge f_1 (2-5 Hz) there are several peaks as well. Leaf suspension experiences larger peaks than air suspension, which is probably due to the frequency content being closer to the eigenfrequencies for the suspension units (compare with mode 1 and 2 for Truck 2 in Figure 4.17) rather than the tires where the stiffness, k_t , have the same values for both suspension types. Noteworthy is that at the bridge f_1 of 2.8 Hz, which coincides with air suspension eigenfrequency f_3 for Truck 3-3 and f_4 for Truck 3-3-3, that leaf suspension gives a larger contribution even though its eigenfrequencies does not coincide with the bridges' f_1 . It is therefore assumed that lower modes, which are related to the suspension units, gives a larger DAF for leaf suspension even when an air suspension eigenfrequency is closer to the bridges' f_1 .

For higher vehicle modes (above 8 Hz) it depends on how close the eigenfrequency is to the bridges' f_1 , instead of suspension type since the tire stiffness is equal. For larger bridge f_1 , i.e. above the highest vehicle modes, the DAF is quite similar for both air and leaf suspension since no coincidental frequencies occur.

It is also evident that the Swedish norm is quite conservative and that the Swiss norm for single truck loading (SIA-T), dotted line in the figure, is much more appropriate. The Swiss norm can therefore be seen to be well adjusted to take coincidental frequencies into consideration. It is however quite conservative for values above 10 Hz.

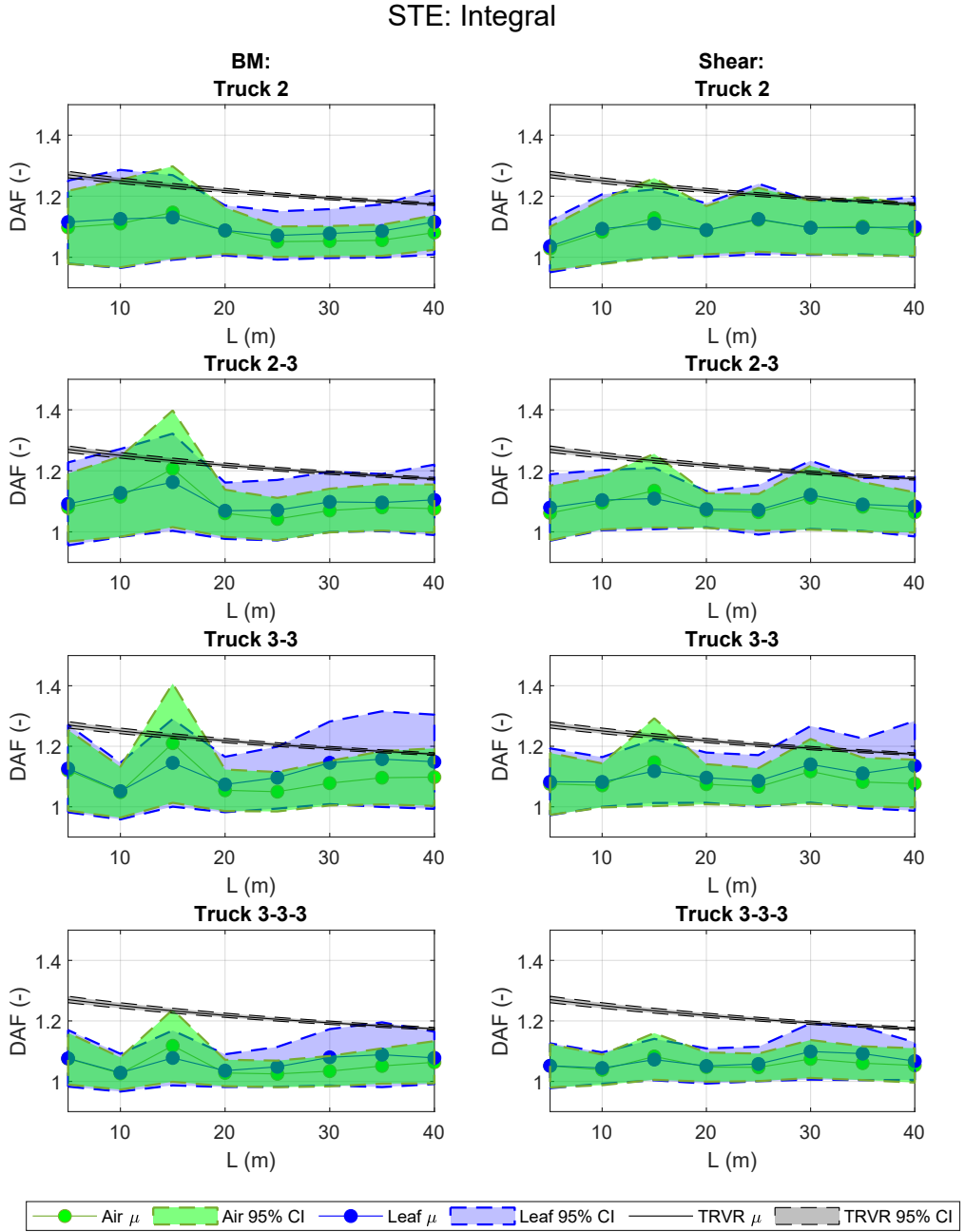


Figure 9.3: DAF for the STE depending on bridge length for the integral bridges. The values are plotted versus the Swedish norm (TRVR).

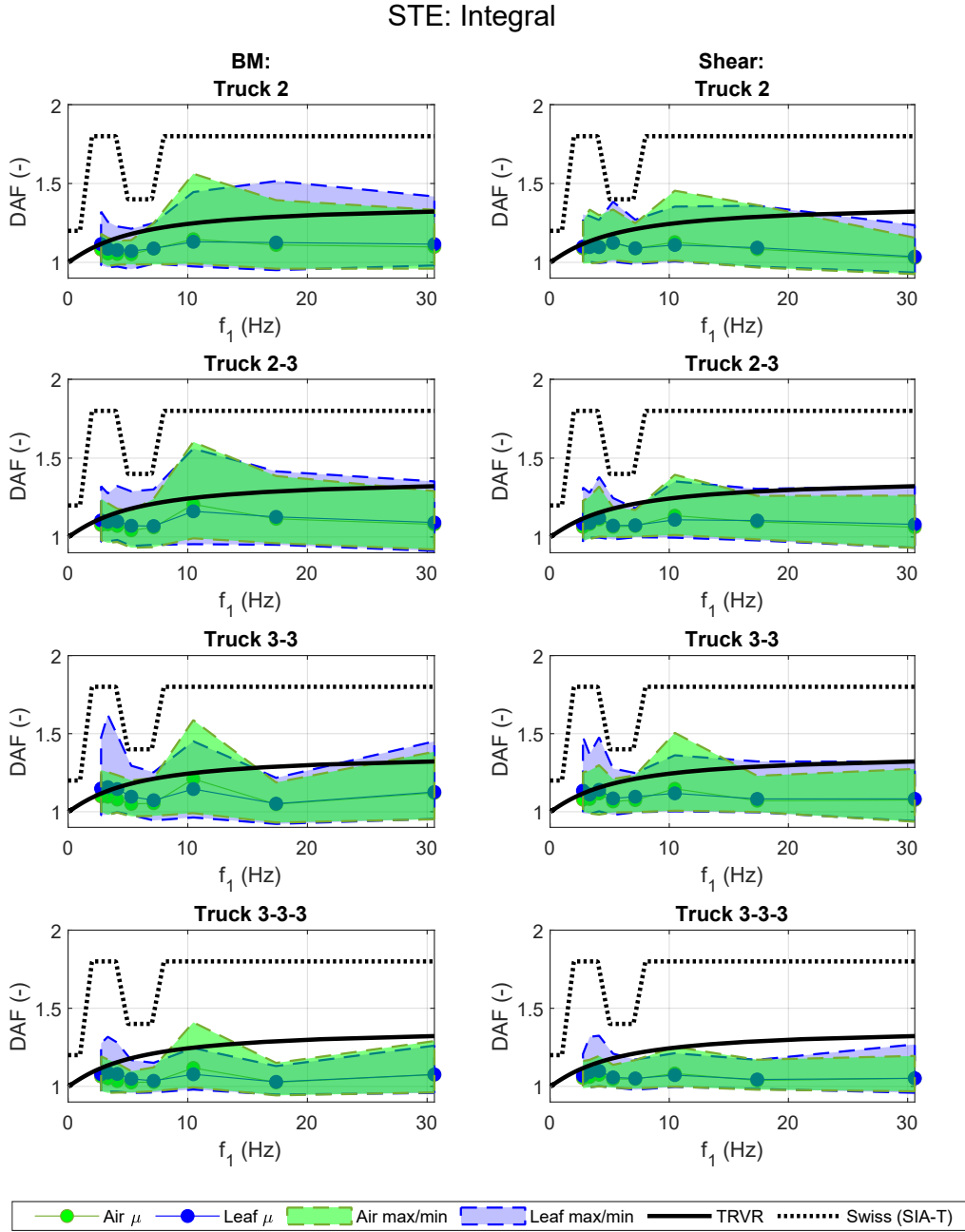


Figure 9.4: DAF for the STE depending on bridge fundamental frequency for the integral bridges. The values are plotted versus the Swedish (TRVR) and Swiss norm.

An FFT analysis, see Figure 9.5, of the wheel forces for Truck 2 with air suspension on the bridge and of the acceleration at the mid-span shows the reason to the amplification of the DAF for a bridge length of 15 m (10.5 Hz). The two highest modes of the vehicle, tire modes, are contributing the most to the bridge acceleration.

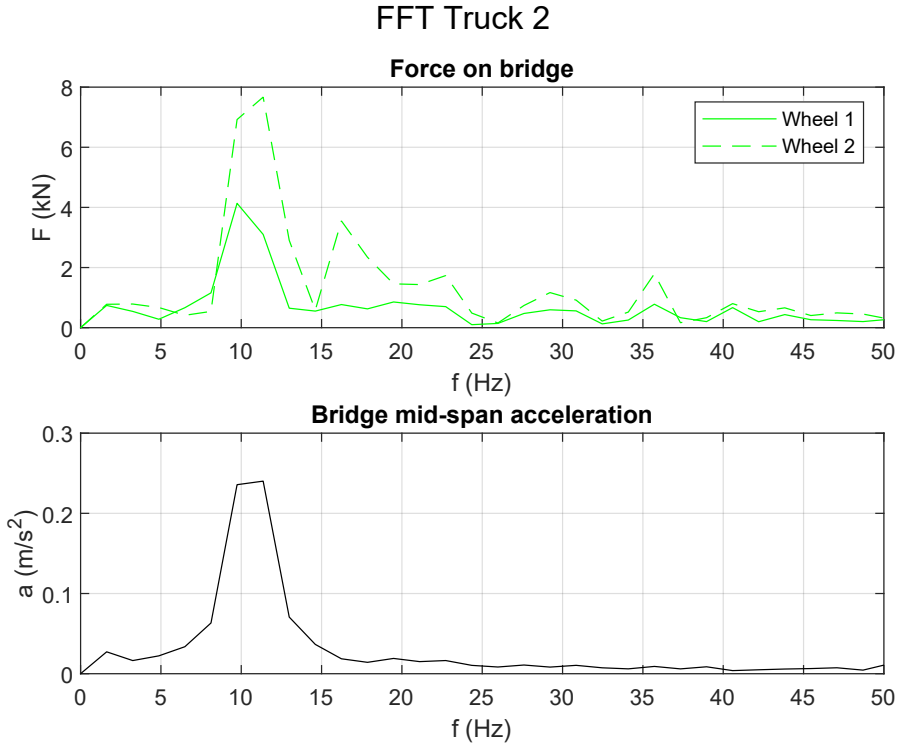


Figure 9.5: FFT of the wheel contact forces on the bridge for Truck 2 and bridge mid-span displacement for a bridge length of 15 m (10.5 Hz).

The larger values of the DAF for leaf compared to air suspension at low bridge frequencies is assumed to correspond to the lower suspension modes. However, the second bridge frequencies at these values, see Table 9.4, are quite close to the higher modes of the vehicles as well. In order to distinguish which modes contribute to the bridge excitation an FFT analysis is performed of Truck 3-3 with leaf suspension for bridge lengths of 25-40 m (2-6 Hz). An evaluation of the truck wheel forces and bridge mid-span acceleration shows that it is mainly the first mode of the bridge that is induced, see Figure 9.6. As can be seen the first vehicle modes contributes largely to the bridge response, whereas the higher modes around 8-12 Hz are not contributing as

much. The first modes are suspension modes, which means that the stiffer leaf suspension give a larger DAF at low bridge frequencies.

Table 9.4: Bridge second eigenfrequency, f_2 .

L (m)	25	30	35	40
f_2 (Hz)	14.8	11.5	9.3	7.7

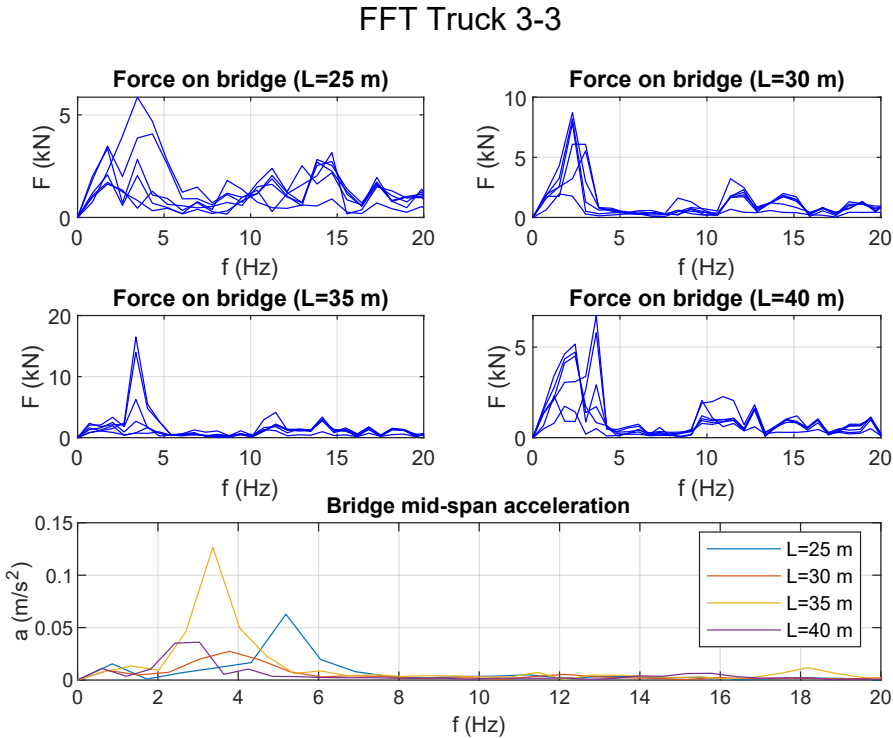


Figure 9.6: FFT of the wheel contact forces on the bridge for Truck 3-3 and bridge mid-span acceleration for a bridge length of 25-40 m.

9.2.3 Summary

The Swedish norm is exceeded for all the vehicle models, and approximations based on fundamental frequency is better adjusted to take coincidental frequencies into account. Similar studies have shown the same behaviour such as Jung, G. Kim, and Park (2013), which can be seen in Figure 9.7.

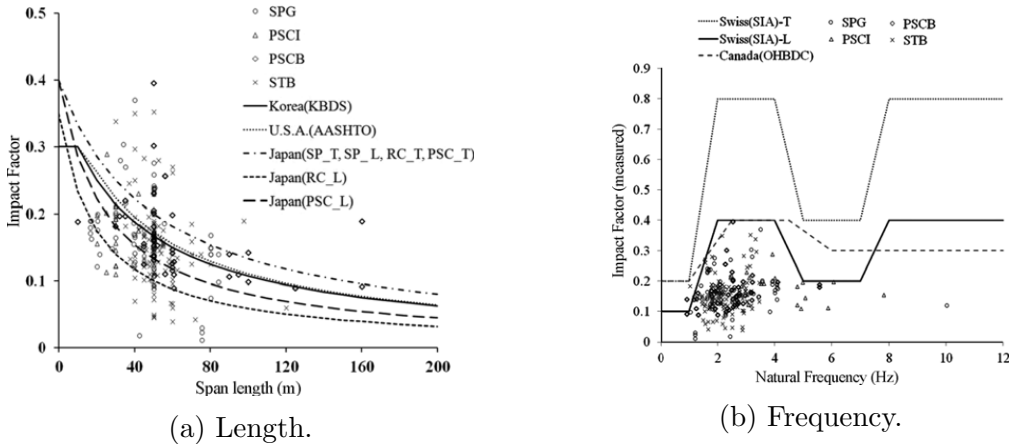


Figure 9.7: DAF depending on length and fundamental frequency for different bridge types (Jung, G. Kim, and Park 2013).

A comparison between air and leaf suspension based on the mean values is presented in Table 9.5 and 9.6. The difference is calculated as:

$$\frac{DAF_{\text{air}} - DAF_{\text{leaf}}}{DAF_{\text{leaf}}} \tag{9.1}$$

Negative values correspond to a lower DAF for air suspension. Air suspension can give almost a 5-6 % lower DAF at low frequencies but it is almost 6 % larger when its eigenfrequency coincides with the integral bridges' at around 10 Hz. However, the opposite situation could have been found at a bridge frequency of around 11 Hz, where leaf suspension experiences a coincidental frequency. Air suspension can be seen to give a 1-3 % (μ) smaller contribution to the DAF compared to leaf suspension in general.

Table 9.5: Difference (%) of the DAF (BM) between air and leaf suspension.

DAF (BM)												
Bridge	Truck											
	2			2-3			3-3			3-3-3		
	μ	max	min	μ	max	min	μ	max	min	μ	max	min
Slab	-1.9	0.8	-4.4	-1.7	-0.4	-3.1	-2.7	1.3	-5.6	-0.8	0.7	-3.1
Integral	-1.5	1.4	-3.1	-1.1	3.8	-2.7	-2.1	5.7	-5.9	-1.1	3.7	-4.2

Table 9.6: Difference (%) of the DAF (shear) between air and leaf suspension.

DAF (Shear)												
Bridge	Truck											
	2			2-3			3-3			3-3-3		
	μ	max	min									
Slab	-1.1	0.4	-5.3	-1.3	0.2	-2.9	-1.9	1.0	-4.1	-1.0	0.6	-4.3
Integral	-0.1	1.6	-1.0	-0.6	2.3	-1.8	-1.6	2.6	-5.2	-0.9	1.0	-2.9

9.3 Multiple truck event

The following sections present results from multiple trucks traversing the different bridges. The study is made in order to compare the DAF when multiple vehicles are present on the bridge. The conditions for the parameter study can be found in section 8.10. The bridge properties is set to mean values, see section 8.4. The amount of vehicle events simulated for each bridge length is set to 1000. The speed is varied according to section 8.7. The road surface is set to class A. The preconditions can be seen in Table 9.7.

Table 9.7: Preconditions for the parameter study. ¹ See section 8.4. ² See section 8.7. ³ See section 4.4.4.

Preconditions	
Bridge type	Slab/Integral
Bridge properties	Mean values ¹
Road surface	Class A
Velocity	$N(100, 10^2)$ ²
Suspension	Air/Leaf ³
Vehicle events	1000

9.3.1 Slab bridges

The percentage of each vehicle model and number of vehicles for each bridge length is presented in Table 9.8. As can be seen in the table, the number of vehicles increases with bridge length, and Truck 2 is the most common vehicle model.

The result from the study of the slab bridges can be seen in Figure 9.8 and 9.9. The mean values in the figures are below the Swedish norm but the 95 % confidence interval (CI) and maximum values are mainly above. The same

Table 9.8: Percentage of vehicle model and number of vehicles during the simulations.

L	Suspension	Truck (%)				Number of vehicles (%)				
		2	2-3	3-3	3-3-3	2	3	4	5	6
5	Air	71	9	9.9	10.1	97.5	2.5	0	0	0
	Leaf	71	9	10	10.1	98.3	1.7	0	0	0
10	Air	70	10	9.8	9.9	86.4	12.9	0.7	0	0
	Leaf	70	10	9.9	9.9	88.2	10.7	1.1	0	0
15	Air	70	9.7	11	9.9	76.8	21.2	1.9	0.1	0
	Leaf	70	9.7	11	10	75.9	22	2.1	0	0
20	Air	70	11	8.8	10.6	67.2	28.5	4.1	0.2	0
	Leaf	70	11	8.9	10.6	69.4	26.7	3.8	0.1	0
25	Air	69	11	11	9.9	61.1	33.2	5.4	0.3	0
	Leaf	69	11	11	9.9	56.3	36.8	6.5	0.4	0
30	Air	71	10	9.6	9.4	52.8	36.7	10	0.5	0
	Leaf	71	10	9.7	9.4	51.8	37.2	10	0.8	0
35	Air	70	10	9.7	9.6	43.4	38.6	16	1.6	0
	Leaf	70	10	9.7	9.7	44.9	41.3	13	1.3	0
40	Air	71	10	9.3	9.6	38.7	43.3	15	2.7	0.3
	Leaf	71	10	9.3	9.6	41.9	37.7	18	2.7	0.1

peaks experienced for the STE for the different vehicle models are retrieved and is magnified for some frequencies, for example at 1.85 Hz. It can be seen that the approximation according to the Swiss norm for single truck loading (SIA-T) is accurate in this case as well as for the STE. This is mainly due to coincidental frequencies between 1-3 Hz. For shear the values corresponding to lane loading (SIA-L) is more appropriate except for some peaks.

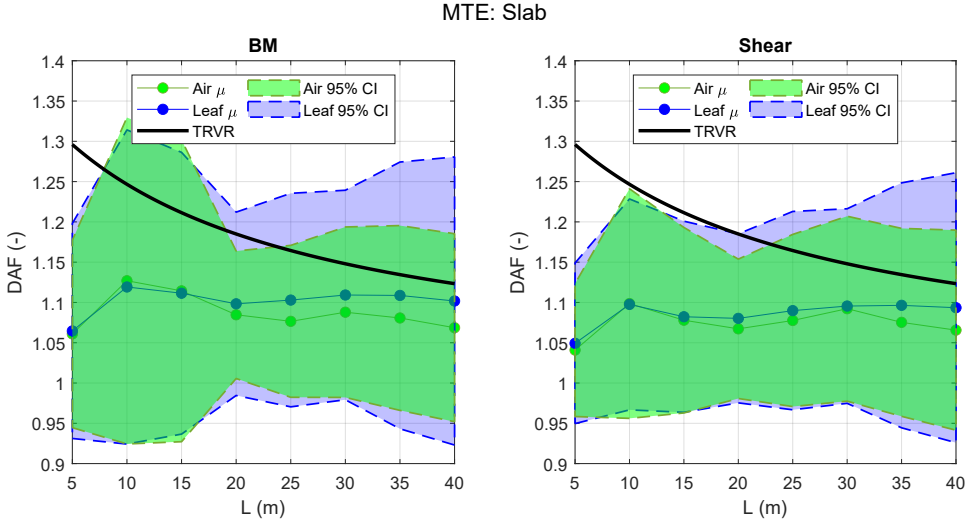


Figure 9.8: DAF for the MTE depending on bridge length for the slab bridges. The values are plotted versus the Swedish norm (TRVR).

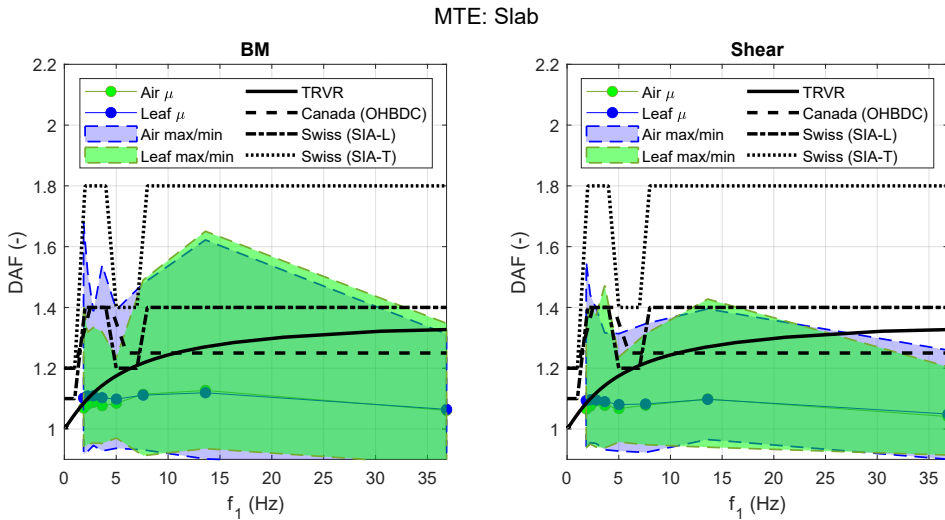


Figure 9.9: DAF for the MTE depending on bridge fundamental frequency for the slab bridges. The values are plotted versus the Swedish (TRVR), Swiss and Canadian norm.

9.3.2 Integral bridges

The percentage of each vehicle model and number of vehicles for each bridge length is presented in Table 9.9. As can be seen in the table the number of vehicles increases with bridge length, and Truck 2 is the most common

vehicle model.

Table 9.9: Percentage of vehicle model and number of vehicles during the simulations.

L	Suspension	Truck (%)				Number of vehicles (%)				
		2	2-3	3-3	3-3-3	2	3	4	5	6
5	Air	70	10	11	9.5	97.9	2.1	0	0	0
	Leaf	70	10	11	9.5	97.6	2.3	0.1	0	0
10	Air	70	10	9.9	9.6	86.6	12.6	0.8	0	0
	Leaf	70	10	9.9	9.6	86.8	12.6	0.6	0	0
15	Air	69	9.4	11	10.2	76	22.6	1.4	0	0
	Leaf	69	9.4	11	10.3	77.7	20.3	2	0	0
20	Air	71	10	9.9	9.5	69.5	26.8	3.7	0	0
	Leaf	70	10	9.9	9.5	64.8	31.4	3.6	0.2	0
25	Air	70	10	11	9.6	58.2	35.9	5.5	0.4	0
	Leaf	70	10	11	9.7	57.6	34.8	7.1	0.5	0
30	Air	70	9.9	9.9	10.1	50.6	39.1	9.5	0.8	0
	Leaf	70	9.9	9.9	10.2	48.2	40.5	11	0.6	0.2
35	Air	70	10	10	9.5	44.4	41.7	12	1.7	0.2
	Leaf	70	10	10	9.5	47.7	37.5	14	1.1	0
40	Air	70	11	10	9.7	38	43.7	16	2.7	0.1
	Leaf	70	11	10	9.7	41.5	39.6	16	2.8	0.3

The result from the study of the integral bridges can be seen in Figure 9.10 and 9.11. The mean values and the 95 % confidence interval (CI) in the figures are mainly below the Swedish norm but the maximum values are mainly above. It can be seen that the approximation according to the Swiss norm for lane loading (SIA-L) is more appropriate than the Swedish norm except for some outliers. Since the integral bridges have higher frequencies than the slab bridges, no large peaks can be seen around 1-3 Hz which occurred for the slab bridges.

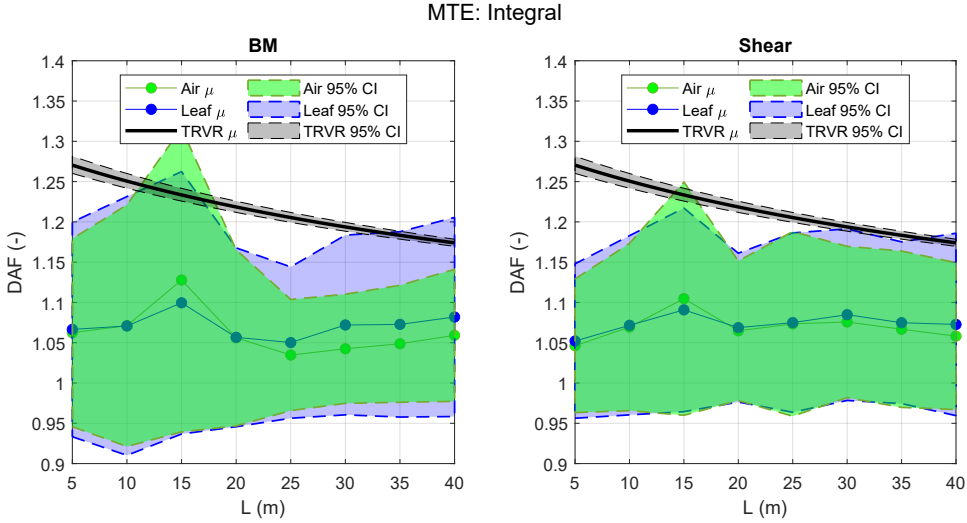


Figure 9.10: DAF for the MTE depending on bridge length for the integral bridges. The values are plotted versus the Swedish norm (TRVR).

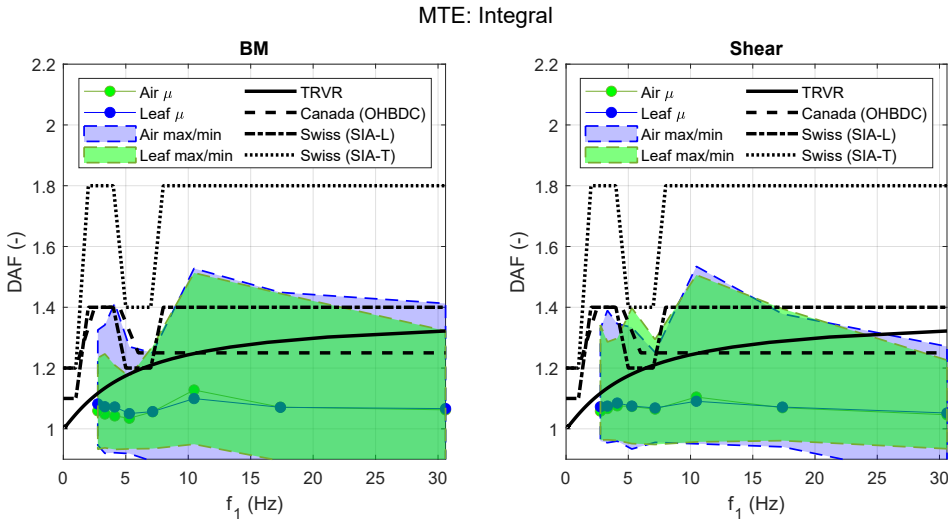


Figure 9.11: DAF for the MTE depending on bridge fundamental frequency for the integral bridges. The values are plotted versus the Swedish (TRVR), Swiss and Canadian norm.

9.3.3 Summary

A comparison between air and leaf suspension based on the mean values is presented in Table 9.10. The difference is calculated according to equation

9.1. Negative values correspond to a lower DAF for air suspension. The maximum and minimum values for the integral bridge can be seen to be quite similar but with opposite sign. The maximum value is mainly due to the coincidental frequency at 10 Hz, which gives a peak for air suspension. The same effect is not seen for the slab bridges, where the largest difference is around 2.5-3 %. However, air suspension gives around 1 % (μ) less contribution to the DAF in general. The same effect as for the single truck event is that air suspension gives smaller values at low fundamental frequencies, i.e. for longer bridges, and a smaller difference at higher fundamental frequencies, i.e. shorter bridges.

Table 9.10: Difference of the DAF between air and leaf suspension.

Bridge	BM			Shear		
	μ	max	min	μ	max	min
Slab	-1.3	0.7	-3.0	-1.0	0.1	-2.5
Integral	-0.8	2.6	-2.8	-0.4	1.3	-1.4

9.4 Platooning

Since equal distances might give a larger DAF, see section 8.9.2, a comparative study is made for equal and random distances between the vehicles in a platoon. The amount of vehicle events is set to 1, which is insufficient when simulating random distances since there will be an upper and lower limit. This is however neglected in order to retrieve time-efficient results and the study is only made in order to show the difference. The preconditions for the parameter study can be seen in Table 9.11

Table 9.11: Preconditions for the parameter study. ¹ See section 8.4. ² See section 8.7. ³ See section 4.4.4.

Preconditions	
Bridge type	Slab/Integral
Bridge properties	Mean values ¹
Road surface	Smooth
Velocity	100 km/h ²
Suspension	Air ³
Vehicle events	1

9.4.1 Slab bridges

The result from platooning for the slab bridges can be seen in Figure 9.12 and 9.13.

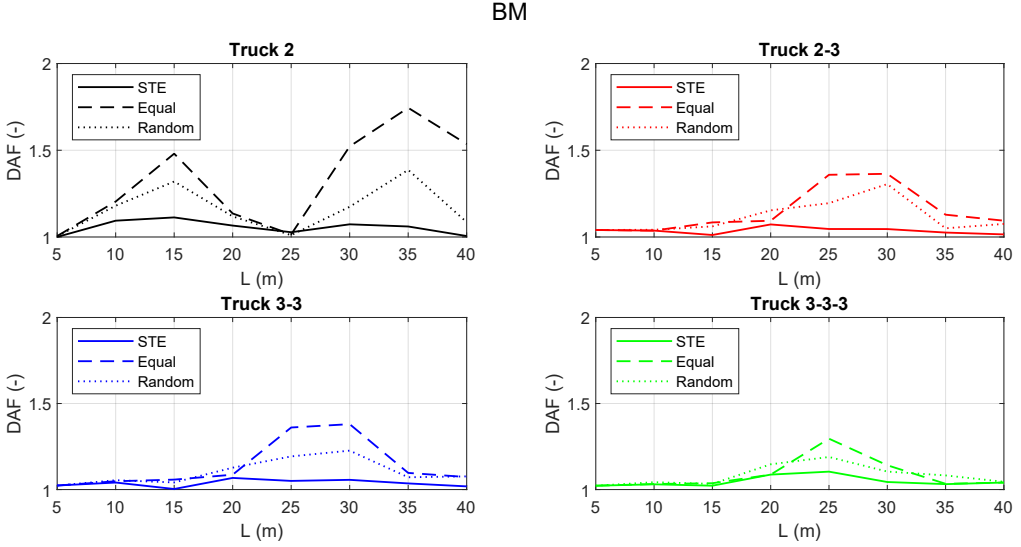


Figure 9.12: DAF (BM) for platoons with equal and random distances and for a single truck event (STE).

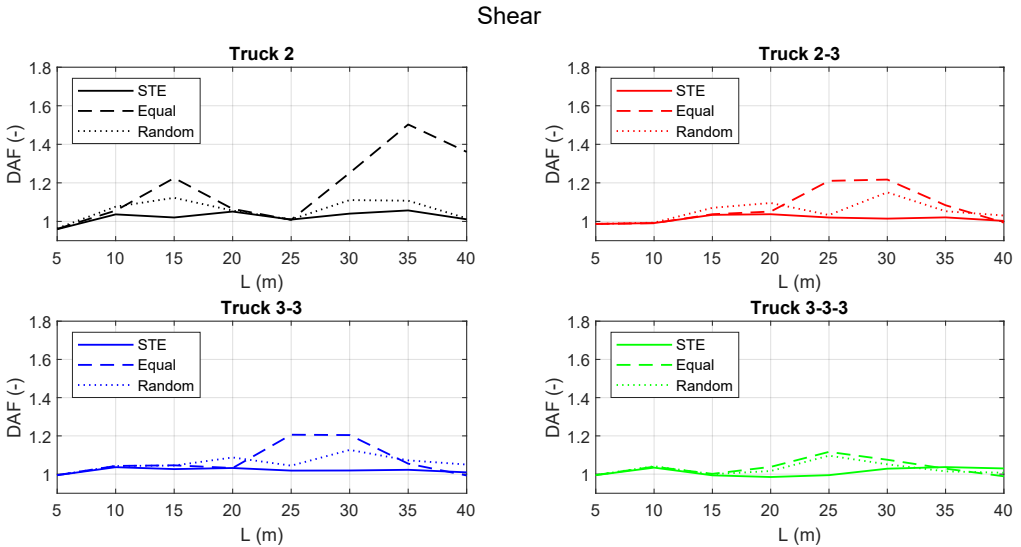


Figure 9.13: DAF (Shear) for platoons with equal and random distances and for a single truck event (STE).

As can be seen there are not large peaks for the DAF for every bridge length. This is due to the fact that distances between axles also fall within the range of cancellation distances, see section 4.3.3 about cancellation. The phenomena can be seen for both random and equal distances which confirms the assumption of cancellation. Note also that the DAF is mainly amplified for bridge lengths that are longer than the axle length of the vehicle, $L_{v,ax}$.

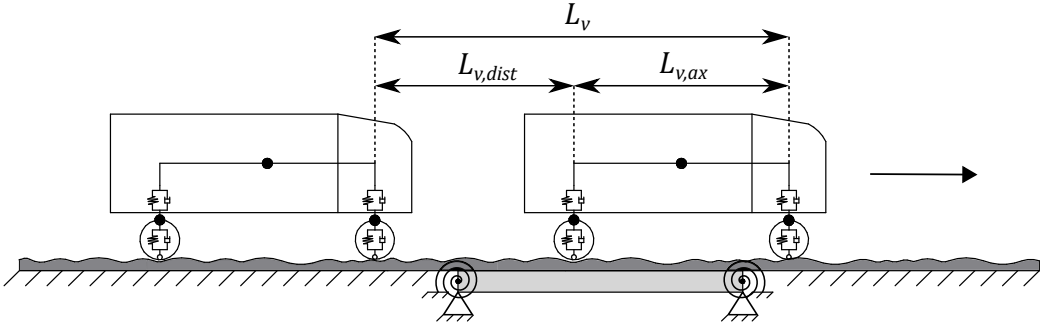


Figure 9.14: Different distances between vehicles that can induce resonance and cancellation for Truck 2, $L_{v,ax}$ and $L_{v,dist}$.

The different lengths that can induce resonance or cancellation for Truck 2 can be seen in Figure 9.14. The closest cancellation lengths, L_{canc} , to the two distances, $L_{v,ax}$ or $L_{v,dist}$, as well as the difference in length, ΔL_{canc} , is presented in Table 9.12 for Truck 2. The resonant length, L_{res} , closest to $L_{v,ax}$ is also presented and the difference ΔL_{res} . As can be seen the closer to a cancellation length, i.e. smaller ΔL_{canc} , the smaller the DAF, see Figure 9.12. Note especially for the bridge length of 25 m for Truck 2, where a cancellation length of 3.85 m is close to the axle distance of 3.75 m. It can be seen that the resonant length is close to $L_{v,ax}$ at a bridge length of 5 m. However, since ΔL_{canc} is quite small the effect of resonance is not amplified as it is for other bridge lengths.

Coincidental frequencies could also be a factor when studying the peaks in the figures. Both Truck 2-3 and 3-3 experiences peaks at bridge lengths of 25 and 30 m, which are at coincidental frequencies. Note also that the peak for Truck 3-3-3 at a bridge length of 25 m can also be seen in the STE for the slab bridges, see Figure 9.1. Note also that the bridge to vehicle mass ratio, m_b/m_v , is a significant factor, where Truck 2 experiences much larger peaks than the heavier semi-trailers.

Table 9.12: Distances $L_{v,ax}$ (rounded to 3.8 m) or $L_{v,dist}$ and the closest cancellation length L_{canc} for the bridge length L for Truck 2. The difference in length, ΔL_{canc} , is also given. The resonant length, L_{res} , closest to $L_{v,ax}$ is also presented and the difference ΔL_{res} .

L	5	10	15	20	25	30	35	40
L_v	14.5	14.4	14.8	16.8	15.6	20.0	12.5	15.1
$L_{v,dist}$ or $L_{v,ax}$	10.7	10.7	3.8	13.0	3.8	3.8	3.8	3.8
L_{canc}	10.9	11.2	5.5	13.8	3.9	5.0	6.2	7.5
ΔL_{canc}	0.2	0.5	1.7	0.8	0.1	1.2	2.4	3.7
L_{res}	3.8	4.1	3.7	5.6	7.8	10.0	12.5	15.1
ΔL_{res}	0.1	0.4	0.1	1.8	4.0	6.3	8.7	11.4

9.4.2 Integral bridges

The result from platooning for the integral bridges can be seen in Figure 9.15 and 9.16.

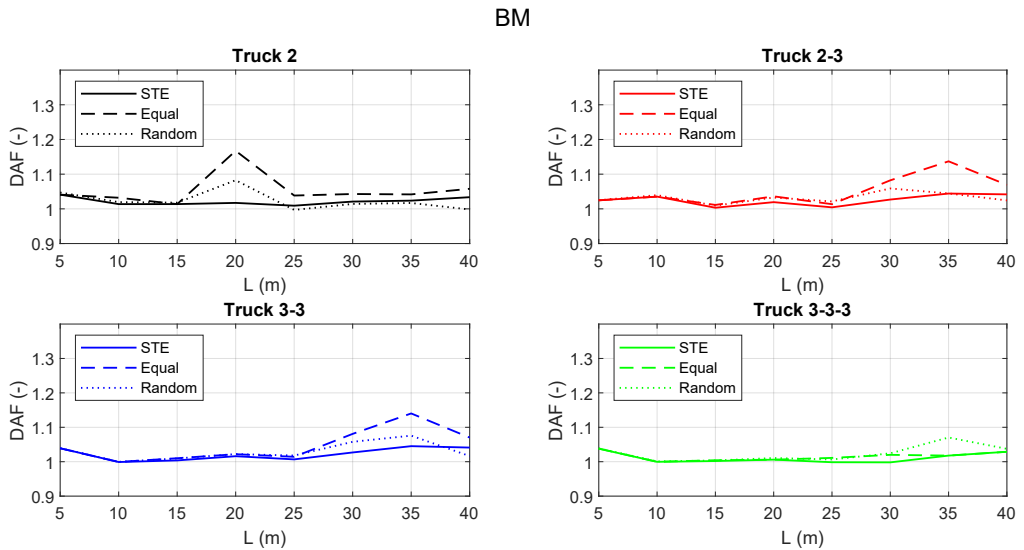


Figure 9.15: DAF (BM) for platoons with equal and random distances and for a single truck event (STE).

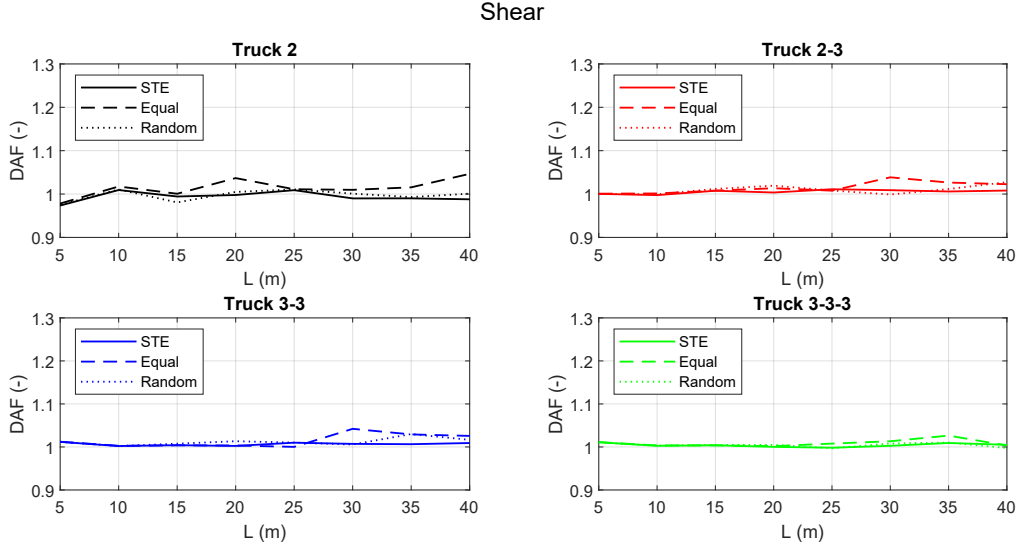


Figure 9.16: DAF (Shear) for platoons with equal and random distances and for a single truck event (STE).

As can be seen there are not large peaks for the DAF at every bridge length. This is also due to the fact that distances between axles fall within the range of cancellation distances here as well. Note for example that at the bridge length of 20 m for Truck 2 that the cancellation distances closest to the axle length is 2 and 6 m, whereas for other bridge lengths are closer to 3.75 m.

The closest cancellation lengths for Truck 2, L_{canc} , to the two distances, $L_{v,ax}$ or $L_{v,dist}$ in Figure 9.14, as well as the difference in length, ΔL_{canc} , is presented in Table 9.13. The resonant length, L_{res} , closest to $L_{v,ax}$ is also presented and the difference ΔL_{res} . It can be noted that at 20 m, L_{res} is close to the axle length and that the response is amplified for the equidistant platoon with resonant distance L_v compared to one with random distances.

Table 9.13: Distances $L_{v,ax}$ (rounded to 3.8 m) or $L_{v,dist}$ and the closest cancellation length L_{canc} for the bridge length L for Truck 2. The difference in length, ΔL_{canc} , is also given. The resonant length, L_{res} , closest to $L_{v,ax}$ is also presented and the difference ΔL_{res} .

L	5	10	15	20	25	30	35	40
L_v	13.8	14.5	16.1	15.7	15.9	20.5	16.9	20.3
$L_{v,dist}$ or $L_{v,ax}$	3.8	3.8	3.8	11.9	12.2	16.7	3.8	3.8
L_{canc}	4.1	4.0	4.0	13.6	13.1	16.9	4.2	5.0
ΔL_{canc}	0.3	0.2	0.2	1.7	1.0	0.2	0.4	1.3
L_{res}	3.7	3.2	2.7	3.9	5.3	6.8	8.4	10.2
ΔL_{res}	0.1	0.5	1.1	0.2	1.6	3.1	4.7	6.4

9.4.3 Summary

The vehicle distances induces cancellation as well as resonance since not all axle positions are at equal lengths. Since there are many axles for vehicle models 2-3, 3-3, 3-3-3 there will be many possible combinations for both cancellation and resonance. It is possible to simulate a constant distance of the total axle length for the vehicles. For Truck 2 this is not applicable in practice since the vehicle distances would be too short. A study also shows that using $L_{v,ax}$ between vehicles instead of L_v does not induce a larger DAF with the constant speed of 100 km/h. In order to get larger values on the DAF, the velocity would need to be changed accordingly but that would give a large variation of the velocity.

It is also noted that the bridge to vehicle mass ratio, m_b/m_v , is a factor also for platooning, where Truck 2 experiences the largest peaks which corresponds well to the trend of m_b/m_v in Figure 4.19. Coincidental frequencies are also a factor. It is also possible that using a lower velocity than 100 km/h would induce a larger DAF for some bridge lengths, but it is still assumed that the largest peaks are found at the present speed of 100 km/h.

The difference in percentage for equal and random distances can be seen in Table 9.14 based on all vehicle models. Positive values indicate that a platoon of equal distances induces a larger DAF than one with random. The largest peaks can be found for slab bridges since there is no rotational stiffness at the boundary nodes and that a larger mass is attributed to these bridges.

As much as around 46 % increase of the DAF can be seen for slab bridges whereas integral bridges have a maximum of approximately 9 %.

Table 9.14: Difference (%) between equal and random distances in a platoon for the bridge lengths of 5-40 m for BM and Shear. The positive values indicate that equal distances induce a larger DAF than random.

Bridge	Type	Suspension	L							
			5	10	15	20	25	30	35	40
Slab	BM	Air	0.1	2.1	12.2	1.5	14.1	29.6	25.8	41.5
		Leaf	0.3	1.8	9.2	0.7	12.9	31.6	46.2	27.2
	Shear	Air	0.0	0.0	9.1	2.1	17.2	12.7	35.7	33.9
		Leaf	0.2	1.0	8.3	3.4	17.5	17.6	48.2	26.9
Integral	BM	Air	0.0	1.2	0.2	7.8	4.2	2.8	8.9	6.0
		Leaf	0.0	0.7	0.2	5.9	3.9	2.5	5.3	5.1
	Shear	Air	0.3	0.7	2.0	3.2	1.1	4.0	2.3	4.6
		Leaf	0.3	0.3	1.7	0.4	1.3	4.5	2.4	5.4

9.5 Soil-structure interaction

The preconditions when evaluating the soil-structure interaction can be seen in Table 9.17. The soil properties of moraine is evaluated since this is the most common soil in Sweden (SGU 2000). Sand and gravel gives a similar response but gives a larger DAF than moraine, see Figure 8.12. The stiffness and damping used for the maximum, mean and minimum values of the soil can be seen in Table 9.15. The soil mass is set to 0 according to section 5.2. The speed is varied according to section 8.7. The difference between air and leaf suspension is negligible and therefore only air suspension is used. The bridge fundamental frequencies can be seen in Table 9.16. The frequencies can be seen to vary according to the stiffness of the soil.

Table 9.15: Properties for moraine (Mn) used in the parameter study.

Property	Max	μ	Min
Stiffness, K (GN/m)	46.7	14.2	1.6
Damping, C (MNs/m)	834.8	311.0	49.8

Table 9.16: Bridge fundamental frequencies, f_1 , for the maximum, mean and minimum values on the soil stiffness, K , according to Table 9.15.

L (m)	5	10	15	20	25	30	35	40
Min (Hz)	14.17	10.51	7.79	5.88	4.58	3.68	3.03	2.56
μ (Hz)	28.66	16.50	10.15	7.00	5.20	4.06	3.29	2.74
Max (Hz)	30.14	17.13	10.37	7.11	5.26	4.10	3.31	2.75

Table 9.17: Preconditions for the parameter study. ¹ See section 8.4. ² See section 8.5. ³ See section 8.7. ⁴ See section 4.4.4.

Preconditions	
Bridge type	Integral
Bridge properties	Mean values ¹
Soil properties	Moraine ²
Road surface	Smooth
Velocity	100 to 110 km/h ³
Suspension	Air ⁴
Vehicle events	1

9.5.1 Integral bridges

The results for the STE and SSI for BM can be seen in Figure 9.17. The result when applying the maximum, mean and minimum values on the soil properties according to Table 9.15 is plotted in dotted, dashed and dash-dotted lines. As can be seen, the major difference occur at short bridges, especially for Truck 2 and 2-3. At longer bridge lengths the difference is not as large.

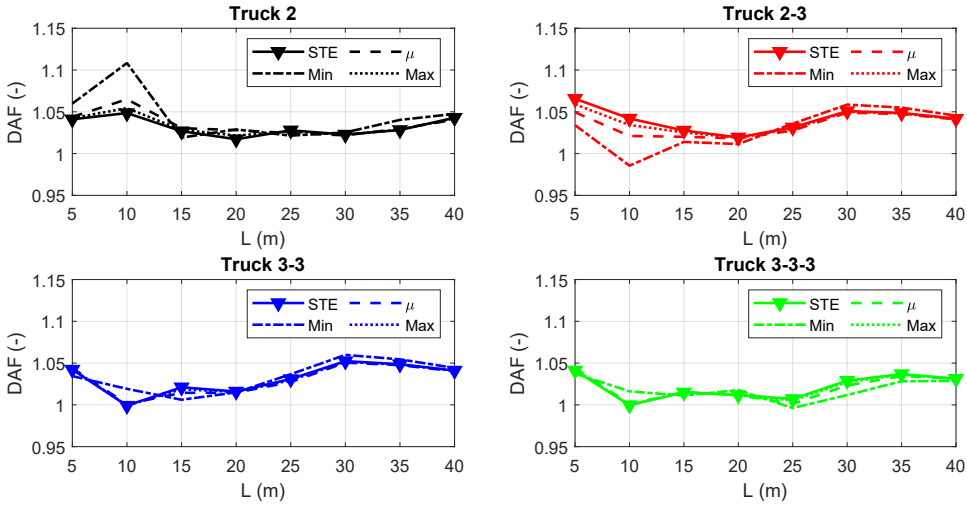


Figure 9.17: DAF (BM) for a STE and when implementing SSI with minimum, μ and maximum values on Mn.

The difference in percentage between the STE and when implementing SSI can be seen in Figures 9.18 - 9.21 for the different vehicle models. Negative values correspond to a lower DAF for the SSI. The limits of the evaluation is coloured in the figures.

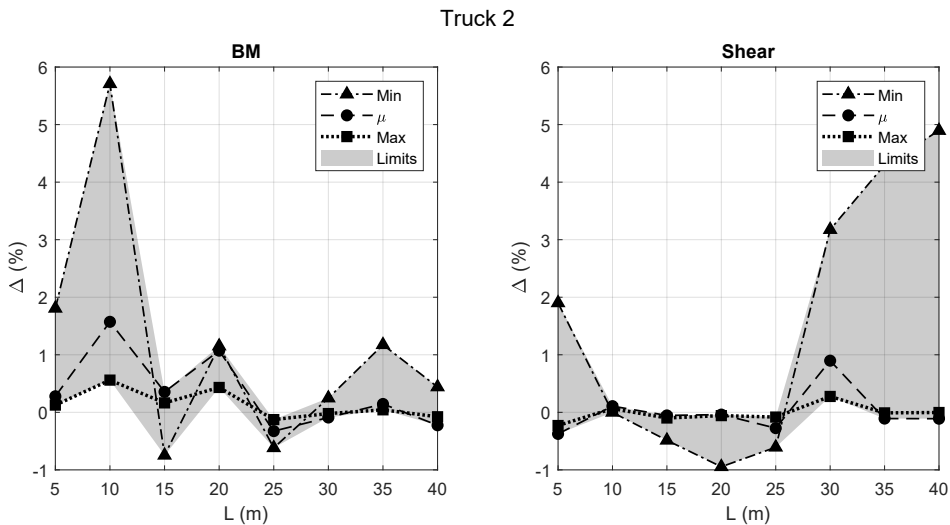


Figure 9.18: Difference (%) of the DAF for Truck 2 between a STE and when implementing SSI with minimum, μ and maximum values on Mn.

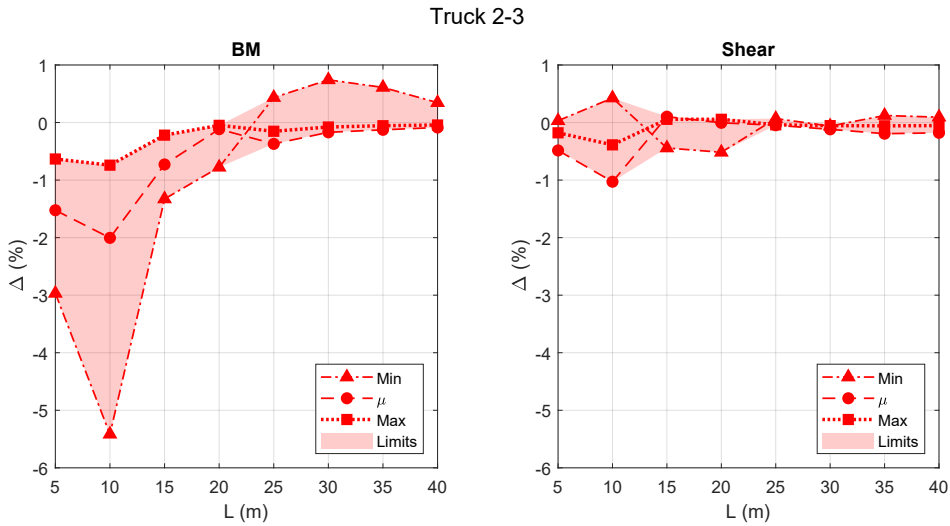


Figure 9.19: Difference (%) of the DAF for Truck 2-3 between a STE and when implementing SSI with minimum, μ and maximum values on M_n .

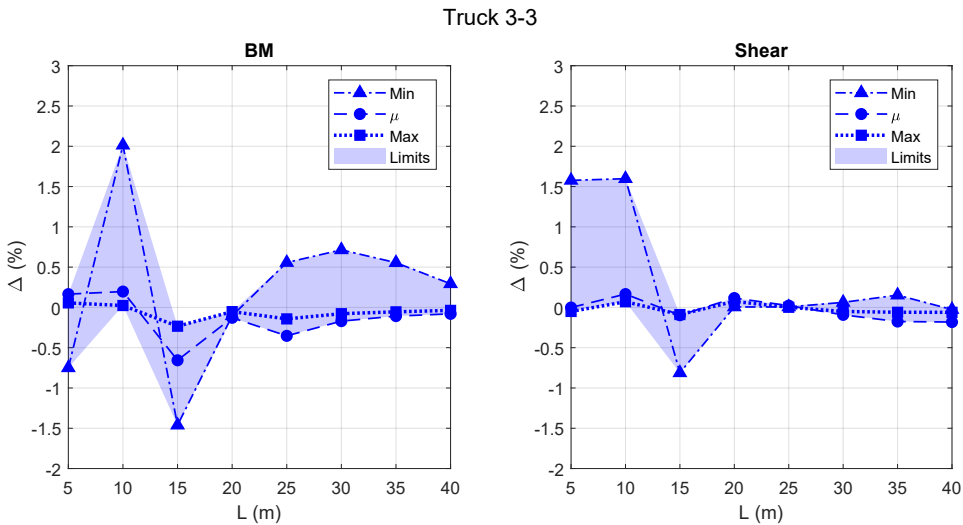


Figure 9.20: Difference (%) of the DAF for Truck 3-3 between a STE and when implementing SSI with minimum, μ and maximum values on M_n .

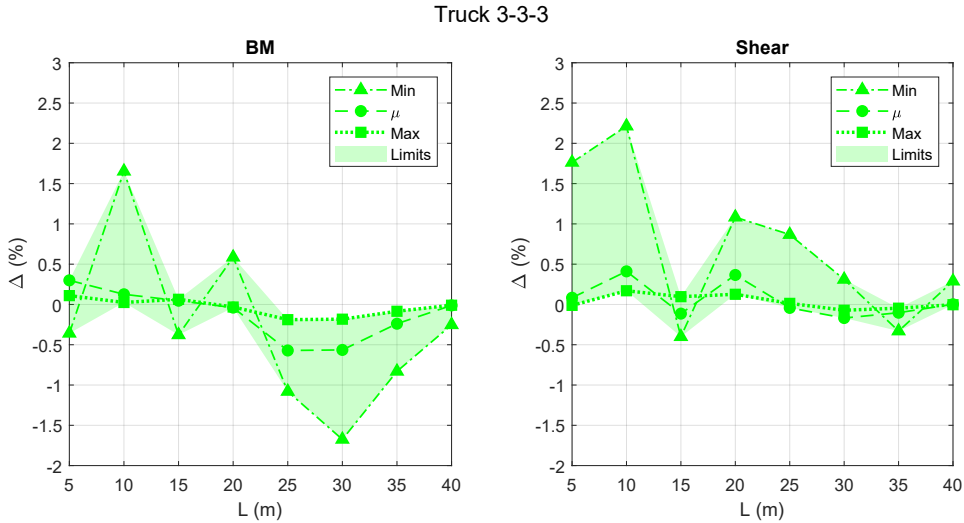


Figure 9.21: Difference (%) of the DAF for Truck 3-3-3 between a STE and when implementing SSI with minimum, μ and maximum values on Mn.

As can be seen the difference is largest for Truck 2-3 at the length of 10 m for the minimum values on the soil properties. This could have to do with resonant lengths as well as an effect of the SSI. An analysis of the time signal for BM at a bridge length of 10 m for Truck 2-3 shows the reason to the lower DAF. As can be seen in Figure 9.22, the dynamic BM is amplified at the first peak, i.e. at the blue ring marker for the dash-dotted line. This is due to the elastic spring at the boundaries that induces a different behaviour than when having no vertical translation, i.e. the average response from bridge and vehicle is amplified. The STE and SSI events for the maximum DAF are at different velocities, and they are therefore out of phase to each other in the figure.

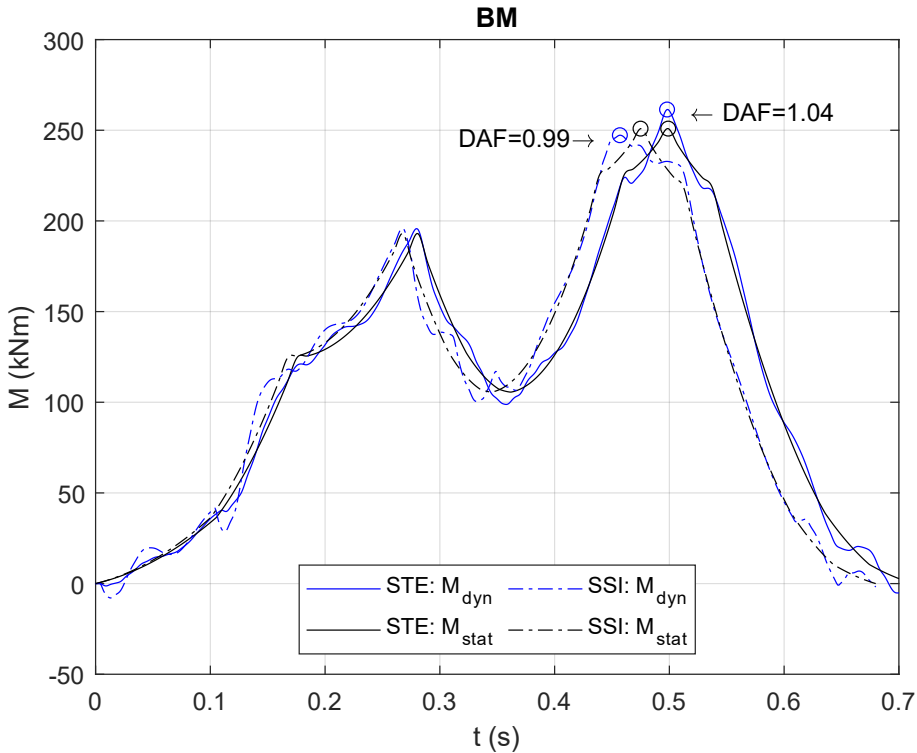


Figure 9.22: Dynamic and static BM for a STE and when implementing SSI (minimum values on M_n) for Truck 2-3 at a bridge length of 10 m.

An FFT analysis of the same vehicle and bridge length shows that the forces at the wheels are larger when implementing SSI with minimum values on the soil properties. The acceleration at mid-span is also amplified, see Figure 9.23. It is also seen that the vehicle eigenfrequencies coincide with the bridges' for the SSI, note the wheel forces at around 10 Hz. It is therefore assumed that the elastic springs at the boundaries gives a larger acceleration and response in most cases, and that the smaller values on the DAF is mainly due to peaks of the DAF at other locations than the usual maxima, i.e. for the STE's, with relaxation afterwards due to an upward deflection of the bridge due to the boundary conditions and vehicle response.

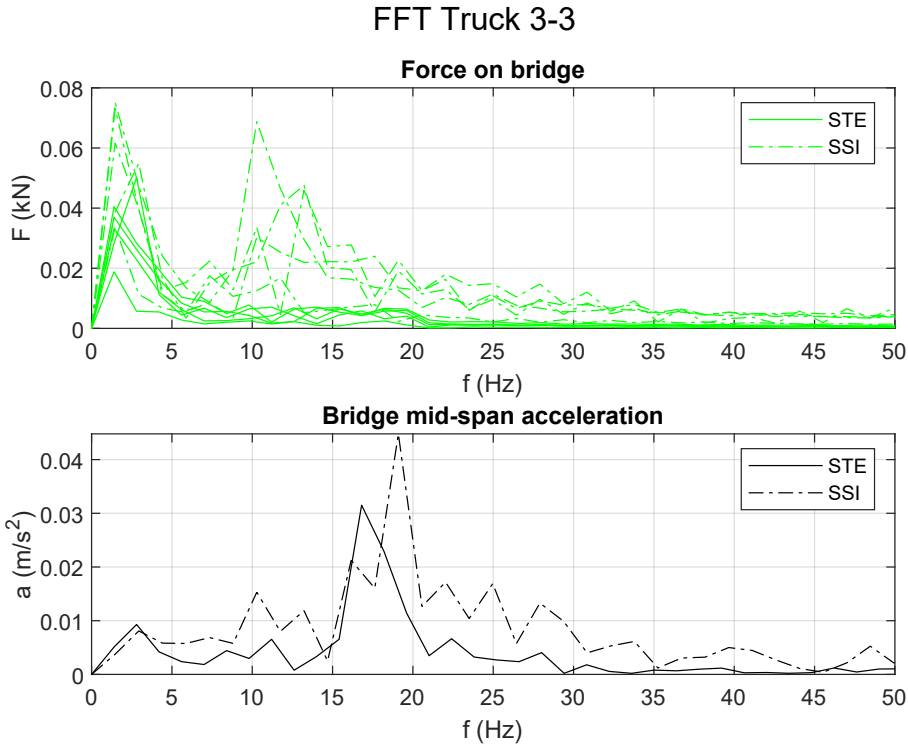


Figure 9.23: FFT analysis of the wheel forces for Truck 2-3 and the bridge mid-span acceleration at a bridge length of 10 m for a STE and when implementing SSI (minimum values on Mn).

To confirm the previous behaviour, an analysis of Truck 3-3 is also performed for bridge lengths of 5, 10 and 15 m with all properties (minimum, μ and maximum) of the soil. The BM for the bridge lengths can be seen in Figures 9.24 - 9.26. As can be seen, the response is amplified when having elastic boundaries. Note for example in Figure 9.26 that the DAF experiences a peak for SSI (min) right before the STE maximum, i.e. the response is amplified at around 0.56 s. This is due to an amplified response of the vehicle and bridge at that point. If the DAF for SSI (min) were to be based on the maximum BM and the static BM at that point the DAF would be 1.03, i.e. larger than for the STE. It is therefore also highly dependent on the assumptions on how the DAF is retrieved.

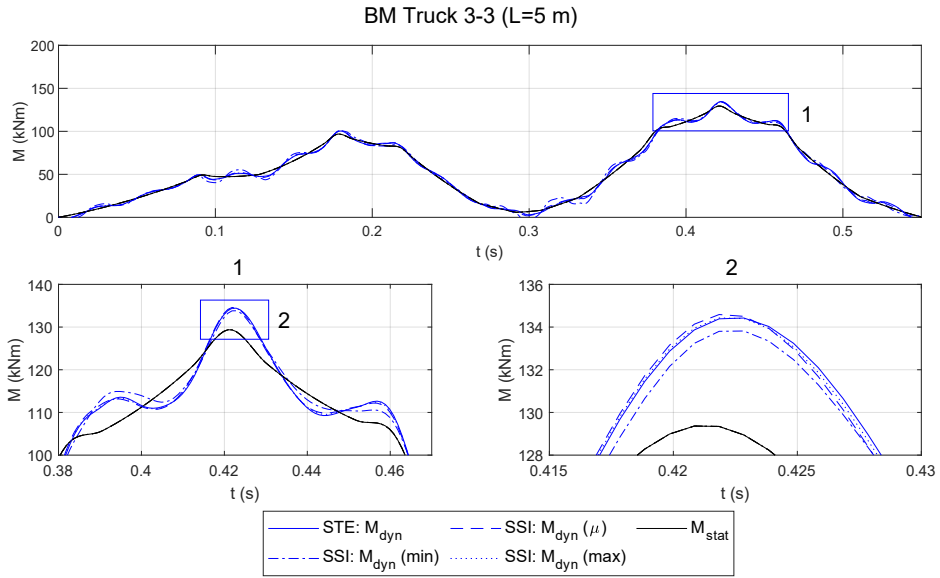


Figure 9.24: Dynamic and static BM for a STE and when implementing SSI for Truck 3-3 at a bridge length of 5 m. The two bottom subplots are zoomed in at the maximum.

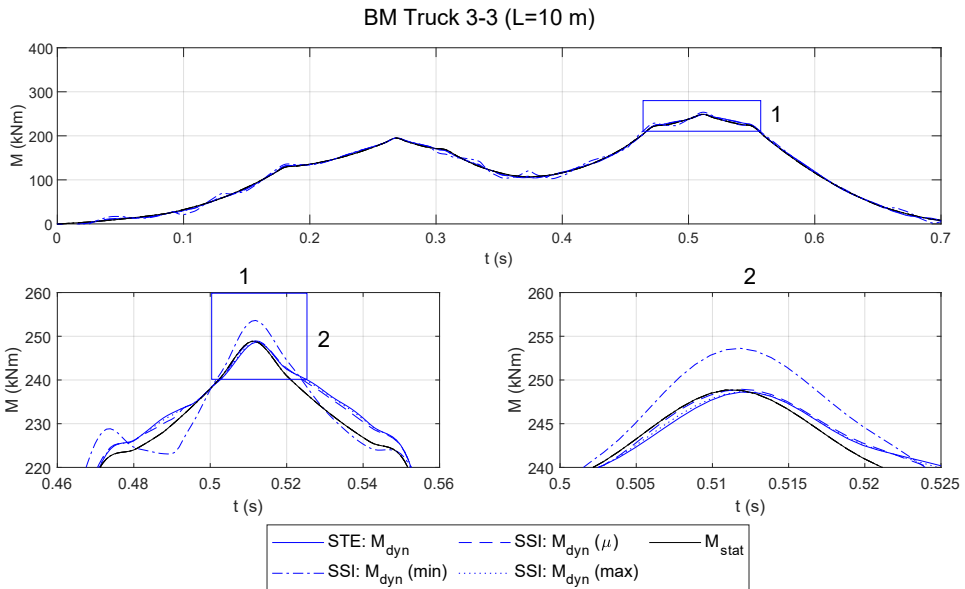


Figure 9.25: Dynamic and static BM for a STE and when implementing SSI for Truck 3-3 at a bridge length of 10 m. The two bottom subplots are zoomed in at the maximum.

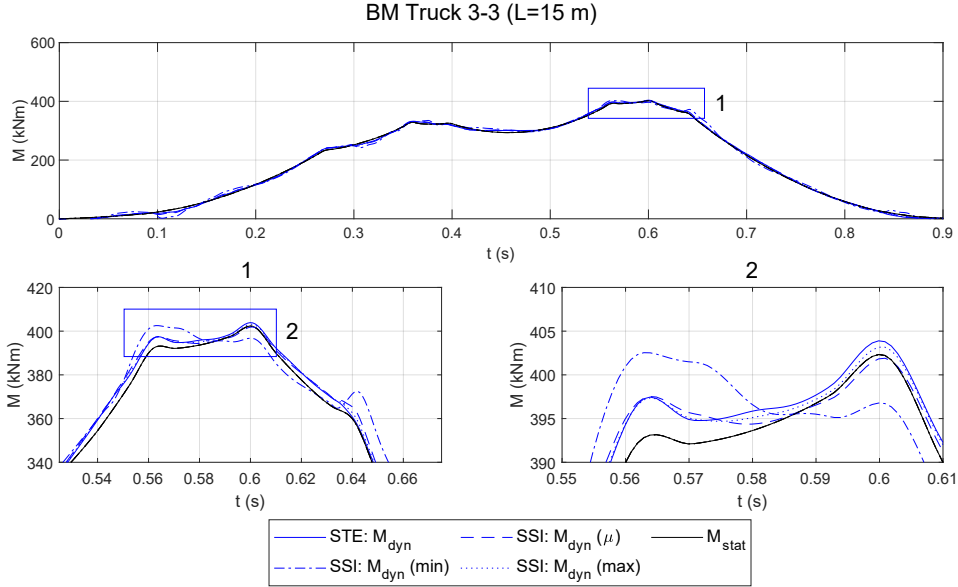


Figure 9.26: Dynamic and static BM for a STE and when implementing SSI for Truck 3-3 at a bridge length of 15 m. The two bottom subplots are zoomed in at the maximum.

The normalized mid-span displacement for the two maxima (at around 0.56 s and 0.6 s) for Truck 3-3 at a bridge length of 15 m and with minimum values on the soil properties can be seen in Figure 9.27. As can be seen, the displacement at the mid-span moves upwards after the first peak, and the difference is much larger for the SSI.

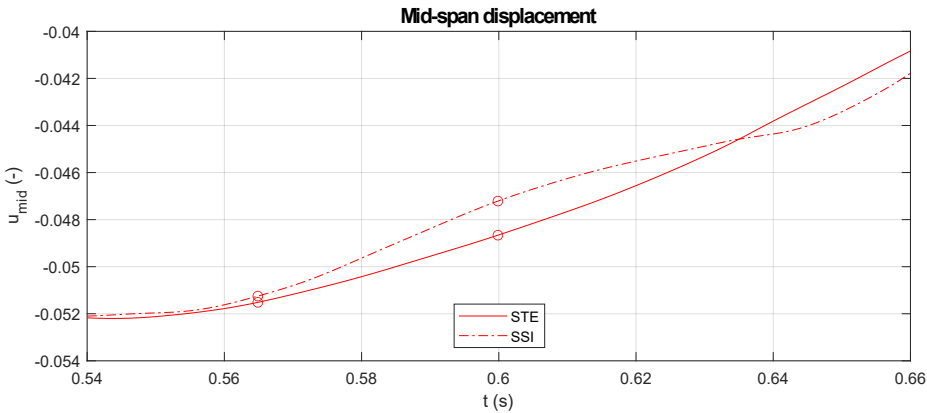


Figure 9.27: Normalized mid-span displacement for the bridge in Figure 9.26 for a STE and SSI with minimum values on the soil.

An FFT analysis of the vehicle force for the first wheel is performed for Truck 3-3 at bridge lengths of 5, 10 and 15 m, see Figure 9.28. The acceleration is yet again larger for the SSI compared to the STE. The same can be seen for the other wheel forces but they are not plotted in the figure. The response is reduced with an increased stiffness of the elastic spring. An FFT of the acceleration at mid-span can be seen in Figure 9.29, and the same behaviour is noted. The acceleration for SSI with μ and maximum values on the soil are barely seen in the figure since they are very close to the STE acceleration. This shows again that the response for the bridges are highly dependent on the stiffness of the soil.

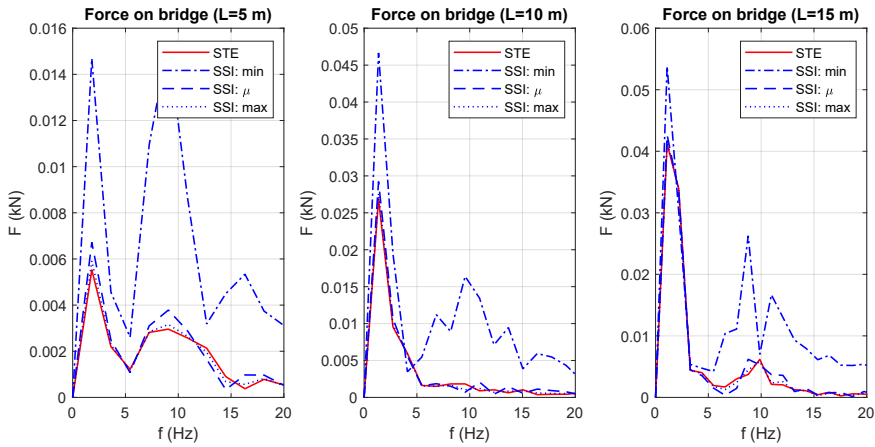


Figure 9.28: FFT analysis of the first wheel force for Truck 3-3 at a bridge length of 5, 10 and 15 m.

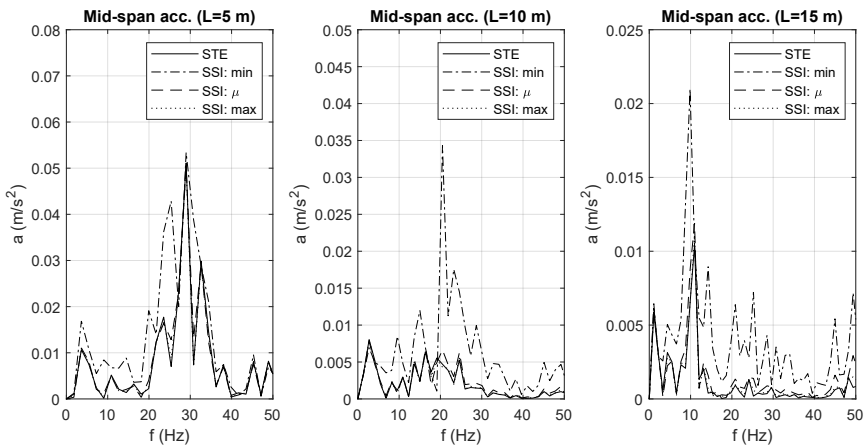


Figure 9.29: FFT analysis for Truck 3-3 of the bridge mid-span acceleration at a bridge length of 5, 10 and 15 m.

Part III

Review

Chapter 10

Discussion

10.1 Bridges

The approximations of the bridge parameters are quite generalized and many parameters such as skewness and slanting of the bridges are not taken into account. The rotational stiffness is also assumed to be for that of a 4-lane bridge, and thus larger than for a bridge with fewer lanes. A lower value of the rotational stiffness could have been used for safe-sided results, but that would not have been realistic values. The DAF for bridges with fewer lanes would therefore have to be investigated further. However, the results for the slab bridges are assumed to be valid for both single- and multi-lane bridges, since safe-sided results are provided due to the larger bridge to vehicle mass ratio. The ratio could be seen to be one of the main factors. More realistic values on the damping ratio, ζ , could also give lower values on the DAF.

10.2 Convergence

The number of vehicle events, ie. 1000, for the STE and MTE are lower than the required in order to achieve convergence. The number of events are however sufficient in order to study the behaviour of the DAF depending on bridge length and frequency. However, in order to retrieve a more accurate value of the upper limit of the DAF, a larger number of events need to be simulated.

10.3 Trafikverket

The DAF according to Trafikverket (2019b) is quite inaccurate for the STE and other norms, such as the Swiss norm for single truck loading (SIA-T) is more appropriate. For very short bridges, with a high f_1 , the Swedish norm is more in agreement with the STE. However, for longer bridges with a lower f_1 the norm is insufficient for the STE due to coincidental frequencies.

For the MTE it can also be concluded that the Swedish norm is inaccurate. The Swiss (SIA-T) is a better fit for the slab bridges. For the integral bridges, which have no f_1 around 1.0-2.7 Hz, the Swiss norm for lane loading (SIA-L) is a better fit except for some outliers, for example at around 10 Hz which is a coincidental frequency.

Since the loading scenarios in Trafikverket (2019b) consists of single as well as multiple vehicles it is therefore assumed that the maximum DAF should be retrieved from the STE and MTE, and an approximation based on bridge fundamental frequency could be appropriate.

Air suspension gives a smaller contribution to the DAF compared to leaf suspension for low bridge f_1 close to the lowest vehicle modes (suspension modes). This is due to the increased stiffness of leaf suspension. Another explanation could be that the bridge f_1 gets lower values due to the increased mass from the vehicle, see Figure 4.7, and coincides with an eigenfrequency for leaf suspension. However, since peaks are experienced for leaf suspension for both the slab and integral bridges it is assumed that the increased stiffness is the main factor. In order to determine a lower value on the DAF due to air suspension it would require all vehicles to have this suspension type which might prove difficult in practice.

Heavier vehicles gives a smaller value on the DAF and it is possible that the axle loads in the vehicle scenarios in Trafikverket (2019b) could be attributed different values on the DAF based on the weight of the vehicle.

Information if a bridge is installed with a tuned mass damper could also be useful when evaluating the DAF, since this will lower the response at coincidental frequencies.

10.4 Platooning

Since resonance is an issue for platoons with equal distance, it might be beneficial if the trucks are installed with data information of the location

of bridges in the road network. When a platoon reaches a bridge the distance between trucks can be changed to random distances in order to not induce resonance in the bridge. If a system like this is too expensive or gruesome to develop, an easier approach is to always have random distances as a precaution.

The random distances generated in section 9.4 need to be generated for several events in order to retrieve an upper and lower limit, much like the one for the STE and MTE. This would ensure an accurate ratio, i.e. amplification, for a platoon with random distances and a single truck event for example. Further studies would therefore need to be made and information about an upper limit on the platoon length would be needed, which unfortunately could not be found for this thesis.

The analysis in section 9.4 focuses only on platoons with individual vehicle models and there might exist a combination of vehicles, most likely a combination of the lighter vehicle models 2, 2-3 and 3-3, that would induce a worse situation for some bridge lengths. However, a scenario like that would be statistically unlikely.

10.5 Soil

The dynamic stiffness in this thesis is only retrieved for a dimensionless frequency, a_0 , below 1.5 which is quite inadequate. A study on the dynamic stiffness for higher frequencies, e.g. retrieving a rigorous solution and approximating with lumped parameter models with more DOF's than the one used in this thesis could improve the results.

In order to incorporate the soil when classifying bridges it would be beneficial with information of the soil properties beneath and behind the integral legs. A software that calculates a DAF based on these parameters as well as the bridge properties would be an interesting approach when determining a bearing capacity class. Otherwise, a simplification could be to retrieve a maximum percentage increase of the DAF based on which soil surrounds the bridge without having to perform additional calculations.

Chapter 11

Conclusions

The DAF depends mainly on:

- Coincidental frequencies: An amplified response of the DAF is obtained when the eigenfrequencies of the vehicle and bridge fundamental frequency coincide.
- Vehicle speed and road irregularities: A higher velocity and a rougher road surface gives a larger DAF. A comparison of the results for a STE with smooth and class A road surface shows that a rougher surface gives a larger DAF.
- Bridge to vehicle mass ratio, m_b/m_v : A larger ratio gives a larger DAF.
- Suspension stiffness: Leaf suspension gives a larger DAF for low bridge fundamental frequencies close to the lowest vehicle modes, i.e. suspension modes.
- Resonance and cancellation: Platooning might induce resonance and higher values on the DAF. Random distances for future platoons is recommended.
- Soil-structure interaction: The vehicle and bridge response is amplified with a decrease in soil stiffness with the current soil model, but a smaller DAF is obtained for certain bridge lengths and vehicle models.

The Swedish norm is quite inaccurate and the following conclusions are recommended:

- Basing the DAF on bridge fundamental frequency instead of bridge span seems to be a better approach due to coincidental frequencies.

- The Swiss norm for single truck loading (SIA-T) is quite accurate based on the results, except for conservative values above 15-20 Hz.
- The DAF for shear could perhaps be attributed lower values than for BM, see Figure 11.1, much like the DAF for one-lane bridges in the Eurocode.
 - A varying DAF based on speed limit could be an improvement to a DAF based on fundamental frequency. Other road surface classes than class A might be needed during simulations with lower speed limits since the required IRI values are higher.
 - Heavier vehicles in the vehicle scenarios in Trafikverket (2019b) could be attributed lower values on the DAF whereas lighter vehicles could be attributed higher values due to the bridge to vehicle mass ratio m_b/m_v .
 - If future vehicles would be produced with mainly air suspension, the DAF could perhaps be lowered with 1-6 % based on mean values (could be higher based on maximum values), at least for low bridge frequencies. However, at the current situation where traffic is a mixture between both suspension types this is not possible.

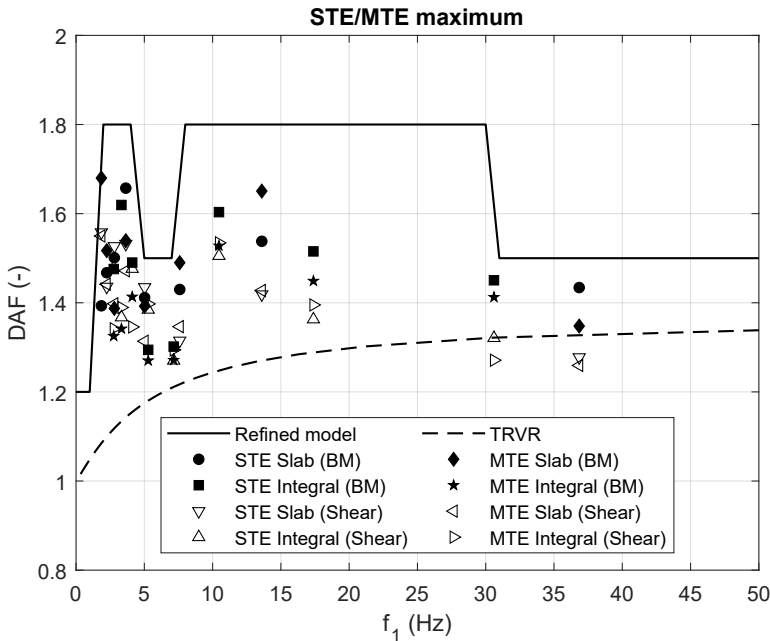


Figure 11.1: Maximum values from the STE and MTE as well as the DAF according to Trafikverket (TRVR) and a refined model.

The maximum values from the STE and MTE is plotted in Figure 11.1, as well as an example of a refined model and the DAF according to Trafikverket (2019b) with $f_1 = 82L^{-0.9}$. The DAF is unknown for values between 20-30 Hz and the top peak (DAF = 1.8) is therefore continued until 30 Hz. An example of how the DAF could be constructed based on fundamental frequency, f_1 , and the speed limit, v , of the road can be seen in Figure 11.2.

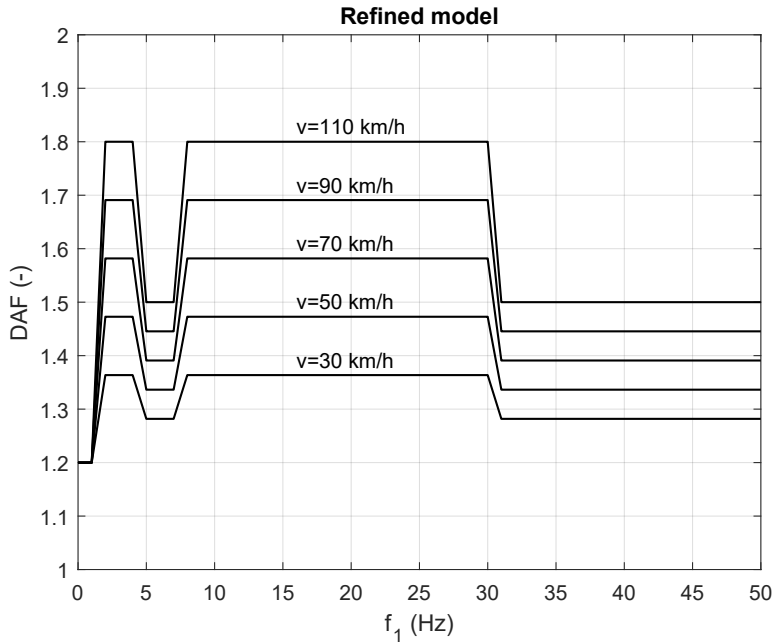


Figure 11.2: An example of how the DAF could be based on fundamental frequency, f_1 , and the speed limit, v .

Chapter 12

Further work

12.1 Bridges

Since this thesis only focus on single lane loading, further work could be to investigate the DAF based on multi-lane loading. Bridges with fewer lanes, i.e. with lower mass and less rotational stiffness, would also need to be investigated. Having smaller increments than 5 m on the bridge lengths would also be necessary in order to retrieve values of the DAF for other bridge fundamental frequencies. Investigation of other types of bridges and multiple span bridges is also needed.

12.2 Vehicles

The studies show that the Swedish norm is insufficient which can be confirmed with previous studies such as Jung, G. Kim, and Park (2013). The vehicles used in this thesis are the most common vehicles on European roads, except for Truck 3-3-3. However, since coincidental frequencies is the main issue more extensive studies with more vehicle models and varying parameters is recommended. Using standard deviation on the vehicle properties, i.e. mass, suspension etc., such as in the study by Cantero, Gonzalez, and Eugene OBrien (2011) could prove valuable in further studies.

Evaluating bridge response based on semi-active or active suspension would also be interesting since the DAF most likely would be lowered. The problem is that the numerical solution would be time-consuming and studies such as Harris, E.J. OBrien, and A. González (2007) where an optimal damping coefficient is used based on the surface irregularities could therefore be a good strategy.

12.3 Speed limit

Since the values on the vehicle velocity has been set between 90-110 km/h, an upper value on the DAF is assumed to have been retrieved and it is mainly for bridges of a speed limit of 90 km/h and above. Studies of bridges where the speed limit is lower could be valuable for further studies. A combination of the Swedish norm with an expression based on fundamental frequency, f_1 , with a varying velocity, v , based on speed limit could be an interesting approach. This would give a lower DAF and subsequently economical and environmental benefits. Note that if a lower speed is used other road surface classes such as class B-C might need to be used according to Table 4.1.

12.4 Platooning

The MTE is assumed to also be a sufficient evaluation of the DAF for platoons. A study could however be needed in order to confirm this. Further studies would need to be made for platoons with random distances and information about an upper limit on the platoon length would be needed.

12.5 Soil

Further studies could also include a more comprehensive evaluation of the soil surrounding the integral legs by modelling the dynamic stiffness with more accurate soil models. An advanced lumped parameter model according to Ibsen and Liingaard (2006) could be used for the vertical translations. A lumped parameter model could be used to get a representation of the soil behind the integral legs as well as the horizontal and rotational motions of the foundations according to Saitoh (2012). A study on the dynamic stiffness with several soil layers and not only an elastic half-space could also be a good compliment.

Bibliography

Articles

- Bhise, Ankita et al. “Comparison Between Passive And Semi-Active Suspension System Using Matlab/Simulink”. In: *IOSR Journal of Mechanical and Civil Engineering* 13 (Apr. 2016), pp. 01–06. DOI: 10.9790/1684-1304010106.
- Cantero, Daniel, Therese Arvidsson, et al. “Train–track–bridge modelling and review of parameters”. In: *Structure and Infrastructure Engineering* 12 (9 2016), pp. 1051–1064. DOI: 10.1080/15732479.2015.1076854.
- Cantero, Daniel, Arturo Gonzalez, and Eugene OBrien. “Comparison of Bridge Dynamic Amplifications due to Articulated 5-Axle Trucks and Large Cranes”. In: *The Baltic Journal of Road and Bridge Engineering* 6 (Mar. 2011), pp. 39–47. DOI: 10.3846/bjrbe.2011.06.
- Cantero, Daniel, Patrick McGetrick, et al. “Experimental monitoring of bridge frequency evolution during the passage of vehicles with different suspension properties”. In: *Engineering Structures* 187 (2019), pp. 209–219. ISSN: 0141-0296. DOI: <https://doi.org/10.1016/j.engstruct.2019.02.065>. URL: <http://www.sciencedirect.com/science/article/pii/S0141029618318996>.
- Caprani, Colin C. et al. “Assessment dynamic ratio for traffic loading on highway bridges”. In: *Structure and Infrastructure Engineering* 8.3 (2012), pp. 295–304. DOI: 10.1080/15732471003667645. eprint: <https://doi.org/10.1080/15732471003667645>. URL: <https://doi.org/10.1080/15732471003667645>.
- Deng, Lu et al. “State-of-the-Art Review of Dynamic Impact Factors of Highway Bridges”. In: *Journal of Bridge Engineering* 20 (5 2014). DOI: /10.1061/(ASCE)BE.1943-5592.0000672.
- Harris, N.K., E.J. OBrien, and A. González. “Reduction of bridge dynamic amplification through adjustment of vehicle suspension damping”. In: *Journal of Sound and Vibration* 302.3 (2007), pp. 471–485. ISSN: 0022-

- 460X. DOI: <https://doi.org/10.1016/j.jsv.2006.11.020>. URL: <http://www.sciencedirect.com/science/article/pii/S0022460X06008844>.
- Hester, David and Arturo González. “A bridge-monitoring tool based on bridge and vehicle accelerations”. In: *Structure and Infrastructure Engineering* 11.5 (2015), pp. 619–637. DOI: 10.1080/15732479.2014.890631. URL: <https://doi.org/10.1080/15732479.2014.890631>.
- Johansson, C., C. Pacoste, and R. Karoumi. “Closed-form solution for the mode superposition analysis of the vibration in multi-span beam bridges caused by concentrated moving loads”. In: *Computers & Structures* 119 (2013), pp. 85–94. ISSN: 0045-7949. DOI: <https://doi.org/10.1016/j.compstruc.2013.01.003>. URL: <http://www.sciencedirect.com/science/article/pii/S0045794913000138>.
- Jung, Hyunjun, Gyuseon Kim, and Cheolwoo Park. “Impact factors of bridges based on natural frequency for various superstructure types”. In: *KSCE Journal of Civil Engineering* 17 (Mar. 2013). DOI: 10.1007/s12205-013-1760-4.
- Lou, Ping and Francis Au. “Finite element formulae for internal forces of Bernoulli–Euler beams under moving vehicles”. In: *Journal of Sound and Vibration* 332 (Mar. 2013), pp. 1533–1552. DOI: 10.1016/j.jsv.2012.11.011.
- Ludescher, Hannes and Eugen Brühwiler. “Dynamic Amplification of Traffic Loads on Road Bridges”. In: *Structural Engineering International* 19.2 (2009), pp. 190–197. DOI: 10.2749/101686609788220231. URL: <https://doi.org/10.2749/101686609788220231>.
- McGetrick, Patrick et al. “Dynamic axle force and road profile identification using a moving vehicle”. In: *International Journal Architecture, Engineering & Construction* 2 (Mar. 2013).
- Mohammed, Omar and Arturo González. “Static and dynamic moments for any plane within a straight solid slab bridge caused by the crossing of a truck”. In: *Engineering Structures* 150 (2017), pp. 465–480. ISSN: 0141-0296. DOI: <https://doi.org/10.1016/j.engstruct.2017.07.059>. URL: <http://www.sciencedirect.com/science/article/pii/S0141029617323787>.
- Mohammed, Omar, Arturo Gonzalez, and Daniel Cantero. “Dynamic impact of heavy long vehicle with equally spaced axles on short-span highway bridges”. In: *The Baltic Journal of Road and Bridge Engineering* 13 (Mar. 2018), pp. 1–13. DOI: 10.3846/bjrbe.2018.382.
- Mohseni, Iman et al. “Development of Dynamic Impact Factor Expressions for Skewed Composite Concrete-Steel Slab-On-Girder Bridges”. In: *Advances in Materials Science and Engineering* 2018 (July 2018), pp. 1–9. DOI: 10.1155/2018/4313671.

- Paeglite, Ilze and Ainars Paeglitis. “The Dynamic Amplification Factor of the Bridges in Latvia”. In: *Procedia Engineering* 57 (Dec. 2013), pp. 851–858. DOI: 10.1016/j.proeng.2013.04.108.
- Paultre, Patrick, Omar Chaallal, and Jean Proulx. “Bridge dynamic and dynamic amplification factors—a review of analytical and experimental findings”. In: *Canadian Journal of Civil Engineering* 19 (Apr. 1992), pp. 260–278. DOI: 10.1139/192-032.
- Saitoh, Masato. “Lumped parameter models representing impedance functions at the end of a finite beam on a viscoelastic medium”. In: *Computers & Structures* 92-93 (2012), pp. 317–327. ISSN: 0045-7949. DOI: <https://doi.org/10.1016/j.compstruc.2011.10.011>. URL: <http://www.sciencedirect.com/science/article/pii/S0045794911002586>.
- Tyan, Feng et al. “Generation of Random Road Profiles”. In: *J. Advanced Eng.* 4 (Jan. 2009).
- Yang, Y.B. and J.D. Yau. “Resonance of high-speed trains moving over a series of simple or continuous beams with non-ballasted tracks”. In: *Engineering Structures* 143 (2017), pp. 295–305. ISSN: 0141-0296. DOI: <https://doi.org/10.1016/j.engstruct.2017.04.022>. URL: <http://www.sciencedirect.com/science/article/pii/S0141029616308173>.
- Yeong-Bin Yang and Bing-Houng Lin. “Vehicle-Bridge Interaction Analysis by Dynamic Condensation Method”. In: *Journal of Structural Engineering* 121 (11 1995).
- Zhu, X.Q. and S.S. Law. “DYNAMIC LOAD ON CONTINUOUS MULTI-LANE BRIDGE DECK FROM MOVING VEHICLES”. In: *Journal of Sound and Vibration* 251.4 (2002), pp. 697–716. ISSN: 0022-460X. DOI: <https://doi.org/10.1006/jsvi.2001.3996>. URL: <http://www.sciencedirect.com/science/article/pii/S0022460X01939963>.

Books

- Austrell, Per Erik et al. *CALFEM - A finite element toolbox, version 3.4*. English. Studentlitteratur AB, 2004. ISBN: 9789188558237.
- Chopra, Anil K. *Dynamics of Structures. Theory and Applications to Earthquake Engineering*. 4th. Pearson Education, 2013. Chap. 1, 5, 9. ISBN: 978-0-13-285803-8.
- Fřyba, Ladislav. *Dynamics of railway bridges*. Thomas Telford Publishing, 1996. DOI: 10.1680/dorb.34716. eprint: <https://www.icevirtuallibrary.com/doi/pdf/10.1680/dorb.34716>. URL: <https://www.icevirtuallibrary.com/doi/abs/10.1680/dorb.34716>.

- Frýba, Ladislav. *Vibration of solids and structures under moving loads*. Monographs and textbooks on mechanics of solids and fluids. Mechanics of structural systems ; [1]. Noordhoff, 1972. ISBN: 9001324202.
- Ghosn, M. et al. *Design of Highway Bridges for Extreme Events*. CRP-CD. Transportation Research Board, 2003. ISBN: 9780309087506.
- Gonzalez, Arturo. *Vehicle-Bridge Dynamic Interaction Using Finite Element Modelling*. Ed. by David Moratal. Rijeka: IntechOpen, 2010. Chap. 26. DOI: 10.5772/10235. URL: <https://doi.org/10.5772/10235>.
- Guglielmino, Emanuele et al. *Semi-active Suspension Control. Improved Vehicle Ride and Road Friendliness*. Springer-Verlag, 2008. ISBN: 9781848002302.
- Kashem, Saad, Mehran Ektesabi, and Romesh Nagarajah. *Vehicle Suspension Systems and Electromagnetic Dampers*. Springer Tracts in Mechanical Engineering. Springer Singapore, 2018. ISBN: 9789811054778.
- McLean, D.I. et al. *Dynamic Impact Factors for Bridges*. National cooperative highway research program; Synthesis of highway practice. National Academy Press, 1998. ISBN: 9780309068192.
- Mosley, William Henry, Ray Hulse, and John H. Bungey. *Reinforced concrete design to Eurocode 2*. Cham, Switzerland: Palgrave Macmillan, 2012. ISBN: 0230302858.
- Paz, Mario and Young Hoon Kim. *Dynamic Analysis of Beams*. Cham: Springer International Publishing, 2019, pp. 251–289. ISBN: 978-3-319-94743-3. DOI: 10.1007/978-3-319-94743-3_10. URL: https://doi.org/10.1007/978-3-319-94743-3_10.
- Rajapakse, Ruwan. *6 - Elastic Settlement of Shallow Foundations*. Burlington: Butterworth-Heinemann, Jan. 2008, pp. 117–120. ISBN: 978-0-7506-8764-5. URL: <http://www.sciencedirect.com/science/article/pii/B9780750687645500076>.
- Sergio M. Savaresi et, al. *Semi-Active Suspension Control Design for Vehicles*. Butterworth-Heinemann, 2010. ISBN: 9780080966793.
- Sieffert, Jean-Georges and Franck Cevaer. *Handbook of Impedance Functions*. Nantes, France: Editions Ouest-France, 1995. ISBN: 2-908261-32-4.
- Yang, Shaopu, Liqun Chen, and Shaohua Li. *Dynamics of Vehicle-Road Coupled System*. Springer Berlin Heidelberg, 2015. ISBN: 9783662459560.
- Yang, Y B, J D Yau, and Y S Wu. *Vehicle-Bridge Interaction Dynamics*. Singapore: World Scientific, 2004. DOI: 10.1142/5541.

Collections

- Wolf, John P. “Simple physical models for foundation dynamics”. In: *Dynamic Soil-Structure Interaction*. Ed. by Zhang Chuhan and John P. Wolf. Vol. 83. Developments in Geotechnical Engineering. Elsevier, 1998,

pp. 1–70. DOI: [https://doi.org/10.1016/S0165-1250\(98\)80004-7](https://doi.org/10.1016/S0165-1250(98)80004-7). URL: <http://www.sciencedirect.com/science/article/pii/S0165125098800047>.

Conference proceedings

Björnsson, Ivar, Sven Thelandersson, and Fredrik Carlsson. “Simulation of collision loads to bridge supporting structures from heavy goods vehicle traffic on Swedish highways”. English. In: *Safety, Reliability, Risk and Life-Cycle Performace of Structures & Infrastructures*. Ed. by George Deodatis, Bruce R. Ellingwood, and Dan M. Frangopol. United Kingdom: Taylor & Francis, 2013, pp. 2113–2120. ISBN: 978-1-138-00086-5.

Cantieni, Reto. “Dynamic load tests on highway bridges in switzerland - 60 years experience of EMPA”. In: 1983.

Dávila, Arturo and Mario Nombela. “Sartre - Safe Road Trains for the Environment Reducing Fuel Consumption through Lower Aerodynamic Drag Coefficient”. In: *SAE Technical Paper*. SAE International, Oct. 2011. DOI: 10.4271/2011-36-0060. URL: <https://doi.org/10.4271/2011-36-0060>.

González, Arturo, Eugene J. O’Brien, and P. McGetrick. “Detection of Bridge Dynamic Parameters Using an Instrumented Vehicle”. In: 2010.

Hernandez, Eli and John Myers. “Dynamic Load Allowance of a Prestressed Concrete Bridge through Field Load Tests”. In: Sept. 2017.

Internet sources

European Commission. *Cooperative dynamic formation of platoons for safe and energy-optimized goods transportation*. European Commission. Apr. 2017. URL: <https://cordis.europa.eu/project/id/610990> (visited on 02/26/2020).

— *Safe Road Trains for the Environment; developing strategies and technologies to allow vehicle platoons to operate on normal public highways with significant environmental, safety and comfort benefits*. European Commission. May 2017. URL: <https://cordis.europa.eu/project/id/233683> (visited on 02/26/2020).

Lumsden, Kenth. *Truck Masses and Dimensions - Impact on Transport Efficiency*. Oct. 2004. URL: http://modularsystem.eu/download/facts_and_figures/20080522att04.pdf (visited on 01/04/2020).

- NyTeknik. *Se Scantias självkörande "lastbils-plutoner"*. NyTeknik. Dec. 2017. URL: <https://www.nyteknik.se/fordon/se-scantias-sjalvkorande-lastbils-plutoner-6888323> (visited on 02/26/2020).
- Regeringskansliet. *Svensk författningssamling. Förordning om ändring i trafikförordningen (1998:1276)*. 2018. URL: <http://rkrattsdb.gov.se/SFSdoc/18/180102.PDF> (visited on 01/04/2020).
- Tibnor. *Vägräcken*. 2019. URL: https://portal.tibnor.com/sv_SE/Armering/V%5C%C3%5C%A4gr%5C%C3%5C%A4cken/c/20_vr (visited on 04/02/2020).
- Trafikverket. *Bärighetsklass BK4 – vägar för trafik upp till 74 ton*. 2019a. URL: <https://www.trafikverket.se/for-dig-i-branschen/vag-barighetsklass-bk4/> (visited on 01/04/2020).
- Transportation Federal Highway Administration, U.S. Department of. *Load and Resistance Factor Design (LRFD) For Highway Bridge Superstructures - Reference Manual*. 2015. URL: <https://www.fhwa.dot.gov/bridge/pubs/nhi15047.pdf> (visited on 02/11/2020).
- Transportstyrelsen. *Bruttoviktstabeller*. 2018. URL: <https://transportstyrelsen.se/sv/vagtrafik/Yrkestrafik/Gods-och-buss/Matt-och-vikt/Bruttoviktstabeller/> (visited on 01/04/2020).
- *Lastbil*. Transportstyrelsen. June 2013. URL: <https://www.transportstyrelsen.se/sv/vagtrafik/Fordon/Fordonsregler/Lastbil/> (visited on 02/24/2020).

Manuals

- British Standard Institution. *BS EN 1991-2, Eurocode 1: Actions on Structures- Part 2: Traffic Loads on Bridges*. London, UK: British Standard Institution, 2003.
- ISO. *ISO 8608:2016. Mechanical vibration — Road surface profiles — Reporting of measured data*. 2nd. Geneva, Switzerland: ISO, 2016.
- NZ Transport Agency. *Bridge manual (SP/M/022)*. 3rd. SP/M/022. Wellington, NZ: NZ Transport Agency, 2013. ISBN: 978-0-478-37162-8.
- Swedish Standards Institute. *SS-EN 1991-2 Part 2: Traffic loads on bridges*. 1st. Sweden, Stockholm: SIS Förlag AB, 2019.
- Trafikverket. *KRAV Bärighetsberäkningar av broar*. 2013:0267. Version 6.0. Trafikverket, 2019b.

Miscellaneous

- Jacobsson, Bengt. *Vehicle Dynamics. Compendium for Course MMF062*. Gothenburg, Sweden.

Projektarbetet "vägen till vägen". Laborationshandledningar. Lund.

Reports

- Ibsen, Lars Bo and Morten Liingaard. *Lumped-parameter models.* English. 11. Denmark, 2006.
- Karoumi, Raid and Andreas Andersson. *Load testing of the New Svinesund Bridge: presentation of results and theoretical verification of bridge behavior.* Stockholm: KTH Royal Institute of Technology, 2006. ISRN: KTH/BKN/R-96-SE.
- Larsson, Rolf. *Jords egenskaper.* 1. 2008, p. 58.
- Möller, Björn et al. *Geodynamik i praktiken.* 17. 2000, p. 51.
- Plos, Mario and Christoffer Svedholm. *Förstudie: Ökad kapacitet för tunga fordon hos befintliga vägbroar. Förfinad modell för att beräkna fordonsdynamiska effekter.* Göteborg: Chalmers Tekniska Högskola, 2019.
- SGU. *Naturgrus eller morän.* 2000:2. 2000.
- Tobar, Marta and Estrella Martinez. *ENSEMBLE regulatory framework – state of the art. D6.10 of H2020 project ENSEMBLE.* 2019.
- Trafikverket. *Underhållsstandard belagd väg 2011.* 2012:074. Borlänge, Sweden, Mar. 2012.
- Vägverket. *BWIM-mätningar 2002-2003 : Slutrapport.* 2003:165. Borlänge, Sweden, 2004.
- *BWIM-mätningar 2004-2005 - Projektrapport.* 2006:136. Borlänge, Sweden, 2006.

Thesis

- Arvidsson, Therese. "Train–Bridge Interaction: Literature Review and Parameter Screening". Doctoral thesis. Stockholm, Sweden: KTH Royal Institute of Technology, May 2014.
- Caprani, C.C. "Probabilistic Analysis of Highway Bridge Traffic Loading". Doctoral Thesis. Dublin, Ireland: University College, Dublin. School of Architecture, Landscape & Civil Engineering, 2005, p. 409.
- Grave, Samuel. "Modelling of site-specific traffic loading on short to medium span bridges". Doctoral thesis. Dublin, Ireland: Trinity College. Department of Civil, Structural and Environmental Engineering, 2002, p. 401.
- Luttinen, R. Tapio. "Statistical analysis of vehicle time headways". en. Doctoral Thesis. May 1996, p. 193. ISBN: 951-22-8474-X. URL: <http://urn.fi/urn:nbn:fi:tkk-007970>.

- Svedholm, Christoffer. “Efficient Modelling Techniques for Vibration Analyses of Railway Bridges”. QC 20170213. KTH, Structural Engineering and Bridges, 2017, p. 111.
- Zangeneh Kamali, Abbas. “Dynamic Soil-Structure Interaction Analysis of Railway Bridges : Numerical and Experimental Results”. QC 20180315. Licentiate thesis. ELU Konsult AB, 2018. ISBN: 978-91-7729-713-0.